Plasma Sources Sci. Technol. **9** (2000) 528–540. Printed in the UK PII: S0963-0252(00)15188-6

Electron kinetics in atomic and molecular plasmas

C M Ferreira and J Loureiro

Centro de Física dos Plasmas, Instituto Superior Técnico, 1049-001 Lisboa, Portugal

Received 1 December 1999, in final form 22 May 2000

Abstract. In the first part of this paper we briefly review some basic concepts of kinetic theory. The concept of the velocity distribution function is first introduced and its meaning is discussed. Then, the Boltzmann equation is presented on physical grounds and it is shown that the fluid equations are its moments. In the second part, the Boltzmann equation for free electrons in a low-temperature plasma is analysed. It is shown how this equation can approximately be solved for electrons under a HF field of frequency ω (including the particular case of a dc field, which corresponds to the limit $\omega = 0$) by using a first-order double expansion in spherical harmonics in velocity space and a Fourier series in time. The electron transport parameters, particle balance and energy balance are analysed from a general point of view. Finally, an application to argon and nitrogen is given. The effects of changes in the field frequency on the electron energy distribution function, transport parameters and power balance are discussed. The importance of the coupling between the electron and the vibrational kinetics in N_2 is emphasized.

1. Introduction to kinetic theory

In this section we briefly review some basic concepts of kinetic theory which are essential in order to understand the treatment of the electron kinetics to be made later. Detailed analyses of kinetic theory can be found in many textbooks either at an elementary or an advanced level, and the reader should refer to such books (e.g. [1–3]) for more information.

1.1. The meaning of the velocity distribution function

There are many phenomena in ionized gases for which we need to consider the velocity distribution function of the particles, or at least of some particles such as free electrons, and to use a treatment called kinetic theory. In fluid theory, the velocity distribution of each species is assumed to be Maxwellian everywhere and is therefore uniquely specified by the species temperature T. Because inelastic collisions, especially between electrons and neutral particles, play a major role in low-temperature plasmas, significant deviations from thermal equilibrium are usually present in such media, which justifies the need for using the kinetic theory.

By definition, the velocity distribution function $F(\boldsymbol{r}, \boldsymbol{v}, t)$ of a given species represents the number of particles of that species per unit volume of the six-dimensional phase space at position $(\boldsymbol{r}, \boldsymbol{v})$ and time t. This means that the number of particles per unit volume in configuration space with velocity components between v_x and $v_x + \mathrm{d}v_x$, v_y and $v_y + \mathrm{d}v_y$, and v_z and $v_z + \mathrm{d}v_z$ at time t is

$$F(x, y, z, v_x, v_y, v_z, t)\,\mathrm{d}v_x\,\mathrm{d}v_y\,\mathrm{d}v_z.$$

When we consider velocity distributions, we therefore have seven independent scalar variables: $(\boldsymbol{r}, \boldsymbol{v}, t)$. The density in configuration space $n = n(\boldsymbol{r}, t)$, which is a function of only four scalar variables, is obtained by integration of $F(\boldsymbol{r}, \boldsymbol{v}, t)$ over velocity space, that is

$$n(\boldsymbol{r}, t) = \int_{-\infty}^{\infty} \mathrm{d}v_x \int_{-\infty}^{\infty} \mathrm{d}v_y \int_{-\infty}^{\infty} \mathrm{d}v_z\, F(\boldsymbol{r}, \boldsymbol{v}, t) = \int_{-\infty}^{\infty} F(\boldsymbol{r}, \boldsymbol{v}, t)\,\mathrm{d}^3 v. \tag{1}$$

It is often convenient to normalize the velocity distribution to unity, in which case it represents a probability. Thus, if we denote this probability by f, we have

$$F(\boldsymbol{r}, \boldsymbol{v}, t) = n(\boldsymbol{r}, t)\, f(\boldsymbol{r}, \boldsymbol{v}, t) \tag{2}$$

with

$$\int_{-\infty}^{\infty} f(\boldsymbol{r}, \boldsymbol{v}, t)\,\mathrm{d}^3 v = 1. \tag{3}$$

For example, the Maxwellian distribution normalized to unity is:

$$f_M = (m/2\pi KT)^{3/2} \exp(-mv^2/2KT) \tag{4}$$

where $v \equiv (v_x^2 + v_y^2 + v_z^2)^{1/2}$ and m is the particle mass.

There are several average velocities of a Maxwellian distribution that are commonly used. The root-mean-square (rms) velocity is given by

$$(\overline{v^2})^{1/2} = (3KT/m)^{1/2}. \tag{5}$$

The average magnitude of the velocity, $\overline{v}$, is found as follows:

$$\overline{v} = \int_{-\infty}^{\infty} v f(\boldsymbol{v})\,\mathrm{d}^3 v. \tag{6}$$

Since f_M is isotropic, the integral is most easily written in spherical coordinates in v space and taking into account that the volume element of each spherical shell is $4\pi v^2\,\mathrm{d}v$. After some simple calculations, one obtains

$$\overline{v} = 2(2KT/\pi m)^{1/2}. \tag{7}$$

The velocity component in a single direction, say v_x, has a different average. Of course, $\overline{v}_x$ vanishes for an isotropic distribution, but $\overline{|v_x|}$ does not:

$$\overline{|v_x|} = \int |v_x| f_M(\boldsymbol{v})\,\mathrm{d}^3 v = (2KT/\pi m)^{1/2}. \tag{8}$$

The random flux crossing an imaginary plane from one side to the other is given by

$$\Gamma_{random} = \tfrac{1}{2} n \overline{|v_x|} = \tfrac{1}{4} n \overline{v}. \tag{9}$$

For an isotropic distribution like a Maxwellian, it is useful to define another distribution $g(v)$ which is only a function of the scalar magnitude of $\boldsymbol{v}$ such that

$$\int_0^{\infty} g(v)\,\mathrm{d}v = \int_{-\infty}^{\infty} f(\boldsymbol{v})\,\mathrm{d}^3 v. \tag{10}$$

Thus, $g(v) = 4\pi v^2 f$, so that for a Maxwellian we have

$$g(v) = 4\pi (m/2\pi KT)^{3/2} v^2 \exp(-mv^2/2KT). \tag{11}$$

Note that $f_M(v)$ is a maximum for $v = 0$, but $g(v)$ is zero. This is just a consequence of the vanishing of the volume in phase space for $v = 0$.

1.2. The Boltzmann equation

In low temperature plasmas, the distribution of each species $F(\boldsymbol{r}, \boldsymbol{v}, t)$ satisfies in general the well-known Boltzmann equation:

$$\frac{\partial F}{\partial t} + \boldsymbol{v} \cdot \nabla F + \frac{\boldsymbol{X}}{m} \cdot \frac{\partial F}{\partial \boldsymbol{v}} = \left(\frac{\partial F}{\partial t}\right)_c. \tag{12}$$

Here $\boldsymbol{X}$ is the force acting on the particles, and $(\partial F/\partial t)_c$ is the time rate of change of F due to collisions. Considering, for example, free electrons, this collision term must account for elastic and inelastic electron–neutral collisions, and, at relatively high degrees of ionization, for electron–electron and electron–ion collisions. The symbol ∇ stands, as usual, for the gradient in configuration space (x, y, z) while the symbol $\partial/\partial \boldsymbol{v}$ or ∇_v stands for the gradient in velocity space:

$$\frac{\partial}{\partial \boldsymbol{v}} = \hat{\boldsymbol{x}} \frac{\partial}{\partial v_x} + \hat{\boldsymbol{y}} \frac{\partial}{\partial v_y} + \hat{\boldsymbol{z}} \frac{\partial}{\partial v_z}. \tag{13}$$

The meaning of the Boltzmann equation becomes clear if one notes that the left-hand side of this equation represents the total (or the convective) derivative of F in phase space

$$\frac{\mathrm{d}F}{\mathrm{d}t} = \frac{\partial F}{\partial t} + \frac{\partial F}{\partial x}\frac{\mathrm{d}x}{\mathrm{d}t} + \frac{\partial F}{\partial y}\frac{\mathrm{d}y}{\mathrm{d}t} + \frac{\partial F}{\partial z}\frac{\mathrm{d}z}{\mathrm{d}t} + \frac{\partial F}{\partial v_x}\frac{\mathrm{d}v_x}{\mathrm{d}t} + \frac{\partial F}{\partial v_y}\frac{\mathrm{d}v_y}{\mathrm{d}t} + \frac{\partial F}{\partial v_z}\frac{\mathrm{d}v_z}{\mathrm{d}t}. \tag{14}$$

Here, $\partial F/\partial t$ is the rate of change due to the explicit dependence on time. The next three terms are just $\boldsymbol{v} \cdot \nabla F$, while the last three terms, taking into account Newton's third law $m(\mathrm{d}\boldsymbol{v}/\mathrm{d}t) = \boldsymbol{X}$ are recognized as $(\boldsymbol{X}/m) \cdot (\partial F/\partial \boldsymbol{v})$. The total derivative $\mathrm{d}F/\mathrm{d}t$ can be interpreted as the rate of change as seen in a frame moving with the particles in the six-dimensional $(\boldsymbol{r}, \boldsymbol{v})$ space. The Boltzmann equation simply says that $\mathrm{d}F/\mathrm{d}t$ is zero unless there are collisions. Collisions have the effect of removing a particle from one element of velocity space and replacing it in another, or even creating a new particle in the case of ionization. One provides for this by the collision term $(\partial F/\partial t)_c$, which will be further discussed in section 2 for the case of electron collisions.

1.3. Derivation of the fluid equations

The fluid equations are simply moments of the Boltzmann equation.

The lowest moment is obtained just by integrating this equation over velocity space

$$\int \frac{\partial F}{\partial t}\,\mathrm{d}\boldsymbol{v} + \int \boldsymbol{v} \cdot \nabla F\,\mathrm{d}\boldsymbol{v} + \int \frac{\boldsymbol{X}}{m} \cdot \frac{\partial F}{\partial \boldsymbol{v}}\,\mathrm{d}\boldsymbol{v} = \int \left(\frac{\partial F}{\partial t}\right)_c \mathrm{d}\boldsymbol{v} \tag{15}$$

where $\mathrm{d}\boldsymbol{v}$ stands for a three-dimensional volume element in velocity space. By transforming the third term on the left-hand side by Green's theorem and after straightforward calculations one obtains the continuity equation

$$\frac{\partial n}{\partial t} + \nabla \cdot (n\boldsymbol{u}) = S \tag{16}$$

where $\boldsymbol{u}$ is the average (fluid) velocity and S represents the net creation rate of particles per unit volume as a result of collisions (for example, in the case of electrons, this term takes into account new electrons created by ionization and electron losses due to recombination with ions or attachment).

The next moment of the Boltzmann equation is obtained by multiplying it by $m\boldsymbol{v}$ and integrating over $\mathrm{d}\boldsymbol{v}$. We have

$$m\int \boldsymbol{v}\frac{\partial F}{\partial t}\,\mathrm{d}\boldsymbol{v} + m\int \boldsymbol{v}(\boldsymbol{v} \cdot \nabla)F\,\mathrm{d}\boldsymbol{v} + \int \boldsymbol{v}\boldsymbol{X} \cdot \frac{\partial F}{\partial \boldsymbol{v}}\,\mathrm{d}\boldsymbol{v} = \int m\boldsymbol{v}\left(\frac{\partial F}{\partial t}\right)_c \mathrm{d}\boldsymbol{v}. \tag{17}$$

The right-hand side is the change of momentum due to collisions of the particles under analysis (say, the i particles) with other particle species j. This will give a friction term which we will denote by $\boldsymbol{P}_{ij}$.

The first term on the left-hand side gives

$$m\int \boldsymbol{v}\frac{\partial F}{\partial t}\,\mathrm{d}\boldsymbol{v} = m\frac{\partial}{\partial t}\int \boldsymbol{v}F\,\mathrm{d}\boldsymbol{v} \equiv m\frac{\partial}{\partial t}(n\boldsymbol{u}). \tag{18}$$

The third integral on the left-hand side gives, by Green's theorem,

$$\int \boldsymbol{v}\boldsymbol{X} \cdot \frac{\partial F}{\partial \boldsymbol{v}}\,\mathrm{d}\boldsymbol{v} = -\int \boldsymbol{X}F\,\mathrm{d}\boldsymbol{v} = -n\boldsymbol{X}. \tag{19}$$

Finally, to evaluate the second integral on the left-hand side, we first note that

$$\int \boldsymbol{v}(\boldsymbol{v} \cdot \nabla)F\,\mathrm{d}\boldsymbol{v} = \int \nabla \cdot (F\boldsymbol{v}\boldsymbol{v})\,\mathrm{d}\boldsymbol{v} = \nabla \cdot \int F\boldsymbol{v}\boldsymbol{v}\,\mathrm{d}\boldsymbol{v} = \nabla \cdot n\overline{\boldsymbol{v}\boldsymbol{v}}. \tag{20}$$

Now we may separate $\boldsymbol{v}$ into the average (fluid) velocity $\boldsymbol{u}$ and a thermal velocity $\boldsymbol{w}$,

$$\boldsymbol{v} = \boldsymbol{u} + \boldsymbol{w} \tag{21}$$

yielding

$$\boldsymbol{\nabla}\cdot(n\overline{\boldsymbol{v}\boldsymbol{v}}) = \boldsymbol{\nabla}\cdot(n\boldsymbol{u}\boldsymbol{u}) + \boldsymbol{\nabla}\cdot(n\overline{\boldsymbol{w}\boldsymbol{w}}). \tag{22}$$

The quantity $mn\overline{\boldsymbol{w}\boldsymbol{w}}$ is what is called the stress tensor $\boldsymbol{P}$:

$$\boldsymbol{P} \equiv mn\overline{\boldsymbol{w}\boldsymbol{w}}. \tag{23}$$

Collecting the above results and taking into account the continuity equation we finally obtain the fluid equation of motion (or the momentum transport equation)

$$mn\left(\frac{\partial \boldsymbol{u}}{\partial t} + (\boldsymbol{u}\cdot\boldsymbol{\nabla})\boldsymbol{u}\right) + mS\boldsymbol{u} = n\boldsymbol{X} - \boldsymbol{\nabla}\cdot\boldsymbol{P} + \boldsymbol{P}_{ij}. \tag{24}$$

The next moment of the Boltzmann equation is the energy transport equation. The general form of this equation will not be given since we will not make use of it here.

2. Electron kinetics

2.1. The Boltzmann equation for electrons

Now let $F(\boldsymbol{r}, \boldsymbol{v}, t)$ denote the electron distribution function with the normalization $\int F \mathrm{d}^3 v = n(\boldsymbol{r}, t)$, where n is the electron density. We assume that the total electric field acting on the electrons consists of a dc space-charge field and an applied HF field of frequency ω, that is, $\boldsymbol{E} = \boldsymbol{E}_s + \boldsymbol{E}_p \exp(\mathrm{j}\omega t)$, where E_s is the space-charge field intensity and E_p is the complex amplitude of the HF field. The particular case of an applied dc field can be dealt with in the limit $\omega = 0$. The intensity E_s varies with position but E_p will be assumed to be spatially constant.

The Boltzmann equation now takes the form

$$\frac{\partial F}{\partial t} + \boldsymbol{\nabla}_r\cdot(\boldsymbol{v}F) - \boldsymbol{\nabla}_v\cdot\left(\frac{e\boldsymbol{E}}{m}F\right) = \left(\frac{\partial F}{\partial t}\right)_c \tag{25}$$

where e and m are the electron absolute charge and mass, respectively. This equation is usually solved by expanding F in spherical harmonics in velocity space and a Fourier series in time [4]

$$F = \sum_{\ell}\sum_{p} F_p^{\ell} P_l(\cos\vartheta)\exp(\mathrm{j}p\omega t) \tag{26}$$

where P_l are the Legendre polynomials and ϑ is the polar angle.

Let us assume that: (i) the electron–neutral mean free path, λ_e, is much smaller than any relevant dimension of the container, L, i.e. $\lambda_e \ll L$; (ii) the energy gained from the electric field per collision by a representative electron is much smaller than the mean thermal energy of the electrons; (iii) the oscillation amplitude of the electron motion under the action of the HF field is small as compared to L; and (iv) $\omega \gg \tau_e^{-1}$, where τ_e is the characteristic time for electron energy relaxation by collisions. The latter assumption implies that the electrons do not lose appreciable energy during a cycle of the HF field oscillation. Assumptions (i) and (ii) ensure that the anisotropies resulting from the spatial gradients and the field are small. Assumption (iii) ensures that the HF field does not clear the electrons out of the plasma in a half-cycle. Under these assumptions, it is sufficient to consider only the following terms in the expansion of (26)

$$F \simeq F_0^0 + (\boldsymbol{v}/v)\cdot[\boldsymbol{F}_0^1 + \boldsymbol{F}_1^1\exp(\mathrm{j}\omega t)] \tag{27}$$

where F_0^0, $\boldsymbol{F}_0^1$, and $\boldsymbol{F}_1^1$ are time-independent, isotropic functions.

Inserting (27) into (25), expressing the collision operator in terms of the electron–neutral collision frequency for momentum transfer, ν_c, and of the inelastic collision frequencies ν_j and ν_i (j and i holding for the excitation of the jth level and for direct ionization, respectively) and then equating terms of similar time and angle dependence, one obtains one scalar and two vector equations [5]

$$\frac{v}{3}\boldsymbol{\nabla}_r\cdot\boldsymbol{F}_0^1 - \frac{1}{v^2} \times\frac{\partial}{\partial v}\left\{\left(\frac{ev^2}{6m}\right)[\mathrm{Re}\,(\boldsymbol{E}_p\cdot\boldsymbol{F}_1^1) + 2\boldsymbol{E}_s\cdot\boldsymbol{F}_0^1] + \frac{m}{M}\nu_c v^3 F_0^0\right\} = (q - \nu_x - \nu_i)F_0^0 \tag{28}$$

$$\nu_c\boldsymbol{F}_0^1 = -v\boldsymbol{\nabla}_r F_0^0 + \frac{e}{m}\boldsymbol{E}_s\frac{\partial F_0^0}{\partial v} \tag{29}$$

$$(\nu_c + \mathrm{j}\omega)\boldsymbol{F}_1^1 = \frac{e\boldsymbol{E}_p}{m}\frac{\partial F_0^0}{\partial v}. \tag{30}$$

Here m is the mass of the neutrals, Re means the 'real part of' the term, $\nu_x = \sum_j \nu_j$ and q is an operator representing the re-introduction of electrons in the distribution after the inelastic collisions. These processes are treated mathematically as though 'fast' electrons disappeared at the rate $(\nu_x + \nu_i)F_0^0$ and 'slow' electrons appeared at the rate qF_0^0. For the moment, we do not need an explicit expression for qF_0^0, but we just note that the following relation is necessarily satisfied:

$$\int_0^\infty qF_0^0 4\pi v^2\,\mathrm{d}v = n(\overline{\nu}_x + 2\overline{\nu}_i) \tag{31}$$

where the bar represents, as before, the average over the distribution. The factor $2\overline{\nu}_i$ on the right-hand side of (31) accounts for the new free electron produced in each ionizing collision.

The terms on the left-hand side of (28) represent the divergence of the electron flux in configuration (first term) and velocity space. The latter flux is composed of three terms accounting for the fluxes driven by the HF field, the space-charge dc field and the recoil collisions, respectively.

2.2. Electron particle balance

Integrating equation (28) over the velocity space and taking (31) into account one obtains

$$\boldsymbol{\nabla}_r\cdot\int_0^\infty \boldsymbol{F}_0^1\frac{4\pi v^3}{3}\,\mathrm{d}v = \overline{\nu}_i n. \tag{32}$$

The integral on the left-hand side is just the electron particle flow vector $\boldsymbol{\Gamma}$, which taking into account equation (29) is given by

$$\boldsymbol{\Gamma} = \int_0^\infty \boldsymbol{F}_0^1\frac{4\pi v^3}{3}\,\mathrm{d}v = -\boldsymbol{\nabla}_r(D_e n) - n\mu_e\boldsymbol{E}_s \tag{33}$$

where

$$D_e = \frac{1}{n}\int_0^\infty \frac{v^2}{3\nu_c}F_0^0 4\pi v^2\,\mathrm{d}v \tag{34}$$

and

$$\mu_e = -\frac{1}{n}\int_0^\infty \frac{ev}{3m\nu_c}\frac{\partial F_0^0}{\partial v}4\pi v^2\,\mathrm{d}v \tag{35}$$

are the electron free diffusion coefficient and the dc mobility, respectively. Therefore, equation (32) is simply the electron continuity equation

$$\boldsymbol{\nabla}_r\cdot\boldsymbol{\Gamma} = \overline{\nu}_i n. \tag{36}$$

2.3. Electron energy balance

The electron energy balance can be obtained by multiplying equation (28) by the electron energy, $u = mv^2/2$ and then integrating over the velocity space. The resulting equation can be written as

$$\boldsymbol{\nabla}_r\cdot\int_0^\infty \frac{1}{2}mv^2\boldsymbol{F}_0^1\frac{4\pi v^3}{3}\,\mathrm{d}v = \frac{1}{2}\mathrm{Re}\,(\boldsymbol{j}_1\cdot\boldsymbol{E}_p) + \boldsymbol{j}_0\cdot\boldsymbol{E}_s - \frac{2m}{M}\overline{u\nu}_c n - \left(\sum_j eV_j\overline{\nu}_j + eV_i\overline{\nu}_i\right)n \tag{37}$$

where V_j and V_i are the excitation potential of the jth level and the ionization potential, respectively, and $\boldsymbol{j}_1$ and $\boldsymbol{j}_0$ are the ac and dc electron current densities given by

$$\boldsymbol{j}_1 = -e\int_0^\infty \boldsymbol{F}_1^1\frac{4\pi v^3}{3}\,\mathrm{d}v \tag{38}$$

$$\boldsymbol{j}_0 = -e\boldsymbol{\Gamma} = -e\int_0^\infty \boldsymbol{F}_0^1\frac{4\pi v^3}{3}\,\mathrm{d}v. \tag{39}$$

The term on the left-hand side of (37) represents the divergence of an energy flux in configuration space. The various terms on the right-hand side represent, in order, the power gain from the HF field, the power lost by the electrons in flowing against the space-charge field (note that $\boldsymbol{j}_0\cdot\boldsymbol{E}_s$ is a negative term; this power, which is lost by the electrons, is ultimately carried toward the wall by the ions accelerated in the space-charge field) and the power loss due to elastic and inelastic collisions, all per unit volume.

It is convenient at this point to introduce the plasma complex conductivity, σ, defined by the relation $\boldsymbol{j}_1 = \sigma\boldsymbol{E}_p$. From equations (38) and (30) it follows that σ is given by

$$\sigma = -\frac{e^2}{m}\int_0^\infty \frac{1}{\nu_c + \mathrm{j}\omega}\frac{\partial F_0^0}{\partial v}\frac{4\pi v^3}{3}\,\mathrm{d}v. \tag{40}$$

The power absorbed from the HF field is given by $\mathrm{Re}\,(\sigma)E^2$, where E denotes the rms field, and

$$\mathrm{Re}\,(\sigma) = -\frac{e^2}{m}\int_0^\infty \frac{\nu_c}{\nu_c^2 + \omega^2}\frac{\partial F_0^0}{\partial v}\frac{4\pi v^3}{3}\,\mathrm{d}v. \tag{41}$$

2.4. Homogeneous Boltzmann equation. Energy distribution function

Equations (28)–(30) are difficult to solve, even numerically, due to the presence of the space-charge field terms. The difficulties are twofold. First, when we insert into (28) the expressions for $\boldsymbol{F}_0^1$ and $\boldsymbol{F}_1^1$ obtained from (29) and (30), we obtain cross space and velocity terms involving $\boldsymbol{E}_s$, which means that exact separable solutions of the form $F_0^0(\boldsymbol{r}, v) = n(\boldsymbol{r})f_0(v)$ do not exist. Second, to determine $\boldsymbol{E}_s$ self-consistently Poisson's equation must be used, and thus ion motion must also be considered. Therefore, equations (28)–(30) must be coupled to both Poisson's equation and, for example, the ion continuity and momentum transport equations. In recent years, there has been a considerable amount of work performed with the aim at solving this problem self-consistently (see, e.g. [6–9]). This requires, however, complex numerical techniques which are beyond the scope of this presentation. For this reason, we will rather discuss useful approximations.

For discharge modelling, a reasonable approximation in numerous circumstances consists in neglecting the space-charge field term in equation (28) (note, however, that the space-charge field term must be kept in (29), as it nearly balances the diffusion term and makes that the total electron particle flow, $\boldsymbol{\Gamma}$, becomes a small quantity). In fact, it seems physically correct to neglect the flux driven in velocity space by $\boldsymbol{E}_s$ as compared to that driven by the external field. In a self-sustained discharge the electrons must be able to produce ionization at a rate that just compensates for the rate of electron loss. To reach the ionization energy level, an electron has to extract much more energy from the applied field than just the ionization energy, since it makes, on average, several excitations before it ionizes an atom. Additionally, as the electrons try to build up energy they have to overcome the losses resulting from recoil collisions and from their average motion against $\boldsymbol{E}_s$, towards the wall.

Neglecting the term $2\boldsymbol{E}_s\cdot\boldsymbol{F}_0^1$ in equation (28) and taking into account (29) and (30), we obtain the following equation for F_0^0:

$$-\frac{v^2}{3\nu_c}\boldsymbol{\nabla}_r^2 F_0^0 + \frac{ev}{3m\nu_c}\boldsymbol{\nabla}_r\cdot\left(\boldsymbol{E}_s\frac{\partial F_0^0}{\partial v}\right) - \frac{1}{v^2}\frac{\partial}{\partial v}\left[v^2\left(\frac{u_c\nu_c}{3m}\frac{\partial F_0^0}{\partial v} + \frac{m}{M}\nu_c v F_0^0\right)\right] = (q - \nu_x - \nu_i)F_0^0 \tag{42}$$

where we have introduced u_c, the average energy gained from the HF field per collision, given by [10]

$$u_c = \frac{(eE_p)^2}{2m(\nu_c^2 + \omega^2)}. \tag{43}$$

Note that u_c is generally a function of the electron energy through ν_c; the product $\nu_c u_c$, which represents the power transfer from the field to the electrons of energy u, reaches a maximum when $\nu_c(u) = \omega$. This remark will be important later on, when we will discuss the changes in the distribution induced by the changes in ω.

The first two terms on the left-hand side of equation (42) may be each quite large, but they nearly cancel each other

under discharge conditions; their difference being small as compared to the other terms in the equation. It suffices, therefore, to use an approximation for the small difference. Let us assume, following Rose and Brown [5], that $\boldsymbol{E}_s$ can be expressed in the form

$$\boldsymbol{E}_s = -u_s \frac{\boldsymbol{\nabla}_r n}{n} \tag{44}$$

where u_s is a measure of the potential drop associated with the space-charge field. In this case (42) is satisfied by separable solutions of the form $F_0^0(r, v) = n(r) f_0(v)$, and we readily obtain, by integration over all velocities:

$$-D_s \nabla_r^2 n = \overline{\nu}_i n \tag{45}$$

where

$$D_s = D_e - u_s \mu_e \tag{46}$$

represents an effective diffusion coefficient.

We can also write (45) in the form

$$\nabla_r^2 n = -n/\Lambda_e^2 \tag{47}$$

where $\Lambda_e = (D_s/\overline{\nu}_i)^{1/2}$ is an effective diffusion length which can be found by solving (47) with appropriate boundary conditions for n (for example, $\Lambda_e = \Lambda$, where Λ is the characteristic diffusion length for the container, if we assume that n vanishes at the wall).

Taking into account (44) and (47), and introducing the electron energy distribution function $f(u)$ by the renormalization $f_0 4\pi v^2 \,\mathrm{d}v = f(u)\sqrt{u}\,\mathrm{d}u$ (note that $\int_0^\infty f(u)\sqrt{u}\,\mathrm{d}u = 1$), we obtain from equation (42)

$$\frac{2u}{3m\nu_c\Lambda_e^2}\left(f + eu_s\frac{\mathrm{d}f}{\mathrm{d}u}\right) - \frac{2}{3\sqrt{u}}\frac{\mathrm{d}}{\mathrm{d}u}\left[u^{\frac{3}{2}}\nu_c\left(u_c\frac{\mathrm{d}f}{\mathrm{d}u} + \frac{3m}{M}f\right)\right] = (q - \nu_x - \nu_i)f. \tag{48}$$

At breakdown, we can neglect space charge, and thus take $u_s = 0$. We can also assume $\Lambda_e = \Lambda$. In this case, (48) can, in principle, be solved for a given gas (i.e. for a specific set of electron cross sections). The independent parameters involved in (48), as seen by simple inspection, are E_p/N, ω/N (from equation (43) defining u_c) and $N\Lambda$, where N is the gas density. Therefore, the solutions of (48) provide a relationship between these three reduced variables which we can represent, for example, as curves of E_p/N against $N\Lambda$ for constant ω/N. These curves are called the breakdown characteristics [11]. Note that these characteristics implicitly satisfy the equation $D_e/\Lambda^2 = \overline{\nu}_i$, since the latter is exactly obtained by integration of (48), with $u_s = 0$, over all energies.

In a quasineutral, diffusion-controlled discharge at sufficiently high pressures $D_s \simeq D_a$, where

$$D_a = \frac{\mu_i D_e + \mu_e D_i}{\mu_e + \mu_i} \tag{49}$$

is the well known ambipolar diffusion coefficient [12] (μ_i and D_i are the ion mobility and diffusion coefficients, respectively). In this case, we have from equation (46) $u_s = (D_e - D_a)/\mu_e$; since $D_a \ll D_e$ one has $u_s \approx u_k$, where $u_k = D_e/\mu_e$ is the electron characteristic energy expressed in electronvolts. Thus, in principle we can also solve equation (48), with $\Lambda_e = \Lambda$ and $u_s = u_k$, and obtain discharge characteristics for the maintenance field expressed in the form E_p/N against $N\Lambda$ for constant ω/N. The solutions now are more difficult to obtain than for breakdown conditions, since u_k itself is a functional of $f(u)$. The solutions must be such that the equation $D_a/\Lambda^2 = \overline{\nu}_i$ is implicitly satisfied, since this equation is exactly obtained by integration of (48) over all energies.

In spite of the simplifications introduced, solving equation (48) is still a complex problem requiring a great deal of numerical work. The problem is considerably simplified, however, when the diffusion term can be neglected. This term is in the ratio $(N\Lambda_e)^{-2}$ to the remaining terms in equation (48), and can be neglected at sufficiently high pressures. In this case (48) reduces to the much simpler form

$$-\frac{2}{3}\frac{\mathrm{d}}{\mathrm{d}u}\left[u^{3/2}\nu_c\left(u_c\frac{\mathrm{d}f}{\mathrm{d}u} + \frac{3m}{M}f\right)\right] = (q - \nu_x - \nu_i)f\sqrt{u} \tag{50}$$

which is called the homogeneous Boltzmann equation. This is a continuity equation for $f(u)$ along the energy axis alone, expressing the fact that the change in the total electron upflux (the net flux resulting from the applied field and the elastic recoil losses) in an energy interval $\mathrm{d}u$ is equal to the difference between the rates of the re-introduction and the removal of electrons by inelastic collisions.

When the diffusion term is neglected one must also neglect, for consistency, the new electrons produced by ionization (since the diffusion term exactly compensates for the rate of appearance of these new electrons). In this case, ionization must be treated like an ordinary excitation process and $\int_0^\infty q f(u)\sqrt{u}\,\mathrm{d}u = \overline{\nu}_x + \overline{\nu}_i$. The neglect of the diffusion and of the source of new electrons altogether is permissible as long as the energy losses associated with the ionization are much smaller than those resulting from excitation or elastic recoil. In most active plasmas, at not too low pressures, one indeed finds that $\overline{\nu}_x \gg \overline{\nu}_i$, and so equation (50) usually is a good approximation. Note, however, that for the purposes of discharge modelling one must take into account the electron continuity equation independently of (50), since the former is no longer implicit in the latter (as was the case in equations (48) and (28)).

When using (50), the modelling of a discharge can proceed via two independent, successive steps. First, equation (50) is solved and the electron transport and collisional rate coefficients are calculated from $f(u)$. Second, these data are inserted into the continuity and the momentum transfer equations for the electrons and the latter are solved along with the corresponding equations for the ions, taking into account appropriate boundary conditions. The first step involves two independent variables E_p/N and ω/N (from u_c in (43)). The second step involves the solution of a boundary-value problem from which a relationship between E_p/N, ω/N and $N\Lambda$ is obtained as an eigenvalue solution. This relationship is the characteristic for the maintenance field.

Now we return to the general electron energy balance equation (37) in order to discuss useful approximations resulting from equations (48) and (50).

2.5. Approximations to the general electron energy balance equation

The homogeneous Boltzmann equation (50) embodies the following mean energy balance per electron (which is simply obtained by multiplying the equation by u and integrating over all energies)

$$\theta \equiv \frac{\mathrm{Re}\,(\sigma)}{n}\frac{E_p^2}{2} = \frac{2m}{M}\overline{u}\overline{\nu}_c + \sum_j eV_j\overline{\nu}_j + eV_i\overline{\nu}_i. \tag{51}$$

Obviously, this is the same equation as (37) with the energy flux and the space-charge field terms neglected. The power absorbed by the electrons from the HF field is totally spent in collisions with the gas molecules in this case.

The quantity θ is the average absorbed power per electron. Note that θ/N is only a function of E_p/N and ω/N. Since E_p/N is a function of $N\Lambda$ for constant ω/N (see above), the average absorbed power per electron at unit gas density also satisfies the characteristics of the form θ/N against $N\Lambda$ for constant ω/N.

We can estimate the power losses associated with the electron flux toward the wall and the maintenance of the space-charge field using the analysis of the previous sections.

The former of these losses is given by the divergence term on the left-hand side of (37). As an order of magnitude estimate, using equations (32) and (33) we have

$$\boldsymbol{\nabla}_r \cdot \int_0^\infty \frac{1}{2}mv^2\boldsymbol{F}_0^1\frac{4\pi v^3}{3}\,\mathrm{d}v \simeq \overline{u}\boldsymbol{\nabla}_r\cdot\boldsymbol{\Gamma} = \overline{u}\,\overline{\nu}_i n. \tag{52}$$

The average power carried away to the wall per electron is, therefore, of the order of $\overline{u}\,\overline{\nu}_i$, which is just the average rate of escape of electrons (equal to $\overline{\nu}_i$) times the electron mean energy $\overline{u}$.

The power lost by the electrons by flowing against the space-charge field is $\boldsymbol{j}_0 \cdot \boldsymbol{E}_s$ per unit volume, as we have seen in (37). In order to estimate this loss per electron we consider a cylindrical plasma column of radius R and integrate the term $\boldsymbol{j}_0 \cdot \boldsymbol{E}_s$ over the cylinder cross section. We must, however, split the integration into two parts, one corresponding to the quasineutral plasma, between the axis ($r = 0$) and the plasma–sheath boundary ($r = R - \boldsymbol{\Delta}$), and the other to the sheath near the wall, of thickness $\boldsymbol{\Delta} \ll R$, namely,

$$\int_0^R \boldsymbol{j}_0 \cdot \boldsymbol{E}_s 2\pi r\,\mathrm{d}r = -e\int_0^{R-\boldsymbol{\Delta}} \boldsymbol{\Gamma}\cdot\boldsymbol{E}_s 2\pi r\,\mathrm{d}r - e\int_{R-\boldsymbol{\Delta}}^R \boldsymbol{\Gamma}\cdot\boldsymbol{E}_s 2\pi r\,\mathrm{d}r. \tag{53}$$

Assuming a collisionless sheath, $r\boldsymbol{\Gamma}$ is constant across the sheath so that the second integral yields $-2\pi R\Gamma_b e\varphi$, where the subscript b denotes values at the plasma–sheath boundary and φ is the potential drop in the sheath. As is well known [13], $e\varphi \simeq \overline{u}\ln(M/m)^{1/2}$. On the other hand, from the continuity equation we find that $2\pi R\Gamma_b = \pi R^2 n_{av}\overline{\nu}_i$, where n_{av} is the radially-averaged density. Therefore,

$$-e\int_{R-\boldsymbol{\Delta}}^R \boldsymbol{\Gamma}\cdot\boldsymbol{E}_s 2\pi r\,\mathrm{d}r \simeq -\pi R^2 n_{av}\overline{u}\,\overline{\nu}_i \ln\left(\frac{M}{m}\right)^{1/2}. \tag{54}$$

The contribution of the integral over the plasma can be estimated using the approximation (44) for $\boldsymbol{E}_s$. This yields

$$-e\int_0^{R-\boldsymbol{\Delta}} \boldsymbol{\Gamma}\cdot\boldsymbol{E}_s 2\pi r\,\mathrm{d}r \simeq eu_s\int_0^{R-\boldsymbol{\Delta}} \Gamma\frac{\mathrm{d}}{\mathrm{d}r}(\ln n)2\pi r\,\mathrm{d}r = eu_s\left[2\pi R\Gamma_b\ln n_b - \int_0^{R-\boldsymbol{\Delta}}\ln n\frac{1}{r}\frac{\mathrm{d}}{\mathrm{d}r}(r\Gamma)2\pi r\,\mathrm{d}r\right] \tag{55}$$

where the second equality is obtained by integration by parts. Now, we note that $(1/r)\,\mathrm{d}(r\Gamma)/\mathrm{d}r = \overline{\nu}_i n$ and take $\ln n \simeq \ln n_0$ in the integrand term, the subscript zero denoting the axial value. We finally get from (55)

$$-e\int_0^{R-\boldsymbol{\Delta}} \boldsymbol{\Gamma}\cdot\boldsymbol{E}_s 2\pi r\,\mathrm{d}r \simeq -\pi R^2 n_{av} eu_s\overline{\nu}_i\ln\left(\frac{n_0}{n_b}\right). \tag{56}$$

Collecting the results (54) and (56), we find that the average power loss per electron as a result of their flowing against the space-charge field is approximately $\overline{\nu}_i\overline{u}(\ln(M/m)^{1/2} + \ln(n_0/n_b))$, where we have assumed $eu_s \sim \overline{u}$. Taking into account this result together with (52), the average power balance per electron (obtained by integration of (37) over the tube cross section and dividing the result by $\pi R^2 n_{av}$) can be expressed as

$$\frac{\mathrm{Re}\,(\sigma)}{n}\frac{E_p^2}{2} \simeq \frac{2m}{M}\overline{u}\overline{\nu}_c + \sum_j eV_j\overline{\nu}_j + eV_i\overline{\nu}_i + \overline{u}\,\overline{\nu}_i\left[1 + \ln\left(\frac{M}{m}\right)^{1/2} + \ln\frac{n_0}{n_b}\right]. \tag{57}$$

This equation differs from (51), the simplified form obtained from the homogeneous Boltzmann equation, by the last term on the right-hand side. The numerical factor $[1 + \ln(M/m)^{1/2} + \ln(n_0/n_b)]$ may be quite large, of the order of ten or even larger, at relatively high pressures where $n_0 \gg n_b$. However, in this case $\overline{\nu}_i$ is small and energy losses associated with excitation and recoil are predominant. The approximation (51) fails, however, at low pressures, when $\overline{\nu}_i$ and $\overline{u}$ are rather large. In any case, (57) can be used to test the accuracy of (51) and of the homogeneous Boltzmann equation.

2.6. Electron–electron collisions

So far we have neglected electron–electron collisions in the Boltzmann equation, but this should be taken into account at high electron densities. In fact, the degree of ionization can be rather high in HF and microwave discharges, and $f(u)$ can be significantly affected by such collisions.

One can account for such collisions in the homogeneous Boltzmann equation by adding another flux term, G_{ee}, on the left-hand side of equation (50). This equation can be expressed in the general form

$$\frac{\mathrm{d}G}{\mathrm{d}u} = (q - \nu_x - \nu_i)f\sqrt{u} \tag{58}$$

where $G = G_E + G_c + G_{ee}$ is the total electron upflux in energy space; that is the sum of the fluxes driven by the applied field, elastic collisions and electron–electron collisions. The latter flux is obtained from the Fokker–Planck equation and can be expressed as [10, 14]

$$G_{ee} = -2\nu_{ee}u^{3/2}\left[I(u)f(u) + J(u)\frac{\mathrm{d}f}{\mathrm{d}u}\right] \tag{59}$$

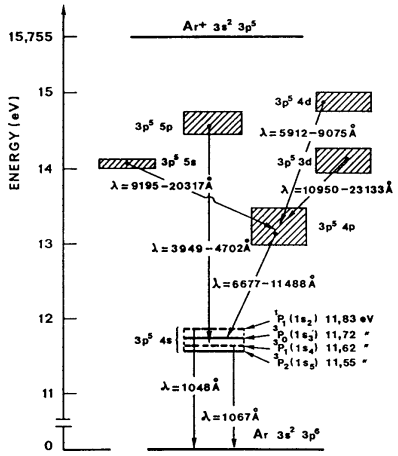

Figure 1. Energy levels of Ar.

where

$$I(u) = \int_0^u f\sqrt{u}\,\mathrm{d}u \tag{60}$$

$$J(u) = \frac{2}{3}\left(\int_0^u f(u)u^{3/2}\,\mathrm{d}u + u^{3/2}\int_u^\infty f(u)\,\mathrm{d}u\right) \tag{61}$$

and

$$\nu_{ee} = 4\pi\left(\frac{e^2}{4\pi\varepsilon_0 m}\right)^2 \frac{\ln\Lambda_c}{v^3}n. \tag{62}$$

Here, ν_{ee} is the electron–electron collision frequency, ε_0 is the permittivity of free space and $\ln\Lambda_c$ is the Coulomb logarithm [10], where $\Lambda_c = 12\pi n\lambda_D^3$, λ_D denoting the electron Debye length.

We have $\int_0^\infty u\,\mathrm{d}G_{ee} = -\int_0^\infty G_{ee}\,\mathrm{d}u = 0$, since electron-electron collisions do not change the total energy of the electron gas. Therefore, the electron power balance equation obtained from (58) is the same as (51). When the distribution becomes Maxwellian, equation (51) constitutes a relationship between T_e, E_p/N and ω/N, where T_e is the electron temperature. In this case, θ/N is a function of T_e alone. Then, since the solutions of the fluid-type equations for the charged particles generally allow one to express T_e as a unique function of $N\Lambda$ (as, for example, in the classical, linear ambipolar diffusion theory for the positive column), θ/N can also be expressed as a unique function of $N\Lambda$, for any ω/N. The single functional dependence of θ/N on $N\Lambda$ constitutes, therefore, a fundamental similarity law for the discharge when $f(u)$ is Maxwellian.

3. Electron kinetics in argon

In this section we present an application of the theory to argon based on numerical solutions to the homogeneous Boltzmann equation (50), using an appropriate set of electron cross sections. Figure 1 shows a simplified energy level diagram of argon. The material presented here has been previously reported [14–16] and the reader should refer to these publications for further details.

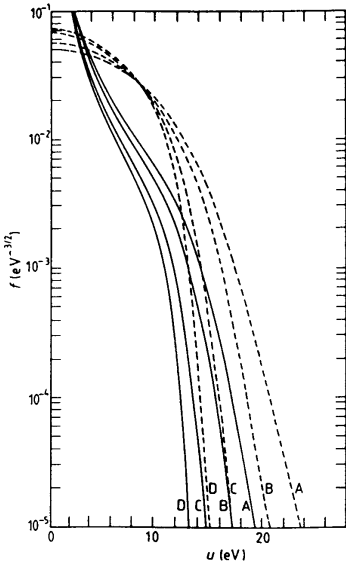

Figure 2. Electron energy distributions in Ar for $\omega/\nu_{ce} = 2$ (full curves) and $\omega \ll \nu_{ce}$ (broken curves) and for the following values of E/N in 10^{-16} V cm^2: 10 (A), 6.5 (B), 3 (C) and 1.5 (D).

We recall that $f(u)$ as obtained from (50) is a function of the two independent parameters E_p/N and ω/N, through $u_c(u)$, the energy gain per collision, defined by equation (43). For the purposes of physical interpretation, a dimensionless parameter ω/ν_{ce}, where ν_{ce} is the collision frequency of a representative electron with a given energy, will be used in place of ω/N (note that ω/ν_{ce} is, in fact, proportional to ω/N, since ν_{ce} is proportional to N). The limiting situations of $\omega \ll \nu_{ce}$ and $\omega \gg \nu_{ce}$ correspond, therefore, to many and to vanishingly few collisions in a cycle of the field oscillation, respectively. It is also useful to introduce an effective field E_e defined as

$$E_e = E\frac{\nu_{ce}}{(\omega^2+\nu_{ce}^2)^{1/2}} \tag{63}$$

where $E = E_p/\sqrt{2}$ is the rms field. This is a similar definition as that currently used when ν_c is assumed to be independent of the electron energy, in which case $f(u)$ is a unique function of E_e/N. As seen from (63), $E_e/N \propto E/\omega$ for $\omega \gg \nu_{ce}$, and $E_e/N \simeq E/N$ for $\omega \ll \nu_{ce}$.

Figure 2 shows two sets of curves of $f(u)$, for $\omega \ll \nu_{ce}$ (similar to the dc case) and $\omega/\nu_{ce} = 2$ and various values of E/N. Here, we have adopted the value $\nu_{ce}/N = 2\times10^{-7}$ cm^3 s^{-1}, which corresponds to electrons of $u \sim 8.5$ eV in argon. This choice makes the rate coefficient of direct ionization, $C_i = \overline{\nu}_i/N$, become nearly a unique function of E_e/N, as shown in figure 3. This peculiarity is

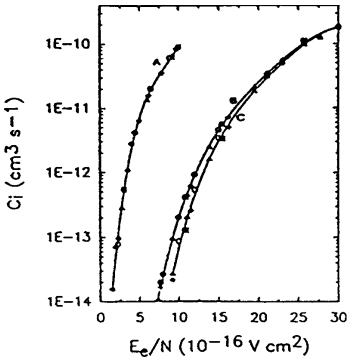

Figure 3. Ionization rate coefficient against E_e/N in Ar (A) and in N_2 for $T_v = 4000$ K (B) and 400 K (C). The data points are from calculations for the various values of ω/ν_{ce} ranging from zero to infinity. The curves are the best fits to these points.

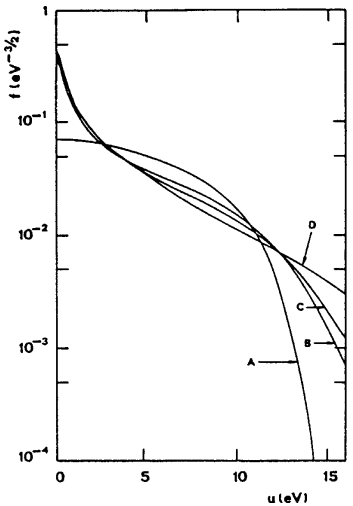

Figure 4. Electron energy distributions in Ar with the same mean energy of 3.5 eV for the following values of ω/ν_{ce}: 0 (A), 0.5 (B), 0.8 (C) and $\gg$1 (D).

useful for the analysis of discharge characteristics for the maintaining field, when stepwise ionization processes are negligible.

The two sets of curves shown in figure 2 exhibit significant differences in the shape of $f(u)$. The distribution peaks at zero energy and becomes much closer to a Maxwellian in the HF case $\omega/\nu_{ce} = 2$. The number of electrons in the high-energy tail relative to that in the body is much larger in this case. In absolute value, the distributions for $\omega \ll \nu_{ce}$ have more electrons in the tail but this results from the fact that they correspond to higher power transfers in absolute value, hence, to a higher range of mean electron energies (note, in fact, that the energy gain per collision u_c given by (43), decreases in absolute value as ω/N increases for constant E/N). For this reason, it is more convenient to compare distributions with the same mean energy but corresponding to different values of ω/ν_{ce}, as shown in figure 4. In order to obtain identical mean energies as ω increases one has also to increase E/N. As seen from figure 4, the relative number of high-energy electrons increases with ω/N although $\overline{u}$ is constant. This is a direct consequence of the fact that the power transfer, $\nu_c u_c$, has a maximum, for a given ω, when $\nu_c(u) = \omega$. As in argon $\nu_c(u)$ is an increasing function of u above the Ramsauer minimum up to $u \sim 12$ eV [17], the maximum power transfer occurs for electrons of increasingly higher energies as ω increases, until $\omega \simeq \nu_c$ (12 eV), which results in a progressive enhancement of the tail. For $u \gtrsim 12$ eV, $\nu_c(u)$ nearly saturates, and a further increase in ω results only in minor changes in the shape of the distribution.

This discussion illustrates that the changes in the shape of $f(u)$ as ω varies can be qualitatively understood from the dependence of the power transfer function $\nu_c u_c$ on the electron energy, as determined by the particular variation of ν_c against u.

The percentage electron energy losses in Ar through elastic collisions, excitation and ionization are represented as a function of θ/N in figure 5, for the two limiting cases of $\omega \ll \nu_{ce}$ and $\omega \gg \nu_{ce}$, when electron–electron collisions are ignored, and also for a Maxwellian distribution. As expected, the changes in ω strongly affect the distribution of the power transfer among the various collisional channels, the curves for $\omega \gg \nu_{ce}$ being shifted towards lower θ/N values as compared to those corresponding to $\omega \ll \nu_{ce}$.

Figure 6 shows the electron characteristic energy, u_k, and the kinetic temperature, $T_e = (2/3)\overline{u}$, as a function of E_e/N, for various values of ω/ν_{ee}. We note that T_e and u_k have quite different values, which is indicative of strong departures from a Maxwellian distribution (in which case $T_e = u_k$) in the body of the distribution. For comparison, figure 6 also shows T_e against E_e/N for the case of a Maxwellian distribution and $\omega \gg \nu_{ce}$. It is interesting to note that u_k strongly decreases as ω/ν_{ce} increases, reaching values well below 1 eV. This fact is connected with the behaviour of the HF distributions at low energies, namely with the strong peak occurring at the origin.

Figure 7 illustrates the effects of electron–electron collisions on the distribution, for $E_e/N = 3\times10^{-16}$ V cm^2 and $n/N = 10^{-4}$, under dc ($\omega = 0$) and microwave ($\omega \gg \nu_{ce}$) fields. The distribution is much more affected by electron–electron collisions in the microwave case; one of the important effects in this case is a significant decrease in the peak at $u = 0$. It is easy to understand on physical grounds why this happens. In argon, low-energy electrons cannot efficiently absorb energy from a microwave field because their collision frequency with the neutrals is very small in the range $u \leqslant 0.5$ eV due to the Ramsauer minimum in the momentum transfer cross section at $u \sim 0.5$ eV (note that the power transferred from the field to the electrons is zero when $\nu_c(u) = 0$). Therefore, electrons tend to accumulate at zero energy, which causes a strong

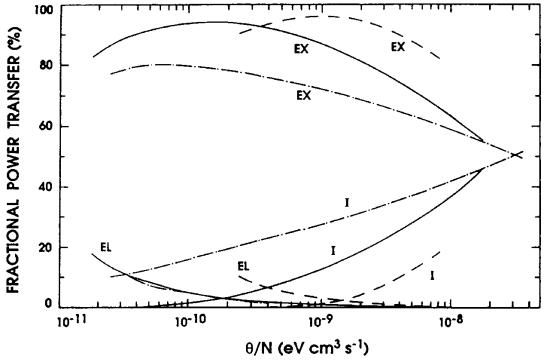

Figure 5. Percentage electron energy losses in Ar through excitation (EX), ionization (I) and elastic recoil (EL) against θ/N in the following cases: no electron–electron interactions, for $\omega \ll \nu_{ce}$ (broken curves) and $\omega \gg \nu_{ce}$ (full curves); and Maxwellian distribution (chain curves).

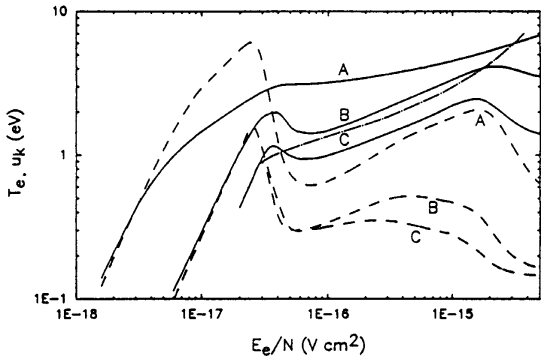

Figure 6. Electron kinetic temperature (full curves) and characteristic energy (broken curves) in Ar against E_e/N, for $\omega/\nu_{ce} = 0.15$ (A), 0.8 (B) and $\gg 1$ (C). The chain curve is for a Maxwellian distribution and $\omega \gg \nu_{ce}$.

peak near $u = 0$. However, these low-energy electrons can interact with other electrons of higher energy, and thus gain energy from electron–electron collisions. Such collisions counteract therefore the accumulation of electrons near $u = 0$ and can significantly contribute to reducing the peak of the distribution, even for moderate degrees of ionization.

These changes induced by electron–electron collisions on the distribution have a huge influence on the electron characteristic energy, u_k a key parameter that determines, as we have seen, the diffusion loss rate (recall that $D_a \simeq \mu_i u_k$, where μ_i is the ion mobility). Figure 8 shows the ratio u_k/T_e as a function of n/N, for three values of E_e/N, in the dc and the microwave case. In the former case, u_k/T_e decreases as n_e/N increases, while in the latter case it is the opposite. The change in u_k/T_e in the microwave case is quite large even at relatively small n/N values, and we can see that u_k becomes of the order of T_e as n/N approaches 10^{-5} or 10^{-4}, depending on E_e/N. This indicates that the body of the distribution nearly Maxwellizes at moderate values of n/N.

4. Electron kinetics in N_2. Coupling with the vibrational kinetics

The solution of the homogeneous Boltzmann equation (50) in a molecular gas such as N_2 is more complex, because it is necessary to account for collisions of electrons with vibrationally excited molecules [18, 19] in the collision term. Moreover, a flux term accounting for rotational excitation must also be included in the total upflux [20]. For consistency, equation (50) must be solved together with the system of rate balance equations determining the populations in the various vibrational levels of the electronic ground state $N_2(X, v)$. Such self-consistent solutions for steady-state discharge conditions have been reported in the literature (see, e.g., [10, 21, 22]).

Let us consider a steady-state HF discharge in nitrogen. Figure 9 shows a schematic energy diagram of the N_2 molecule. The homogeneous electron Boltzmann for this situation can be written in the form [16] (as before, the case of a dc field of intensity $E = E_p/\sqrt{2}$ can be recovered by

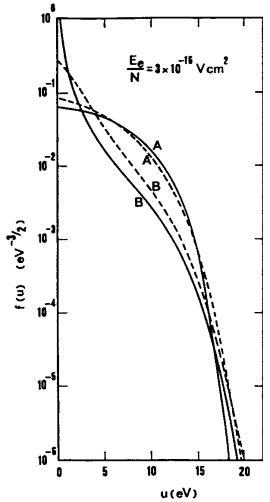

Figure 7. Electron energy distribution in argon for $E_e/N = 3 \times 10^{-16}$ V cm^2, $\omega/\nu_{ce} = 0$ (A) and $\omega/\nu_{ce} = 10$ (B), and the following values of n/N: 0 (full curves) and 10^{-4} (broken curves).

setting $\omega = 0$)

$$\frac{2}{3}\frac{\mathrm{d}}{\mathrm{d}u}\left[u^{3/2}\nu_c\left(u_c\frac{\mathrm{d}f}{\mathrm{d}u}+\frac{3m}{M}f\right)+6B_0u^{1/2}\nu_0 f\right] = \sum_{i,j}[u^{1/2}f(u)\nu_{ij}(u) - (u+V_{ij})^{1/2}f(u+V_{ij})\nu_{ij}(u+V_{ij})] + \sum_{j,i}[u^{1/2}f(u)\nu_{ji}(u) - (u-V_{ij})^{1/2}f(u-V_{ij})\nu_{ji}(u-V_{ij})]. \quad (64)$$

Here, ν_{ij} is the collision frequency for a transition from the ith to the jth molecular state by electron impact, V_{ij} is the energy difference between these states, B_0 is the rotational constant for nitrogen, $\nu_0 = N\sigma_0(2eu/m)^{1/2}$, $\sigma_0 = 8\pi q^2 a_0^2/15$, a_0 is the Bohr radius and $q = 1.01$ is the electric quadrupole moment in units of ea_0^2. The electron–rotation exchanges are treated here in the continuous approximation [20].

In general, the relative populations of electronically excited states are sufficiently low so that electron collisions with such states can be neglected. Furthermore, excitation to electronic states and ionization can usually be treated as single energy loss processes; that is, with no discrimination between individual vibrational levels of the ground and final states. However, electron–vibration energy exchanges with molecules in the ground electronic state; that is, inelastic and superelastic collisions of electrons with $N_2(X, v)$ molecules, must be taken into account, since these vibrational levels are usually highly populated. Equation (64) is therefore coupled, through the collision frequencies ν_{vw}, to the populations N_v of the various ground-state vibrational levels $0 \leqslant v \leqslant 45$ (recall that ν_{vw} is proportional to the density of the initial state

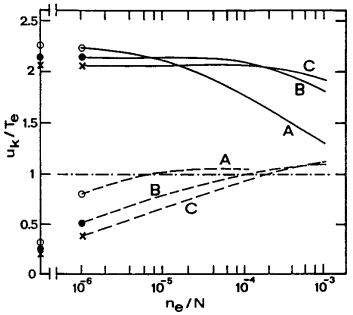

Figure 8. Curves of u_k/T_e against n/N in argon, for dc (full curves), $\omega = 10\nu_{ce}$ (broken curves) and E_e/N (10^{-17} V cm^2) = 10 (A), 50 (B) and 100 (C).

N_v). These populations are given by a system of steady-state rate balance equations for the vibrational levels. The equation for the vth level may be written [18, 21]

$$n\sum_{w=0,w\neq v}^{45} N_w C_{w,v} - nN_v\sum_{w=0,w\neq v}^{45} C_{v,w} + N_{v-1}NP_{v-1,v} + N_{v+1}NP_{v+1,v} - N_v(P_{v,v-1}+P_{v,v+1}) + N_{v-1}\sum_{w=0}^{44} N_{w+1}Q_{v-1,v}^{w+1,w} + N_{v+1}\sum_{w=0}^{45} N_w Q_{v+1,v}^{w,w+1} - N_v\left(\sum_{w=0}^{44} N_{w+1}Q_{v,v+1}^{w+1,w} + \sum_{w=0}^{45} N_w Q_{v,v-1}^{w,w+1}\right) + R(v) = 0 \quad (65)$$

where C, P and Q denote the rate coefficients for electron–vibration, vibration–translation and vibration–vibration processes, respectively, the first and the second subscript indicating the initial and the final state of the colliding molecule. In the case of vibration–vibration exchanges the first and the second superscripts indicate the initial and the final states of the second molecule participating in the process. The term $R(v)$ represents the rate of atomic recombination $N + N \rightarrow N_2(v)$ into the vth level.

The electron–vibration, vibration–translation and vibration–vibration processes considered in equation (65) are the following:

$$\text{electron–vibration} \quad e + N_2(v) \underset{C_{v,w}}{\overset{C_{w,v}}{\rightleftharpoons}} e + N_2(w) \quad (66)$$

$$\text{vibration–translation} \quad \begin{cases} N_2 + N_2(v) \underset{P_{v,v-1}}{\overset{P_{v-1,v}}{\rightleftharpoons}} N_2 + N_2(v-1) \\ N_2 + N_2(v+1) \underset{P_{v+1,v}}{\overset{P_{v,v+1}}{\rightleftharpoons}} N_2 + N_2(v) \end{cases} \quad (67)$$

$$\text{vibration–vibration} \quad \begin{cases} N_2(v) + N_2(w) \underset{Q_{v,v-1}^{w,w+1}}{\overset{Q_{v-1,v}^{w+1,w}}{\rightleftharpoons}} N_2(v-1) + N_2(w+1) \\ N_2(v+1) + N_2(w) \underset{Q_{v+1,v}^{w,w+1}}{\overset{Q_{v,v+1}^{w+1,w}}{\rightleftharpoons}} N_2(v) + N_2(w+1) \end{cases} \quad (68)$$

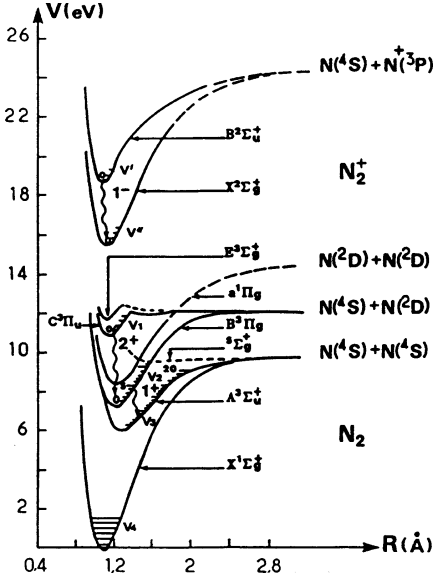

Figure 9. Energy level diagram of N_2.

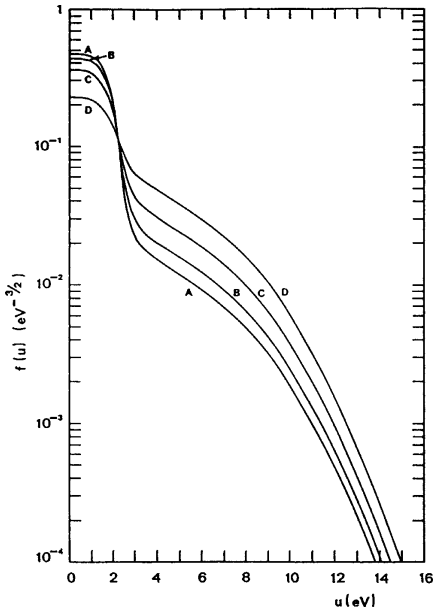

Figure 10. Electron energy distribution functions in N_2 for $E/N = 10^{-15}$ V cm^2 and the following values of T_v in kelvin: 2000 (A), 3000 (B), 4000 (C) and 6000 (D).

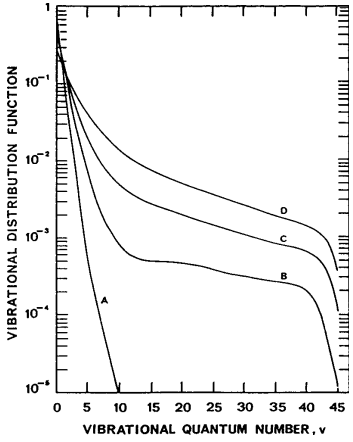

Figure 11. Vibrational distribution functions for the same conditions as in figure 10.

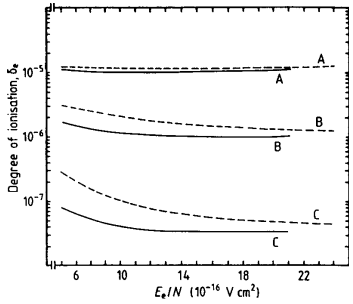

Figure 12. Curves of the degree of ionization against E_e/N in N_2, for $\omega \ll \nu_{ce}$ (full curves) and $\omega \gg \nu_{ce}$ (broken curves) and for the following constant values of T_v in kelvin: 6000 (A), 4000 (B) and 3000 (C).

Note that only single quantum transitions, which are the most likely ones, have been considered in the vibration–translation and vibration–vibration collisional exchange processes.

Figures 10 and 11 show calculated electron energy distributions $f(u)$ and vibrational distribution functions (VDFs), $\delta_v = N_v/N$, for a dc reduced field $E/N = 10^{-15}$ V cm^2 and various values of the characteristic vibrational temperature T_v (defined as the apparent vibrational temperature for the lowest four levels) in the range 2000–4000 K. It is seen that $f(u)$ steeply drops at around 2.5 eV, which is due to the vibrational barrier; the total vibrational excitation cross section has a sharp peak at about this energy, which to a large extent prevents electrons from climbing in energy space. As T_v increases (for example, as a result of an increase in the degree of ionization, and thus in vibrational pumping) this drop in the magnitude of $f(u)$ is significantly attenuated and simultaneously the

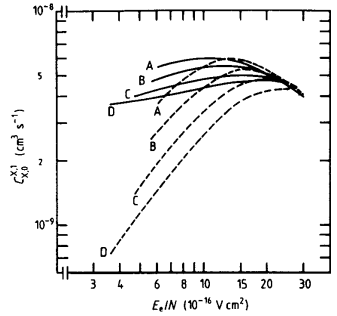

Figure 13. Electron rate coefficient for vibrational excitation from $v = 0$ to $v = 1$ in N_2 against E_e/N, for $T_v = 4000$ K (full curves) and 400 K (broken curves) and for $\omega/\nu_{ce} = 0$ (A), 0.42 (B), 0.83 (C) and 1.67 (D).

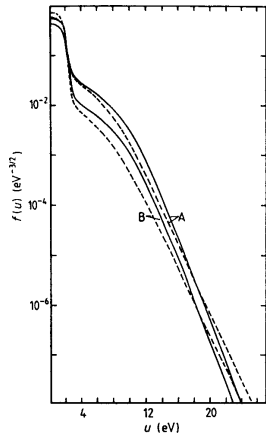

Figure 14. Electron energy distributions in N_2 for $E_e/N = 10^{-15}$ V cm^2, $T_v = 4000$ K (A) and 400 K (B), $\omega/\nu_{ce} = 0.42$ (full curves) and $\omega/\nu_{ce} = 1.67$ (broken curves).

high-energy tail of the distribution is enhanced. This effect is due to electron 'heating' by superelastic electron–vibration collisions.

From the above discussion, it is seen that the coupling to the vibrational kinetics makes the degree of ionization, n/N, become an independent parameter affecting the electron kinetics, even in the absence of electron–electron collisions, in addition to E/N and ω/N (or E_e/N and ω/ν_{ce}). In practice, instead of n/N one can use the characteristic vibrational temperature T_v as an independent parameter, because T_v and n/N are uniquely related to each other for a given E_e/N and ω/ν_{ce} [16].

Figure 12 shows curves of n/N against E_e/N for constant T_v, in the two limiting cases of $\omega \ll \nu_{ce}$ and $\omega \gg \nu_{ce}$. For N_2 we have chosen $\nu_{ce}/N = 2.4 \times 10^{-7}$ cm^3 s^{-1}, which corresponds to electrons of 2.1 eV or 2.9 eV, or

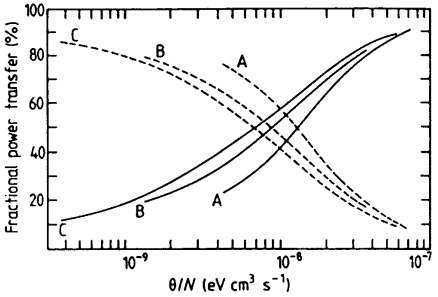

Figure 15. The percentage electron energy losses in N_2 through vibrational excitation (broken curves) and electronic excitation plus ionization (full curves) as a function of θ/N for $\omega/\nu_{ce} = 0$ (A), 0.83 (B) and $\gg 1$ (C).

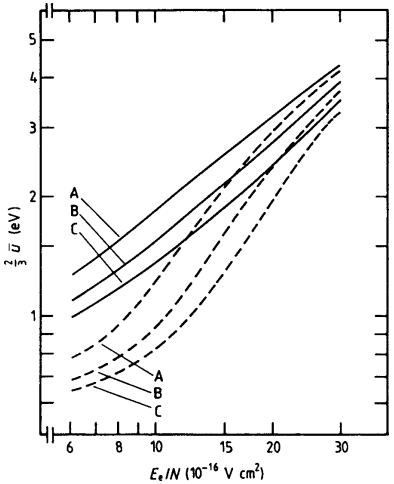

Figure 16. Electron kinetic temperature in N_2 against E_e/N, for $T_v = 4000$ K (full curves) and 400 K (broken curves), and $\omega/\nu_{ce} = 0$ (A), 0.83 (B) and $\gg 1$ (C).

even 10.4 eV (due to the particular shape of $\nu_c(u)$ in N_2 [23]), for the same reasons as in Ar (see figure 3). Producing a given T_v value requires somewhat higher degrees of ionization as ω increases because the rate coefficient for vibrational excitation decreases in this case (figure 13).

Figure 14 shows $f(u)$ for $E_e/N = 10^{-15}$ V cm^2, $T_v = 400$ and $T_v = 4000$ K and two values of ω/ν_{ce}. As in the dc case, higher vibrational temperatures result in higher populations in the tail of $f(u)$, due to the energy gained by the electrons in superelastic collisions.

Changes in ω modify $f(u)$ to a much lesser extent in N_2 than in Ar, but the effects are far from negligible. This can be seen from the curves for the percentage energy losses through vibrational excitation (net power loss, i.e. including the

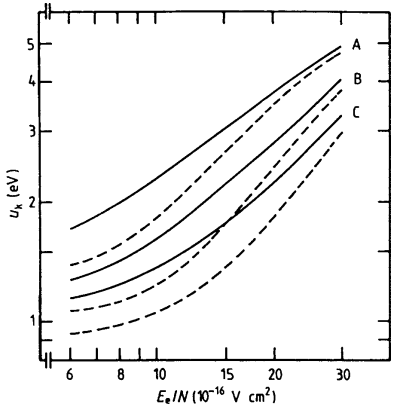

Figure 17. The characteristic energy of N_2 against E_e/N for the same conditions as figure 16.

gain from superelastic collisions) and electronic excitation represented against θ/N in figure 15. The power losses through elastic collisions and rotational excitation are much smaller in the range considered and are not shown on the figure. As ω/ν_{ce} increases the fractional power transferred to the vibrational mode decreases while the losses into electronic excitation and ionization consequently increase. As in Ar, such a behaviour follows from the dependence of $\nu_c u_c$ on u and the fact that this function reaches a maximum for $\nu_c(u) = \omega$. In N_2, $\nu_c(u)$ peaks at around 2.5 eV and grows monotonically at higher energies, so that the maximum power transfer occurs for electrons with increasingly higher energy as ω increases.

Figures 16 and 17 represent, respectively, the electron kinetic temperature $T_e = (2/3)\overline{u}$ and characteristic energy u_k against E_e/N for $T_v = 4000$ and $T_v = 400$ K and various values of ω/ν_{ce}. Both T_e and u_k decrease as ω/ν_{ce} increases for constant E_e/N but the decrease in u_k is much less important in N_2 than in Ar. This is due to the fact the HF distributions in N_2 do not peak at low energies, as seen from figure 14.

References

[1] Chen F F 1984 *Introduction to Plasma Physics and Controlled Fusion* (New York: Plenum)
[2] Huang K 1963 *Statistical Mechanics* (New York: Wiley)
[3] Balescu R 1975 *Equilibrium and Nonequilibrium Statistical Mechanics* (New York: Wiley)
[4] Allis W P and Brown S C 1952 *Phys. Rev.* **87** 419
[5] Rose D J and Brown S C 1955 *Phys. Rev.* **98** 310
[6] Bush C and Kortshagen U 1995 *Phys. Rev.* E **51** 280
[7] Kortshagen U, Pukropski I and Tsendin L D 1995 *Phys. Rev.* E **51** 6063
[8] Uhrlandt D and Winkler R 1996 *J. Phys. D: Appl. Phys.* **29** 115
[9] Alves L L, Gousset G and Ferreira C M 1997 *Phys. Rev.* E **55** 890
[10] Allis W P 1956 *Handbook of Physics* vol 21, p 383
[11] Brown S C 1956 *Handbook of Physics* vol 22, p 531
[12] Allis W P and Rose D J 1954 *Phys. Rev.* **93** 94
[13] Golant V E, Zhilinsky A P and Sakharov I E 1980 *Fundamentals of Plasma Physics* (New York: Wiley)
[14] Ferreira C M and Loureiro J 1984 *J. Phys. D: Appl. Phys.* **17** 1175
[15] Ferreira C M and Loureiro J 1983 *J. Phys. D: Appl. Phys.* **16** 2471
[16] Ferreira C M and Loureiro J 1989 *J. Phys. D: Appl. Phys.* **22** 76
[17] Frost L S and Phelps A V 1964 *Phys. Rev.* A **136** 1538
[18] Capitelli M, Dilonardo M and Gorse C 1981 *Chem. Phys.* **56** 29
[19] Cacciatore M, Capitelli M and Gorse C 1982 *Chem. Phys.* **66** 141
[20] Frost L S and Phelps A V 1962 *Phys. Rev.* **127** 1621
[21] Loureiro J and Ferreira C M 1986 *J. Phys. D: Appl. Phys.* **19** 17
[22] Loureiro J and Ferreira C M 1989 *J. Phys. D: Appl. Phys.* **22** 67
[23] Engelhardt A G, Phelps A V and Risk C G 1964 *Phys. Rev.* A **135** 1566

IOP Publishing — Plasma Sources Science and Technology
Plasma Sources Sci. Technol. **16** (2007) 557–569 doi:10.1088/0963-0252/16/3/015

Fluid modelling of the positive column of direct-current glow discharges*

Luís L Alves[1]

Centro de Física dos Plasmas, Instituto Superior Técnico, Av. Rovisco Pais, Lisboa 1049-001, Portugal

E-mail: llalves@ist.utl.pt

Received 2 February 2007, in final form 28 March 2007
Published 20 June 2007
Online at stacks.iop.org/PSST/16/557

Abstract
This paper presents a tutorial on the fluid modelling of the positive column of direct-current cylindrical glow discharges. The model writes the continuity and momentum-transfer equations for electrons and ions, coupled with Poisson's equation and the electron mean energy transport equations. The model is solved for helium at pressures $p \simeq 0.1$–10 Torr, gas temperature $T_g = 500$ K, discharge currents $I_{dc} = 5$–200 mA, and tube radius $R = 1$ cm. The electron transport parameters and rate coefficients are calculated using the local mean energy approximation in articulation with a two-term Boltzmann solver. Model equations are integrated from the discharge axis to the wall, passing through the space-charge sheath and monitoring the charge separation within it. The results obtained allow a systematic characterization of discharge energy deposition and space-charge sheath formation, as a function of pressure and axial current. A general good agreement is found between model results and experimental measurements available in the literature.

1. Introduction

The study of direct-current (dc) glow discharges has been a subject of interest over the past 80 years [1–54], aiming at the analysis of different plasma properties or with the purpose of applications, for example in material processing or lighting. These fundamental studies focused mainly on the *positive column* region of a dc discharge (corresponding to its most stable, central region), produced in a long glass cylinder (with radius of a few centimetres), limited by a positive anode at one end and a negative cathode at the other (ensuring voltage drops of a few hundred volts, for pressures between 10 mTorr and 10 Torr). Although this discharge configuration is not necessarily the most adopted in processing applications it has the advantage of symmetry, thus converting the cylindrical positive column into the ideal ground to study the basic creation and maintenance mechanisms of a discharge plasma. In fact, in a dc-positive column the externally applied axial electric field is constant, both in space and time, which reduces the problem description to a single (radial) dimension, for a situation with azimuthal symmetry.

This paper presents a tutorial on the fluid modelling of the dc-positive column of glow discharges. The expression *fluid modelling* relates to the type of model used to simulate the physical behaviour of these discharges. It refers to a description where the plasma is treated as a fluid of electrons and ions (both positive and negative), which are transported within a neutral gas background. Hence, the model involves the writing of transport equations (hydrodynamic-like equations) for the plasma charged particles, just as if these species were similar to a flowing fluid. The transport equations are obtained by calculating the *moments* of a microscopic *master equation* [55] (such as the Boltzmann equation [56–58], for the particular case of weakly ionized plasmas), which involves a hierarchical integration of this equation in velocity space.

There are, however, two major differences between the quasi-neutral ensemble of charged particles with a plasma, and an ordinary thermodynamic fluid. The first difference is that the transport of electrons and ions is affected not only by the externally applied field, but also by an electrostatic field that develops as to control charge separation within the

* Paper originally presented at the European Summer School 'Low Temperature Plasma Physics: Basics and Applications' and 'Master Class: Biotechnical and Medical Applications' (Bad Honnef, Germany, 26 September–8 October 2004).

[1] Author to whom any correspondence should be addressed.

0963-0252/07/030557+13$30.00

discharge [59–61]. This so-called *space-charge field* comes as a response to the different transport loss rates of electrons and ions to the walls (due to their different masses), thus being oriented towards the discharge boundaries, with an intensity that increases from the discharge bulk to walls. The self-consistent calculation of the space-charge field (which, in the present case, is radially oriented), as a function of the corresponding electron–ion charge separation, requires the solution to Poisson's equation coupled to the fluid model. The second difference is that a plasma is a reactive medium, within which species are generated and destroyed as the combined result of particle collisions and wall losses. In an active plasma, the net production rate of charged particles must be such as to ensure discharge maintenance. Hence, to satisfy the particle and energy balance equations (for specific wall boundary conditions upon the particle and energy fluxes), the ionization rate and the energy gain rate must compensate for the particle and energy loss rates to the wall. The relationship between these rates allows defining a univocal discharge work-point, for a given set of discharge input parameters. In particular, for given work pressure, geometrical dimensions and discharge current (or charged particle density), it is possible to self-consistently determine the discharge maintenance field (or the input power) as an *eigenvalue* solution to the problem.

2. Fluid model of a dc-positive column

The transport of charged particles in a non-equilibrium dc-positive column is described here using a fluid approach, by solving hydrodynamic-like equations for electrons and ions (particle continuity and momentum-transfer equations; electron mean energy balance and flux equations), coupled to Poisson's equation for the radial space-charge field. The model applies to an axially infinite cylindrical discharge of radius R, maintained by a constant axial electric field, so that equations become one-dimensional in the radial position r. For simplicity, we consider a plasma with a single type of positive ion and no excited species, thus considering only electron collisions with ground state neutrals.

2.1. The stationary Boltzmann equation

The fluid equations for electrons and ions are derived by calculating the moments of the stationary Boltzmann equation

$$\vec{\nabla}_r \cdot (\vec{v} F_\alpha) + \frac{\partial}{\partial \vec{v}} \cdot \left(\frac{q_\alpha \vec{E}}{m_\alpha} F_\alpha \right) = \left(\frac{\partial F_\alpha}{\partial t} \right)_c . \tag{1}$$

Here, $F_\alpha(r, \vec{v})$ is the distribution function of particles $\alpha = e, i$ (electrons and ions, respectively), with the normalization $\int_{-\infty}^{+\infty} F_\alpha(r, \vec{v}) \mathrm{d}\vec{v} = n_\alpha(r)$, where n_α is the corresponding particle density; $q_\alpha = \pm e$ and m_α are the particle charge and mass, respectively (e is the electron absolute charge); $\vec{E}$ is the total electric field, i.e. $\vec{E}(r) = E_r(r)\vec{e}_r + E_z\vec{e}_z$, where E_z is the axial applied field and E_r is the radial space-charge field and $(\partial F_\alpha/\partial t)_c$ is the time rate of change of F_α due to (elastic and inelastic) collisions. As usual, the symbols $\vec{\nabla}_r$ and $\partial/\partial\vec{v}$ stand for the radial component of the gradient in configuration space and the gradient in velocity space, respectively.

The Boltzmann equation measures the total rate of change of F_α. The terms on its left-hand side account for the variation of F_α in configuration and velocity space, respectively, which equal its variation due to collisions (right-hand side).

The Boltzmann equation for electrons is often written in the framework of the so-called *two-term approximation* [56, 62–64]. The latter involves the development of the electron Boltzmann equation (EBE) in spherical harmonics in velocity space, of which only the first two terms are considered. In general, the two-term approximation is valid when the electron distribution function (EDF) exhibits small anisotropic features, in both configuration and velocity space. Details concerning validity conditions and calculations with this approximation can be found in [56, 62–64], and the reader should refer to these papers for more information.

To write the EBE in the two-term approximation we first develop the EDF in spherical harmonics in velocity space as

$$F_e(r, \vec{v}) \simeq F_e^0(r, v) + (\vec{v}/v) \cdot \vec{F}_e^1(r, v), \tag{2}$$

where F_e^0 and $\vec{F}_e^1$ are, respectively, the isotropic and the anisotropic components of F_e, with $\int_0^\infty F_e^0(r, v) 4\pi v^2 = n_e(r)$.

By substituting equation (2) in the EBE (1) one obtains a development for each of its terms [64]:

$$\vec{\nabla}_r \cdot (\vec{v} F_e) \simeq \frac{v}{3} \vec{\nabla}_r \cdot \vec{F}_e^1 + \vec{v} \cdot \vec{\nabla}_r F_e^0, \tag{3a}$$

$$\frac{\partial}{\partial \vec{v}} \cdot \left(\frac{(-e)\vec{E}}{m_e} F_e \right) \simeq -\frac{1}{3v^2} \frac{\partial}{\partial v} \left[\frac{ev^2}{m_e} \left(\vec{E} \cdot \vec{F}_e^1 \right) \right] - \frac{e\vec{E}}{m_e} \cdot \frac{\vec{v}}{v} \frac{\partial F_e^0}{\partial v}, \tag{3b}$$

$$\left(\frac{\partial F_e}{\partial t} \right)_c \simeq \left(\frac{\partial F_e^0}{\partial t} \right)_{\text{elastic}} + \left(\frac{\partial F_e^0}{\partial t} \right)_{\text{inelastic}} - \nu_c \frac{\vec{v}}{v} \cdot \vec{F}_e^1, \tag{3c}$$

with

$$\left(\frac{\partial F_e^0}{\partial t} \right)_{\text{elastic}} \simeq \frac{m_e}{M} \frac{1}{v^2} \frac{\partial}{\partial v} \left(\nu_c v^3 F_e^0 \right), \tag{3d}$$

$$\left(\frac{\partial F_e^0}{\partial t} \right)_{\text{inelastic}} \simeq (q - \nu_x - \nu_l) F_e^0. \tag{3e}$$

Here, M is the mass of heavy species; ν_c is the electron–neutral momentum-transfer collision frequency; $\nu_x \equiv \sum_j \nu_j$ is the electron–neutral collision frequency for total excitation, where ν_j is the corresponding excitation frequency to level j; ν_l is the electron–neutral collision frequency for ionization and q is an operator representing the re-introduction of electrons in the distribution after inelastic collisions (excitations and ionizations), satisfying

$$\int_0^\infty q F_e^0 4\pi v^2 \mathrm{d}v = n_e \left[\langle \nu_x \rangle + 2\langle \nu_l \rangle \right], \tag{4}$$

where $\langle \cdot \rangle$ represents the average over the isotropic part of the distribution. For example, the average ionization frequency by electron impact is given by

$$\langle \nu_l \rangle(r)\, n_e(r) = \int_0^\infty \nu_l(v)\, F_e^0(r, v) 4\pi v^2 \mathrm{d}v. \tag{5}$$

The factor $2\langle \nu_l \rangle$ on the right-hand side of equation (4) accounts for the new free electron produced in each ionizing collision.

By regrouping the terms with equations (3*a*)–(3*e*), the two-term stationary EBE decouples into a scalar equation in F_e^0 and a vector equation in $\vec{F}_e^1$ as

$$\frac{v}{3} \vec{\nabla}_r \cdot \vec{F}_e^1 - \frac{1}{v^2} \frac{\partial}{\partial v} \left\{ \frac{ev^2}{3m_e} \left(\vec{E} \cdot \vec{F}_e^1 \right) + \frac{m_e}{M} \nu_c v^3 F_e^0 \right\} = (q - \nu_x - \nu_l) F_e^0, \tag{6a}$$

$$\nu_c \vec{F}_e^1 = -v \vec{\nabla}_r F_e^0 + \frac{e}{m_e} \vec{E} \frac{\partial F_e^0}{\partial v}. \tag{6b}$$

The terms on the left-hand side of equation (6*a*) represent the divergence of the electron flux in configuration space (first term) and velocity space (second and third terms, accounting for the fluxes driven by the total electric field and by recoil collisions, respectively). The electron flux in configuration space (cf terms on the right-hand side of equation (6*b*)) is controlled by a diffusion gradient term and an electric drift term, respectively.

2.2. Electron particle transport equations

The electron particle balance equation is obtained by integrating the two-term EBE (6*a*) over velocity space (taking into account equation (4))

$$\vec{\nabla}_r \cdot \int_0^\infty \vec{F}_e^1 \frac{4\pi v^3}{3} \mathrm{d}v = n_e \langle \nu_l \rangle, \tag{7}$$

where the term of divergence in velocity space vanishes, by using Green's theorem. The integral on the left-hand side of equation (7) represents the total electron flux $\vec{\Gamma}$, which can be obtained using equation (6*b*)

$$\Gamma_r \equiv \int_0^\infty F_{e_r}^1 \frac{4\pi v^3}{3} \mathrm{d}v = -\nabla_r (D_e n_e) - \mu_e n_e E_r, \tag{8a}$$

$$\Gamma_z \equiv \int_0^\infty F_{e_z}^1 \frac{4\pi v^3}{3} \mathrm{d}v = -\mu_e n_e E_z, \tag{8b}$$

where Γ_r and Γ_z are the radial and axial components of $\vec{\Gamma}$, i.e. $\vec{\Gamma} = \Gamma_r \vec{e}_r + \Gamma_z \vec{e}_z$. In equations (8*a*), (8*b*), the quantities D_e and μ_e are, respectively, the electron diffusion coefficient and the electron dc mobility, given by

$$D_e(r) n_e(r) \equiv \int_0^\infty \frac{v^2}{3\nu_c(v)} F_e^0(r, v)\, 4\pi v^2 \mathrm{d}v, \tag{9a}$$

$$\mu_e(r) n_e(r) \equiv -\int_0^\infty \frac{ev}{3m_e\nu_c(v)} \frac{\partial F_e^0(r, v)}{\partial v} 4\pi v^2 \mathrm{d}v. \tag{9b}$$

The electron continuity equation can finally be written from equations (7) and (8*a*) as

$$\vec{\nabla}_r \cdot \vec{\Gamma}_r = n_e \langle \nu_l \rangle. \tag{10}$$

In summary, the radial description of the electron transport includes the continuity equation (10) and the momentum-transfer equation (8*a*), whose solution gives the electron density $n_e(r)$ and flux $\Gamma_r(r)$.

2.3. Electron energy transport equations

The electron energy balance equation (per unit volume and per unit time) is obtained by multiplying equation (6*a*) by the electron energy (in eV) $u = m_e v^2/2e$, and then integrating over velocity space

$$-\vec{\nabla}_r \cdot \int_0^\infty \frac{m_e v^2}{2e} \vec{F}_{e_r}^1 \frac{4\pi v^3}{3} \mathrm{d}v - \vec{\Gamma} \cdot \vec{E} - \frac{2m_e}{M} \langle u \nu_c \rangle n_e = \left[\sum_j V_j \langle \nu_j \rangle + V_l \langle \nu_l \rangle \right] n_e, \tag{11}$$

where V_j and V_l are the energies (in eV) for the excitation of level j and for ionization, respectively, and where we have used the definition of $\vec{\Gamma}$ (see equations (8*a*), (8*b*)).

The integral in the first term on the left-hand side of equation (11) represents the electron energy radial flux Γ_ε, which can be obtained using equation (6*a*)

$$\Gamma_\varepsilon \equiv \int_0^\infty \frac{m_e v^2}{2e} F_{e_r}^1 \frac{4\pi v^3}{3} \mathrm{d}v = -\nabla_r (D_\varepsilon n_e \varepsilon) - \mu_\varepsilon n_e \varepsilon E_r, \tag{12}$$

where ε is the electron mean energy defined as

$$n_e(r)\, \varepsilon(r) \equiv \int_0^\infty \frac{m_e v^2}{2e} F_e^0(r, v) 4\pi v^2 \mathrm{d}v, \tag{13}$$

and D_ε and μ_ε are, respectively, the electron diffusion coefficient and mobility for energy transport, given by

$$D_\varepsilon(r) n_e(r)\, \varepsilon(r) \equiv \int_0^\infty \frac{m_e v^2}{2e} \frac{v^2}{3\nu_c(v)} F_e^0(r, v)\, 4\pi v^2 \mathrm{d}v, \tag{14a}$$

$$\mu_\varepsilon(r) n_e(r)\, \varepsilon(r) \equiv -\int_0^\infty \frac{m_e v^2}{2e} \frac{ev}{3m_e\nu_c(v)} \frac{\partial F_e^0(r, v)}{\partial v} 4\pi v^2 \mathrm{d}v. \tag{14b}$$

The latter diffusion coefficient relates to the thermal conductivity following $\lambda_T = (3/2) D_\varepsilon n_e$ (in $\mathrm{cm^{-1}\,s^{-1}}$). In the particular case of a Maxwellian EDF, $D_\varepsilon = (k_B T_e/e)\mu_\varepsilon$ (with $k_B T_e/e = (2/3)\varepsilon$, T_e the electron temperature and k_B the Boltzmann constant); if moreover ν_c is energy independent, the electron coefficients for particle and energy transport satisfy the simple relationship $D_\varepsilon = (5/3) D_e$ and $\mu_\varepsilon = (5/3)\mu_e$.

The energy balance equation can finally be written from equations (8*b*), (11) and (12) as

$$\mu_e E_z^2 n_e - \vec{\nabla}_r \cdot \vec{\Gamma}_\varepsilon = \Gamma_r E_r + \frac{2m_e}{M} \langle u \nu_c \rangle n_e + \left[\sum_j V_j \langle \nu_j \rangle + V_l \langle \nu_l \rangle \right] n_e. \tag{15}$$

The terms on the left-hand side of this equation represent, in order, the power gained by the electrons from the applied field (by collisional Joule heating), and the power transfer due to convection (i.e. the transport of energy due to the transport of particles, which can be either a power gain or loss term); the terms on its right-hand side represent, in order, the power lost by the electrons in flowing against the space-charge field (this power is ultimately carried towards the wall by the ions, while accelerated by E_r), and the power lost in elastic, excitation and ionization electron–neutral collisions.

In summary, the radial description of the electron energy transport includes the balance equation (15) and the flux equation (12), whose solution gives the electron mean energy $\varepsilon(r)$ and energy flux $\Gamma_\varepsilon(r)$.

2.4. Ion particle transport equations

The fluid equations for electrons are derived from the moments of the stationary ion Boltzmann equation (IBE) (1) [55, 56]. Since the non-local transport of energy is essentially controlled by electrons (the ions being assumed thermalized with the background gas, at constant temperature T_g), the model considers only the first two moments of the IBE, corresponding to the ion continuity and momentum-transfer equations.

The ion continuity equation is obtained just by integrating equation (1) over velocity space

$$\vec{\nabla}_r \cdot \int \vec{v} F_i \, \mathrm{d}\vec{v} = \int \left(\frac{\partial F_i}{\partial t}\right)_c , \tag{16}$$

where the term of divergence in velocity space vanishes, by using Green's theorem. The integral on the left-hand side of equation (16) defines the radial component of the ion flux $n_i v_i$ (with v_i the corresponding radial drift velocity), whereas its right-hand side yields the net creation rate of ions per unit volume as a result of collisions, which in this case is represented just by the ionization rate $n_e \langle \nu_I \rangle$. Hence, the ion continuity equation writes

$$\vec{\nabla}_r \cdot (n_i \vec{v}_i) = n_e \langle \nu_I \rangle . \tag{17}$$

The ion momentum-transfer equation is obtained by multiplying equation (1) by $m_i \vec{v}$ and integrating over $\mathrm{d}\vec{v}$

$$m_i \int \vec{v}\, \vec{\nabla}_r \cdot (\vec{v} F_i)\, \mathrm{d}\vec{v} + \int \vec{v} \frac{\partial}{\partial \vec{v}} \cdot \left(e\vec{E} F_i\right) \mathrm{d}\vec{v} = m_i \int \vec{v} \left(\frac{\partial F_i}{\partial t}\right)_c \mathrm{d}\vec{v}. \tag{18}$$

The first term on the left-hand side of equation (18) can be transformed as

$$m_i \int \vec{\nabla}_r \cdot (\vec{v}\vec{v} F_i)\, \mathrm{d}\vec{v} = m_i \vec{\nabla}_r \cdot \int \vec{v}\vec{v} F_i \, \mathrm{d}\vec{v} = m_i \vec{\nabla}_r \cdot (n_i \vec{v}_i \vec{v}_i) + k_B T_g \vec{\nabla}_r n_i , \tag{19}$$

where we have separated $\vec{v}$ into the drift velocity $\vec{v}_i$ and the thermal velocity $\vec{v}_{th_i}$ (i.e. $\vec{v} \equiv \vec{v}_i + \vec{v}_{th_i}$), the latter satisfying an isotropic velocity distribution function at temperature T_g, such that $m_i \langle v_{th_i}^2 \rangle / 2 = (3/2) k_B T_g$. The second term on the left-hand side of equation (18) gives, by Green's theorem,

$$e\vec{E} \int \vec{v} \cdot \frac{\partial F_i}{\partial \vec{v}} \, \mathrm{d}\vec{v} = -e\vec{E} \int F_i \, \mathrm{d}\vec{v} = -e n_i \vec{E}. \tag{20}$$

The right-hand side of equation (18) is the change of momentum due to ion collisions with the background gas (mainly), which we will denote by

$$m_i \int \vec{v} \left(\frac{\partial F_i}{\partial t}\right)_c \mathrm{d}\vec{v} \equiv -\nu_i m_i n_i \vec{v}_i , \tag{21}$$

with ν_i the energy averaged ion–neutral momentum-transfer collision frequency.

The ion momentum-transfer equation can finally be written from equations (19)–(21) (taking $m_i \simeq M$) as

$$\vec{\nabla}_r \cdot (n_i \vec{v}_i \vec{v}_i) = \frac{e}{M} n_i \vec{E} - \frac{k_B T_g}{M} \vec{\nabla}_r n_i - \nu_i n_i \vec{v}_i . \tag{22}$$

Equation (22) can be rewritten by developing its nonlinear inertia term $\vec{\nabla}_r \cdot (n_i \vec{v}_i \vec{v}_i)$ and by using the continuity equation (17), yielding (for its radial component)

$$\left[n_i + \frac{\langle \nu_I \rangle}{\nu_i} n_e\right] v_i + \frac{n_i}{\nu_i} \left(\vec{v}_i \cdot \vec{\nabla}_r\right) v_i = \mu_i u_{k_0} n_i \left[\frac{1}{u_{k_0}} E_r - \tau \frac{\nabla_r n_i}{n_i}\right], \tag{23}$$

where $\mu_i \equiv e/(M\nu_i)$ is the ion mobility and

$$\tau \equiv \frac{k_B T_g}{e u_{k_0}} \tag{24}$$

is the reduced gas temperature, normalized to the value of the electron characteristic energy at the discharge axis $r = 0$, i.e

$$u_{k_0} \equiv u_k(0) \equiv \frac{D_e(0)}{\mu_e(0)}. \tag{25}$$

Notice that if the EDF is a Maxwellian then $D_e = (k_B T_e/e)\mu_e$, in which case u_{k_0} is just the electron temperature (in eV) at the discharge axis.

In summary, the radial description of the ion transport includes the continuity equation (17) and the momentum-transfer equation (23), whose solution gives the ion density $n_i(r)$ and drift velocity $v_i(r)$.

2.5. Ambipolar limit. The Schottky condition

From simulation results (see section 4) it is possible to show that the radial profiles of the charged particle densities, the space-charge field and the electron mean energy exhibit the following features:

$$\nabla_r [\ln n_e(r)] \simeq \nabla_r [\ln n_i(r)] , \tag{26}$$

$$E_r(r) \simeq -u_k(r)\, \nabla_r [\ln n_e(r)] , \tag{27}$$

$$u_k(r) \simeq u_{k_0}. \tag{28}$$

Equation (26) confirms the quasi-neutrality of plasma medium; equation (27) shows that the space-charge field is well represented by its ambipolar expression [7, 65, 66], provided $n_e(r)$ is obtained from the self-consistent solution to the problem and equation (28) comes from the fact that the electron mean energy is almost constant, for the range of pressures considered here. Obviously, such conditions are always violated within the space-charge sheath, where charge separation becomes important (thus yielding an intense space-charge field), and particle densities strongly decrease (thus leading also to a decrease in the electron mean energy). Therefore, conditions (26)–(28) are better satisfied at high pressures and high discharge currents, in which cases the thickness of the space-charge sheath is considerably reduced.

Substituting conditions (26)–(28) in equation (23) yields

$$\left[n_i + \frac{\langle \nu_I \rangle}{\nu_i} n_e\right] v_i + \frac{n_i}{\nu_i} \left(\vec{v}_i \cdot \vec{\nabla}_r\right) v_i \simeq -\mu_i u_{k_0} \frac{n_i}{n_e} (1+\tau)\, \nabla_r n_e . \tag{29}$$

At high pressures, the ion–neutral momentum-transfer collision frequency dominates over the ionization frequency (i.e. $\nu_i \gg \langle \nu_I \rangle$), and the ion drift velocity is almost constant between two successive collisions with neutral species (i.e. $\nabla_r v_i / v_i \ll 1$), in which case it is possible to neglect the second and third terms on the left-hand side of equation (29) to write

$$n_i v_i \simeq -\mu_i u_{k_0} \frac{n_i}{n_e} (1+\tau)\, \nabla_r n_e . \tag{30}$$

Equation (30) can be used to deduce the charge particle flux in the *ambipolar limit* [7, 65, 66], i.e. under the conditions of neutrality and flux conservation

$$n_e = n_i \tag{31}$$

$$\Gamma_r = n_i v_i , \tag{32}$$

which yields (for $\tau \ll 1$)

$$\Gamma_a \simeq -D_a \nabla_r n_e , \tag{33}$$

where Γ_a is the ambipolar flux and D_a is the ambipolar diffusion coefficient defined as

$$D_a \equiv \mu_i u_{k_0}. \tag{34}$$

When expression (33) is used in the continuity equation (10), one obtains the Bessel differential equation

$$\nabla_r^2 n_e + \frac{n_e}{\Lambda^2} = 0 \Longrightarrow n_e(r) = n_e(0)\, J_0(r/\Lambda), \tag{35}$$

where J_0 is the zeroth-order Bessel function, and Λ is the characteristic discharge length given by the Schottky condition [2]

$$\Lambda^2 = \frac{D_a}{\langle \nu_I \rangle}, \tag{36}$$

to be calculated from the boundary condition to the problem.

The classical ambipolar boundary condition corresponds to a zero electron density at discharge wall, i.e.

$$n_e(R) = 0 \Longrightarrow \frac{\Lambda_a}{R} \simeq 0.42, \tag{37}$$

which can be articulated with the Schottky condition (36) to calculate the ionization frequency $\langle \nu_I \rangle$ (or the applied field E_z at given pressure), as an *eigenvalue* solution to the problem.

2.6. Critical point. Cold ion approximation

The ion transport equations introduce a critical velocity in the problem, corresponding to the ion sound velocity

$$v_{i_c} = \left(\frac{k_B T_g}{M}\right)^{1/2} , \tag{38}$$

which can be confirmed by solving equations (17) and (23) with respect to $\nabla_r n_i$ and $\nabla_r v_i$, and then by taking the determinant of this system equal to zero.

The problem has been extensively studied by different authors [13, 67], and it comes to introduce, at critical position r_c where the ion velocity equals the sound velocity (38), an internal boundary condition corresponding to (the subscript c indicates calculations at $r = r_c$)

$$\mu_i n_{i_c}^2 E_{r_c} - n_{i_c} v_{i_c} \left(n_{i_c} + 2\frac{\langle \nu_I \rangle_c}{\nu_i} n_{e_c}\right) = -\frac{n_{i_c} v_{i_c}}{\nu_i} \frac{n_{i_c} v_{i_c}}{r_c}. \tag{39}$$

Notice that the notion of critical position is only relevant from a mathematical standpoint. There is no special physical phenomenon occurring at r_c (besides the fact that $v_i = v_{i_c}$), which by the way justifies removing the singularity introduced by equation (38) using boundary condition (39), so as to ensure a smooth and continuous problem solution.

In general, the critical position is not known *a priori*, which adds some extra difficulties to the numerical solution of the problem. However, the situation can be considerably simplified by neglecting the term associated with the relative gas temperature τ (cf equations (23) and (24)), which corresponds to the so-called *cold ion approximation*. In the particular case of $\tau \to 0$ we have $v_{i_c} \to 0$ and $E_{r_c} \to 0$ (cf equations (38) and (39)), which indicates that the critical position r_c coincides with the discharge axis, thus converting the internal boundary condition (39) into an axis boundary condition for the ion density $n_i(r_c = 0)$. Numerical tests using the complete equation (23) (developing all variables in power series around τ [67]) show that the ion diffusion term has only a little effect on model results, hence justifying the use of the cold ion approximation.

2.7. Poisson's equation

The full description of the electron and ion transport, in a non-equilibrium cylindrical positive column, requires a model formulation covering the region from the discharge axis to the wall, going through the space-charge sheath and monitoring the charge separation within it. The correct way to deal with this problem is to use Poisson's equation [7, 10, 11, 39, 68]

$$\vec{\nabla}_r \cdot \vec{E}_r = \frac{e}{\varepsilon_0} (n_i - n_e) , \tag{40}$$

where ε_0 is the vacuum permittivity.

In this framework, there is no point in separating the *plasma region* from the *sheath region*, since Poisson's equation provides a unified description of the entire discharge. This also avoids the controversial question of determining the sheath thickness, which is ultimately associated with the size of the region exhibiting a more intense charge separation (or space-charge field).

2.8. Boundary conditions

The electron flux equation (8*a*) and continuity equation (10), the electron energy flux equation (12) and balance equation (15), the ion continuity equation (17) and momentum-transfer equation (23) and Poisson's equation (40) constitute a system of seven first-order differential equations, which require seven boundary conditions to be solved.

At the discharge axis ($r = 0$) the set of boundary conditions that respect axis-symmetry is

$$\nabla_r n_e|_0 = 0, \tag{41}$$

$$\nabla_r \varepsilon|_0 = 0, \tag{42}$$

$$E_r(0) = 0. \tag{43}$$

At the discharge wall ($r = R$) the electron particle and energy fluxes are set to verify

$$\Gamma_r(R) = \frac{1}{2} n_e(R)\langle v\rangle(R), \tag{44}$$

$$\Gamma_\varepsilon(R) = \frac{1}{2} n_e(R)\langle uv\rangle(R), \tag{45}$$

where $n_e(R)\langle v\rangle(R)$ and $n_e(R)\langle uv\rangle(R)$ represent, respectively, the average values of v and uv over the isotropic part of the EDF at the wall. Conditions (44) and (45) were obtained for totally absorbing physical boundaries, by imposing that the backward perpendicular fluxes are equal to zero [38, 39, 69]. As an example for the particle flux ($\vec{e}_\perp$ is the outward normal to the wall)

$$\int_{\vec{v}\cdot\vec{e}_\perp<0} F_e(R,\vec{v}) v_r \mathrm{d}\vec{v} = 0 \Longrightarrow$$

$$\int_0^\infty v^2 \mathrm{d}v \int_\pi^{\pi/2} \sin\theta \mathrm{d}\theta\, 2\pi \left[F_e^0(R,v) + F_{e_r}^1(R,v)\cos\theta\right] \times v\cos\theta = 0,$$

or

$$\int_0^\infty F_{e_r}^1(R,v)\frac{4\pi v^3}{3}\mathrm{d}v = -\frac{\int_\pi^{\pi/2}\sin\theta\cos\theta d\theta}{\int_\pi^{\pi/2} 3\sin\theta\cos^2\theta d\theta} \times \int_0^\infty v F_e^0(R,v) 4\pi v^2 \mathrm{d}v,$$

which yields equation (44).

Conditions (44) and (45) can be generalized by introducing a mean (energy independent) reflection coefficient ξ, defined as

$$\xi \equiv \frac{\int_{\vec{v}\cdot\vec{e}_\perp<0} F_e(R,\vec{v}) v_r \mathrm{d}\vec{v}}{\int_{\vec{v}\cdot\vec{e}_\perp>0} F_e(R,\vec{v}) v_r \mathrm{d}\vec{v}}, \tag{46}$$

in which case the electron fluxes at discharge wall become $\Gamma_r(R) = (1-\xi)/(1+\xi)\, n_e(R)\langle v\rangle(R)/2$ and $\Gamma_\varepsilon(R) = (1-\xi)/(1+\xi)\, n_e(R)\langle uv\rangle(R)/2$. As expected, the value of ξ depends on the surface nature and electric condition, ranging from $\xi = 0$ (total absorption) to $\xi = 1$ (total reflection).

The remainder two boundary conditions are associated with the ions. According to the discussion in section 2.6, the reduced ion density at discharge axis can be obtained (in the cold ion approximation) from an asymptotic analysis of the internal boundary condition (39), using $\nabla_r n_i|_0 = E_r(0) = v_i(0) = 0$, which gives an algebraic third-order equation on $n_i(0)$ [13, 67]

$$\frac{e}{\varepsilon_0}\mu_i \frac{n_i^2(0)}{n_e^2(0)}\left[n_i(0) - n_e(0)\right] - \langle\nu_1\rangle(0)\left[\frac{n_i(0)}{n_e(0)} + \frac{3}{2}\frac{\langle\nu_1\rangle(0)}{\nu_i}\right] = 0. \tag{47}$$

Moreover, since the discharge wall is of dielectric nature, the total radial current equals zero at this boundary, which means that

$$\Gamma_r(R) = n_i(R) v_i(R). \tag{48}$$

Also, by subtracting equation (17) from (10) one obtains

$$\vec{\nabla}_r \cdot \left[\vec{\Gamma}_r(r) - n_i(r)\vec{v}_i(r)\right] = 0, \tag{49}$$

which can be combined with condition (48) to give

$$\Gamma_r(r) = n_i(r) v_i(r). \tag{50}$$

2.9. Reduced equations. Eigenvalue solution

Equations (8*a*), (10), (12), (15), (17), (23) and (40) can be written in terms of reduced parameters, calculated with respect to the gas density $N = p/k_B T_g$ (where p is the gas pressure), the electron density at discharge axis $n_{e_0} \equiv n_e(0)$, and the discharge radius R. The resulting equation set writes (developing the differential operator ∇_r and after taking $\tau = 0$)

$$\frac{1}{x}\frac{\mathrm{d}}{\mathrm{d}x}\left[x\frac{\Gamma_r(x)}{n_{e_0}}\right] = NR\, k_1(x) g(x), \tag{51}$$

$$\frac{\Gamma_r(x)}{n_{e_0}} = -\frac{1}{NR}\frac{\mathrm{d}}{\mathrm{d}x}\left[(D_e N)(x)\, g(x)\right] - (\mu_e N)(x)\frac{E_r}{N}(x)\, g(x), \tag{52}$$

$$(\mu_e N)(x)\left(\frac{E_z}{N}\right)^2 g(x) - \frac{1}{NR}\frac{1}{x}\frac{\mathrm{d}}{\mathrm{d}x}\left[x\frac{\Gamma_\varepsilon(x)}{n_{e_0}}\right] = \frac{\Gamma_r(x)}{n_{e_0}}\frac{E_r}{N}(x) + \frac{\theta_{\mathrm{coll}}}{N}(x), \tag{53}$$

$$\frac{\Gamma_\varepsilon(x)}{n_{e_0}} = -\frac{1}{NR}\frac{\mathrm{d}}{\mathrm{d}x}\left[(D_\varepsilon N)(x)\,\varepsilon(x) g(x)\right] - (\mu_\varepsilon N)(x)\frac{E_r}{N}(x)\,\varepsilon(x) g(x), \tag{54}$$

$$\frac{1}{x}\frac{\mathrm{d}}{\mathrm{d}x}\left[x\, t(x) v_i(x)\right] = NR\, k_1(x) g(x), \tag{55}$$

$$\left[t(x) + \frac{k_1(x)}{\nu_i/N} g(x)\right] v_i(x) + \frac{1}{NR}\frac{t(x) v_i(x)}{\nu_i/N}\frac{\mathrm{d}v_i}{\mathrm{d}x} = (\mu_i N)\, t(x)\frac{E_r}{N}(x), \tag{56}$$

$$\frac{1}{x}\frac{\mathrm{d}}{\mathrm{d}x}\left[x\frac{E_r}{N}(x)\right] = \frac{e n_{e_0} R^2}{\varepsilon_0 NR}\left[t(x) - g(x)\right]. \tag{57}$$

Here, $x \equiv r/R$ is the normalized radial position; $g(x) \equiv n_e(x)/n_{e_0}$ and $t(x) \equiv n_i(x)/n_{e_0}$ are the reduced electron and ion densities, respectively; $k_1(x) \equiv (\langle\nu_1\rangle/N)(x)$ is the electron–neutral ionization rate coefficient; and

$$\frac{\theta_{\mathrm{coll}}}{N}(x) \equiv \frac{2m_e}{M}\frac{\langle uv_c\rangle}{N}(x)\, g(x) + \left[\sum_j V_j \frac{\langle\nu_j\rangle}{N}(x) + V_I\frac{\langle\nu_1\rangle}{N}(x)\right] g(x) \tag{58}$$

is the electron power lost (per electron, at unit gas density) in elastic and inelastic collisions with neutral particles.

The inspection of equations (51)–(58) and of boundary conditions (41)–(47) and (50) reveals that the problem solution depends only on the values of three reduced quantities, namely E_z/N, NR and $n_{e_0}R^2$. For example, when using reduced parameters, condition (47) writes $(e/\varepsilon_0)\, n_{e_0} R^2/(NR)\,\mu_i N\, t^2(0)[t(0) - 1] - NR\, k_1(0)[t(0) + (3/2) k_1(0)/(\nu_i/N)] = 0$. Note that the values of the different transport parameters and rate coefficients are to be independently determined, e.g. from the literature or by solving the corresponding Boltzmann equation (see section 3). Further note that the quantity $n_{e_0}R^2$ can be combined with the reduced applied field E_z/N to give the total axial discharge current

$$I_{\mathrm{dc}} = e\int_0^R \mu_e(r) E_z n_e(r)\, 2\pi r \mathrm{d}r = 2\pi e (n_{e_0}R^2)\frac{E_z}{N}\int_0^1 (\mu_e N)(x) g(x)\, x\mathrm{d}x. \tag{59}$$

The problem solution must simultaneously satisfy the particle balance equation (51) and the electron power balance equation (53), that is it must give an ionization rate and a Joule heating rate that exactly compensate for the loss rates of particle and energy to the wall, by strictly satisfying the flux boundary conditions (44)–(45). As in the ambipolar limit (see section 2.5), these conditions yield a relationship between the quantities E_z/N, NR and $n_{e_0}R^2$ (or I_{dc}), to be determined as an *eigenvalue* solution to the problem, for example by obtaining E_z/N as a function of NR and I_{dc}. Figure 1 presents the flowchart of the calculation scheme adopted. The latter determines E_z/N using a two-step procedure, which involves the normalization of the electron mean energy profile to its value $\varepsilon(0)$, at the discharge axis.

In summary, equations (51)–(57), subject to the boundary conditions presented in section 2.8, are solved given NR and I_{dc}, yielding the *eigenvalue* E_z/N and the radial profiles of the reduced charged particle densities $[g(x)$ and $t(x)]$, fluxes $[\Gamma_r(x)/n_{e_0}, t(x)v_i(x)$ and $\Gamma_\varepsilon(x)/n_{e_0}]$, mean energy $\varepsilon(x)$, and space-charge field $(E_r/N)(x)$.

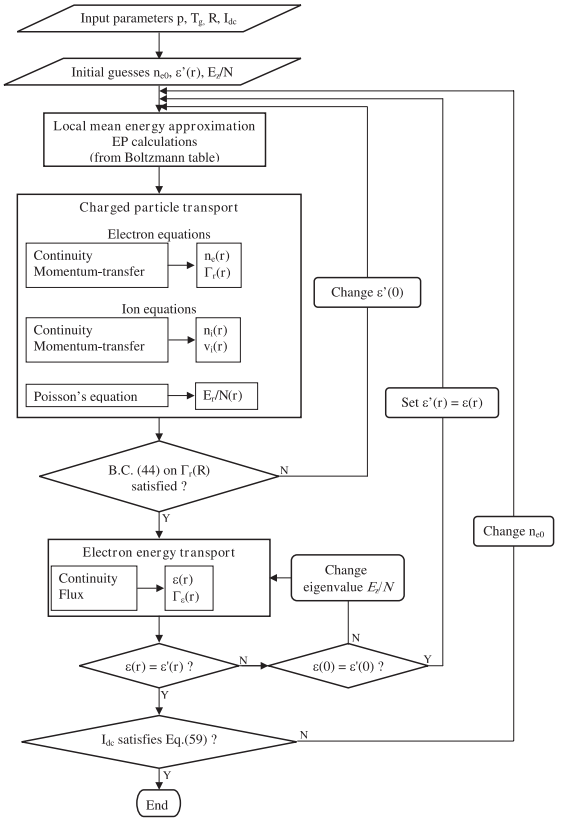

Figure 1. Flowchart of the calculation scheme adopted in the fluid modelling of a dc-positive column.

3. Transport parameters and rate coefficients

Charged particle transport parameters and rate coefficients play a key role in discharge modelling, as they have a direct

influence upon the description of both particle and energy transport. The problem is mainly with the evaluation of the electron parameters (EP) for different positions in space, when adopting a kinetic approach that calculates the EDF from the corresponding Boltzmann equation (see equations (5), (9*a*)–(9*b*), (13)–(14*b*) and (58)). In general, the complex problem of solving the space-dependent EBE is circumvented by adopting the homogeneous (i.e. space-independent) form of its two-term approximation (see equations (6*a*), (6*b*))

$$-\frac{1}{v^2}\frac{\partial}{\partial v}\left[\frac{ev^2}{3m_e}\frac{e}{m_e(\nu_c/N)}\left(\frac{E_z}{N}\right)^2\frac{\partial F_e^0}{\partial v}+\frac{m_e}{M}\frac{\nu_c}{N}v^3F_e^0\right] = \left(\frac{q}{N}-\frac{\nu_x}{N}-\frac{\nu_I}{N}\right)F_e^0, \tag{60}$$

which is used to calculate F_e^0 for different values of the reduced applied field E_z/N. In this case, the spatial dependence of F_e^0 (hence the EP) is accounted for indirectly, by using either the *local field approximation* or the *local mean energy approximation*.

The local field approximation [34, 41, 70, 71] writes the isotropic part of the EDF as the product of the space-dependent electron density, $n_e(r)$, by the so-called electron energy distribution function (EEDF), $f(u)$, whose profile is assumed to depend only on the reduced applied electric field, E_z/N (see equation (60)), i.e.

$$F_e^0(r,u) = n_e(r)\ f(u)|_{(E_z/N)(r)}\,, \tag{61}$$

where we have replaced v by u in the functional dependence of F_e^0. Consequently, equation (60) is solved for $f(u)$, given the (local) value of E_z/N at each position r, and the EP (5), (9*a*), (9*b*), (13)–(14*b*) and (58) become independent of $n_e(r)$, yet keeping a spatial dependence via $f(u)|_{(E_z/N)(r)}$. The local field approximation is valid only at high pressures, when electron collision frequencies are sufficiently high as to justify a local equilibrium between the energy gained by the electrons from the applied field and the energy lost in electron collisions (see equation (15)). Surely, this approximation is not satisfied at low pressures or within discharge sheaths (regardless of the pressure), due to the enhanced anisotropic features then observed.

The local mean energy approximation [39, 41, 53, 72–76] assumes that the spatial dependence of the EEDF is introduced by the electron mean energy $\varepsilon(r)$. In this case, the isotropic part of the EDF writes

$$F_e^0(r,u) = n_e(r)\ f(u)|_{\varepsilon(r)}\,, \tag{62}$$

and the EP (5), (9*a*), (9*b*), (13)–(14*b*) and (58) become spatially resolved via $f(u)|_{\varepsilon(r)}$. This work calculates the EP by adopting the local mean energy approximation as follows: (i) the homogeneous two-term EBE is solved at different electric fields; (ii) the results so obtained are used to construct a table of EP as a function of the electron mean energy $\varepsilon_{\rm Boltz}$ and (iii) the solution to the fluid model yields the spatial distribution of the electron mean energy $\varepsilon(r)$. The latter is used to obtain the spatial profiles of the EP by resorting to the table constructed in (ii).

Concerning the ion transport parameters, we adopt the cold ion approximation (see section 2.6), which comes to say that the ion velocity has only a drift component v_i. For most gases, at moderate v_i values, the ion–neutral momentum-transfer cross-section exhibits a Langevin's profile, being proportional to $1/v_i$. Therefore, the ion momentum-transfer collision frequency (hence, the ion mobility) can be considered as independent of the radial position, and has been taken from the literature.

4. Results and discussion

As an application example, the model is solved for the dc-positive column of cylindrical discharges in helium, for $p \simeq 0.1$–10 Torr, $T_g = 500$ K, $I_{dc} = 50$–200 mA, and $R = 1$ cm. The model adopts the electron cross-section set deduced in [77, 78], which accounts for ground state excitations to all singlet and triplet states up to level $n = 7$, and for ionization. The model uses the He^+ mobility value proposed in [79], $\mu_i N = 3.26 \times 10^{20}$ V^{-1} cm^{-1} s^{-1}. Details about the numerical solution to the model can be found in [53].

Figure 2 shows the *discharge characteristic curves*, corresponding to a plot of E_z/N versus NR, for 50 and 200 mA axial currents. Typically, when NR increases the reduced applied field E_z/N (also termed *reduced maintenance field*) decreases, following the limitation in the electron losses with the discharge. Note that, at high pressures, the discharge characteristics become independent of I_{dc} (or, equivalently, of n_{e_0}, see section 2.9), in agreement with the Schottky condition (36). However, the application of the Schottky condition to model results yields a characteristic length whose value differs from the one predicted by the classical ambipolar

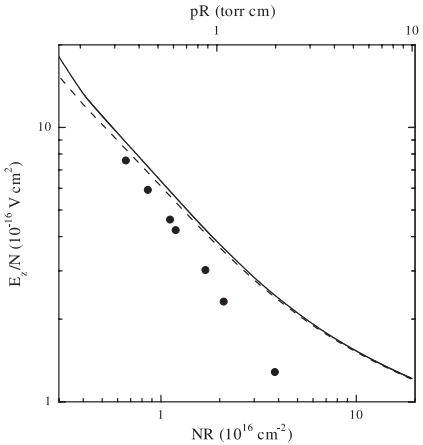

Figure 2. Discharge characteristic curves in helium: axial reduced electric field E_z/N as a function of the product NR (and pR). The curves are calculations for $I_{dc} = 50$ mA (solid line) and 200 mA (dashed). The points are measurements of Kaneda [80] for $I_{dc} = 30$ mA.

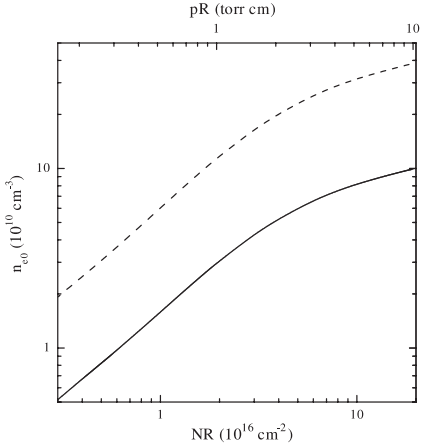

Figure 3. Electron density at discharge axis as a function of NR (and pR), for the same axial currents as in figure 2.

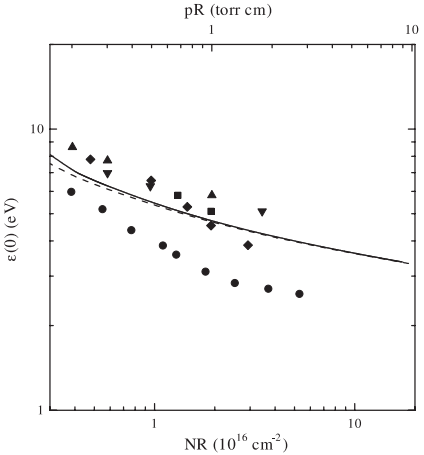

Figure 4. Electron mean energy at discharge axis as a function of NR (and pR). The curves are calculations for the same axial currents as in figure 2, which were divided by a factor of 2 for representation purposes. The points are measurements of Kaneda (circles) [80] (for $I_{dc} = 30$ mA), Karelina (squares) (as reported by Sato [81], and by Dote and Shimada [19]), Klarfeld (up triangles) (as reported by Sato [81], and by Dote and Shimada [19]), Bickerton and von Engel (down triangles) [82] (as reported by Sato [81]), and by Dote and Shimada (diamonds) [19] (as reported by Sato [81]).

theory. For $E_z/N = 1.30 \times 10^{-16}$ V cm^{-2} (corresponding to $NR = 1.93 \times 10^{17}$ cm^{-2}) and $\varepsilon(0) = 6.60$ eV (which gives $k_I \simeq 2.80 \times 10^{-13}$ cm^3 s^{-1} and $u_k \simeq 4.46$ eV), we have $\Lambda = 0.37$ cm (see equations (34) and (36)), in contrast with the typical ambipolar characteristic length $\Lambda_a = 0.42$ cm (for a zero electron density at discharge wall) (see equation (37) at $R = 1$). Figure 2 plots also E_z/N versus NR, as measured by Kaneda [80] at $I_{dc} = 30$ mA. In general, the model seems to overestimate the values of the maintenance field with respect to measurements, particularly at high pressures, which is most probably due to the fact that stepwise excitation and ionization mechanisms were not considered.

The results in figure 2 are connected to those in figure 3, which represents the self-consistent values of the electron density at discharge axis n_{e_0}, as a function of NR, for the axial currents considered. As expected, from equation (59) and figure 2, n_{e_0} increases with NR (at constant I_{dc}) and with I_{dc} (at constant NR or E_z/N).

The conclusions obtained from the analysis of figure 2 are well confirmed by figure 4, which represents calculated and measured values of the electron mean energy at discharge axis $\varepsilon(0)$, as a function of NR, for the same axial currents as in figure 2. In figure 4, and for comparison purposes, the (overestimated) calculated curves were divided by a factor of 2, thus approaching the experimental values reported by Kaneda [80] and by Sato [81]. Note the significant dispersion in the experimental data presented in this figure. As in figure 2, simulations clearly deviate from the measurements of [80] at high pressures, but this trend is not confirmed by the measurements of [81].

An alternative representation for the discharge characteristic curves is shown in figure 5, which plots the plasma wall potential $V(R)$, as a function of NR, for the same axial currents as in figure 2. The decrease in the absolute values

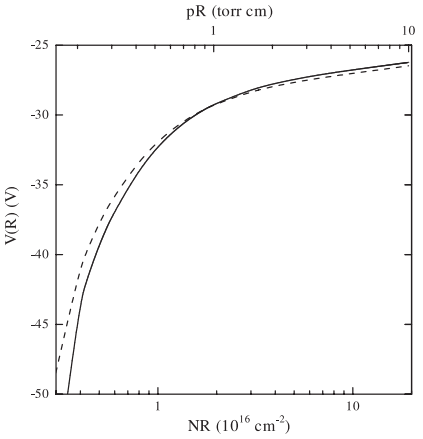

Figure 5. Plasma wall potential as a function of NR (and pR), for the same axial currents as in figure 2.

of $V(R)$, as pressure increases, is associated with a reduction in the thickness of the charge separation region, hence a decrease in the potential drop $|\Delta V_s|$ across the space-charge sheath. From the results of figures 4 and 5 one concludes

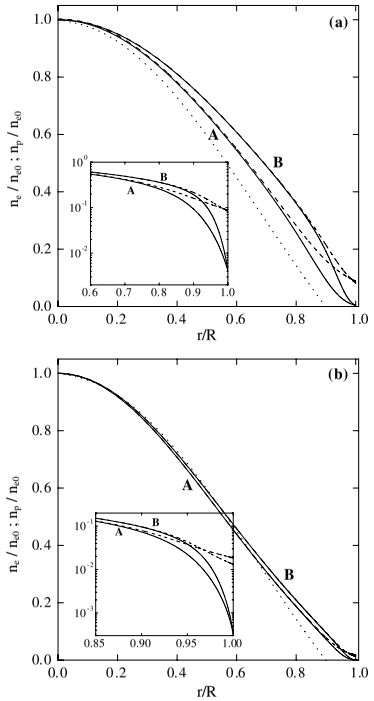

Figure 6. Radial distribution of the reduced charged particle densities, as a function of r/R, for $I_{dc} = 50$ mA (lines A) and 200 mA (B), at $p = 0.3$ Torr (*a*) and 5 Torr (*b*). Solid lines, reduced electron density n_e/n_{e0}; dashed, reduced ion density n_i/n_{e0}; dotted, Bessel's distribution $J_0(r/\Lambda)$, for a characteristic discharge length $\Lambda = 0.37$ cm.

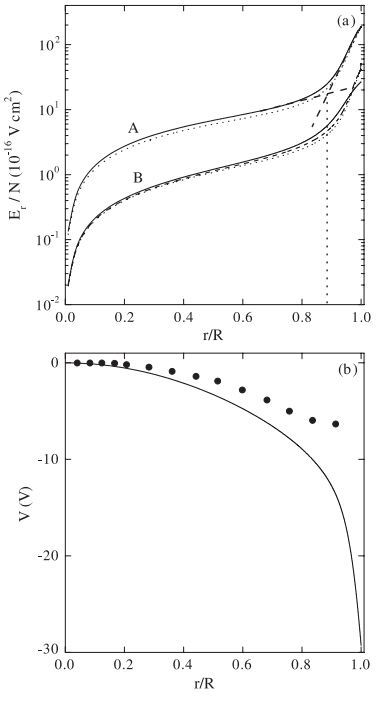

Figure 7. (*a*) Radial profile of the reduced space-charge electric field, as a function of r/R, for the following conditions: A, $p = 0.4$ Torr and $I_{dc} = 150$ mA (both lines); B, $p = 5$ Torr and $I_{dc} = 50$ mA (solid line) or 200 mA (dashed and dotted). The dotted lines were obtained using the ambipolar expression $E_r/N = -(u_k/NR)(\nabla_s n_e/n_e)$. The dashed tangents to solid line A sketch a procedure to roughly locate the plasma-sheath interface. (*b*) Radial profile of the plasma potential, as a function of r/R, for $p = 0.4$ Torr and $I_{dc} = 150$ mA. The curves are calculations and the points are measurements of Kimura *et al* [83].

that $|V(R)| \simeq 3.3\varepsilon(0)$, which agrees with the simple estimation of the potential drop across a Debye sheath [61], $|\Delta V_s| \simeq (\varepsilon/3)\ln(2M/\pi m_e) \simeq 2.8\varepsilon$.

The main differences between low- and high-pressure dc discharges are particularly well featured by plotting the radial profiles of the charged particle densities, as in figures 6(*a*) and 6(*b*) for $p = 0.3$ Torr and 5 Torr, respectively, and for $I_{dc} = 50, 200$ mA. An observation of this figure confirms that, as pressure increases, the space-charge sheath (identified with the region close to the wall where charge separation occurs) becomes thinner (starting around $x \simeq 0.85$ at 0.3 Torr and $x \simeq 0.95$ at 5 Torr, for $I_{dc} = 200$ mA) and sharper (yielding a relative charge separation at the wall of ~ 0.1 at 0.3 Torr, and $\sim 2 \times 10^{-2}$ at 5 Torr). Note that, in the bulk region, the relative profiles of the electron and ion densities are quite similar, as previously expressed in equation (26). For comparison purposes, figures 6(*a*) and 6(*b*) also show the Bessel profile $J_0(r/\Lambda)$ for a characteristic discharge length $\Lambda = 0.37$ cm, obtained by applying the Schottky condition (36) to simulation results. As one could expect, this value of Λ yields a Bessel distribution that reproduces quite well the charged particle density profiles in the discharge bulk, at high pressures (cf equation (35) and figure 6(*b*)). Note that this agreement in the discharge bulk is accompanied by negative values of the Bessel distribution near the wall, which confirms the fact that the sheath region is not correctly described by ambipolar theory. Nevertheless, the reduced space-charge field obtained from simulations is well represented by its ambipolar expression $(E_r/N)(x) = -(u_k(x)/NR)(\mathrm{d}\ln[g(x)]/\mathrm{d}x)$ (provided $g(x)$ is obtained from the self-consistent solution to the problem) (cf equation (27)), as one can see from figure 7(*a*) that plots E_r/N versus r/R for $p = 0.4$ Torr, $I_{dc} = 150$ mA and for $p = 5$ Torr, $I_{dc} = 50, 200$ mA. The results in this figure show also that the reduced space-charge field is less intense for higher

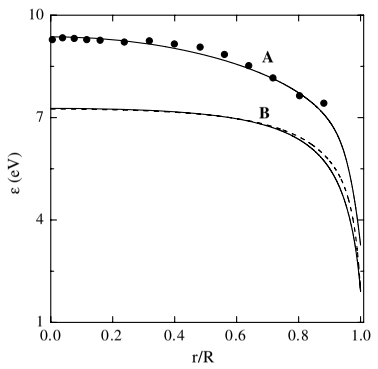

Figure 8. Radial profile of the electron mean energy, as a function of r/R, for the same conditions as in figure 7(*a*). The curves are calculations and the points are measurements of Kimura *et al* [83], which were multiplied by a factor of 1.15 for representation purposes.

pressures, thus for smaller charge separations. Notice that the representation of the space-charge field profile in figure 7(*a*) can be used to roughly locate the plasma-sheath interface, for example by identifying the crossing-point of the tangents to the *plasma* and *sheath* sections of this profile. The procedure is sketched in figure 7(*a*) for the curve at $p = 0.4$ Torr and $I_{dc} = 150$ mA. Figure 7(*b*) represents calculated and measured values of the radial profile of the plasma potential $V(r) = -\int_0^r E(r')\mathrm{d}r'$, obtained for $p = 0.4$ Torr and $I_{dc} = 150$ mA. Notice that the experimental data of Kimura *et al* [83] were obtained by probe measurements, which can explain the observed deviation from simulations near the discharge wall.

Figure 8 shows ε as a function of r/R, for the same conditions as in figure 7(*a*). An observation of this figure reveals that the electron mean energy is practically constant across the discharge bulk (cf equation (28)), although it strongly decreases near the discharge wall following the electron density profile. Notice that the electron energy profile becomes flatter as pressure increases, due to the enhanced influence of collisions in transport. For comparison purposes, figure 8 also plots $\varepsilon(r)$ as measured by Kimura *et al* [83] at $p = 0.4$ Torr and $I_{dc} = 150$ mA; these results were multiplied by a factor of (only) 1.15, and are found to be in good agreement with simulations. As already observed for the discharge characteristic curves, figures 7(*a*) and 8 confirm the independence of simulation results on I_{dc} (or n_{e0}) at high pressures, in agreement with the Schottky condition (36).

The total fractional power transfer, as a function of r/R, is represented in figures 9(*a*) and 9(*b*), at $p = 0.3$ Torr and 5 Torr, respectively, and for $I_{dc} = 50$ mA. The plotted curves correspond to the different power transfer channels considered in equation (15). In this figure, percentages were calculated relative to the total (radially integrated across the discharge) power gained from the applied field. An observation of this figure shows that (i) the power balance is dominated by Joule heating and by collisions all across the discharge, until the edge

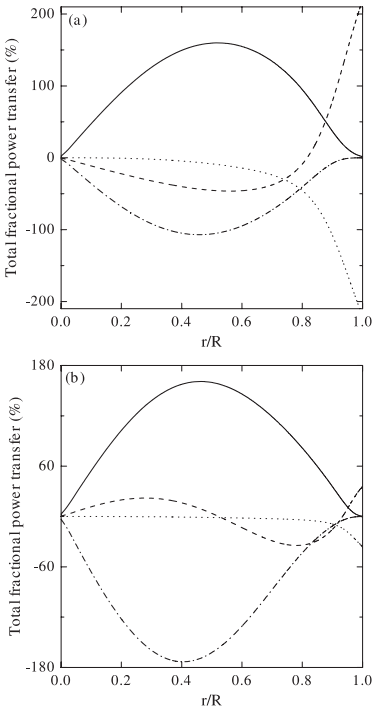

Figure 9. Total fractional power transfer, as a function of r/R, for $I_{dc} = 50$ mA at $p = 0.3$ Torr (*a*) and 5 Torr (*b*). The different curves correspond to the following power transfer channels (cf equations (15), (53) and (58)): Joule heating due to the applied field, $\mu_e E_z^2 n_e$ (solid lines); convection flow, $-\overline{\nabla}_r \cdot \overline{\Gamma}_r$ (dashed); flow against the space-charge field, $\Gamma_r E_r$ (dotted); elastic and inelastic collisions, $\theta_{coll} n_{e0}$ (dashed–dotted). The positive (negative) values indicate an electron power gain (loss). Percentages were calculated relative to the total (radially integrated across the discharge) power gained from the applied field.

of the space-charge sheath region; (ii) within the sheath, the power lost in maintaining the space-charge field is balanced by the power gained from convection, and these are the two dominant power transfer channels in this region. At low pressures, the relative values of these terms are higher, which confirms the development of a more extended space-charge sheath, under these conditions (see also figures 5–7) and (iii) in the discharge bulk (roughly for $x \simeq 0$–0.8), the power lost in flowing against the space-charge field is practically zero, due to its very small intensity therein. Note, finally, that in the discharge bulk, at low pressures, the power transfer due to convection is always negative (corresponding to a power loss mechanism), while at high pressures it can be either positive or negative. This observation is a direct result of collisions, and it can be explained by analysing, in figure 10, the impact

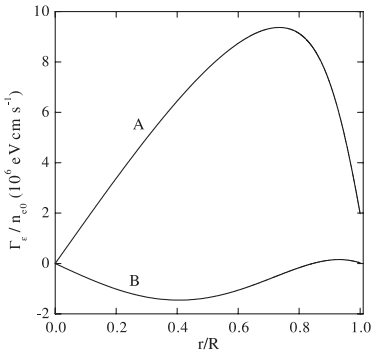

Figure 10. Radial profile of the reduced electron energy flux, as a function of r/R, for $p = 0.3$ Torr (line A) and 5 Torr (B), at $I_{dc} = 50$ mA.

of pressure on the radial profile of the electron energy flux (cf equation (12)). In fact, at low pressures Γ_ε is always positive (thus directed towards the wall), increasing from the discharge axis to the sheath's edge, and decreasing therein. This behaviour is associated with a small collision rate, which allows for a loss of energy due to electron transport across the discharge bulk, and a gain of energy within the sheath due to an enhanced space-charge field confinement. However, at high pressures Γ_ε decreases from zero, for $x \simeq 0$–0.5, thus yielding a gain of energy associated to the convection mechanism, near the discharge axis, as a result of the strong influence of collisions in particle transport.

5. Final remarks

This paper has presented a fluid model describing the transport of charged particles in the non-equilibrium dc-positive column of helium cylindrical discharges. The model includes the continuity and momentum-transfer equations for electrons and ions, coupled with Poisson's equation and the electron mean energy transport equations. The model was solved for pressures $p \simeq 0.1$–10 Torr, gas temperature $T_g = 500$ K, discharge axial currents $I_{dc} = 5$–200 mA and tube radius $R = 1$ cm. We have used an *eigenvalue* formulation to find an univocal solution to the particle and energy balance equations. The model has adopted the *local mean energy approximation* [39,41,53], by computing the electron transport parameters and rate coefficients as a function of the electron mean energy, using the results of a two-term Boltzmann equation solver [77].

Results obtained allowed a systematic study, as a function of pressure and axial current, of the discharge energy deposition features, in association with the analysis of the space-charge sheath formation. At low and intermediate pressures (up to 5 Torr), the presence of an extended collisional space-charge sheath confirms that the correct description of the problem should involve the axis-to-wall integration of Poisson's equation and the electron mean energy transport equations. At high pressures, it was shown that the model reproduces the basic features of *Schottky's ambipolar theory* [2], up to the edge of the very thin space-charge sheath. A general good agreement was found between model results and experimental measurements available in the literature.

The model can be further improved by upgrading the transport equations for electrons and ions. The inclusion of nonlinear inertia terms in the electron particle and energy flux equations (8*a*) and (12) can introduce important corrections in the description of the space-charge sheath region. Moreover, by keeping the diffusion term (proportional to τ) in the ion momentum-transfer equation (23) one can expect some (small) corrections in the description of charged particle transport near the discharge axis. The formulation can also be generalized to a multi-ion component situation, by writing equations (17) and (23) for *each* (positive and negative) ion species, by adding as many axis boundary conditions (47) as different ion species, and by rewriting condition (48) for the conservation of the total radial current at discharge wall as $\sum_i n_i(R)v_i(R) = \Gamma_r(R)$, where the sum on the left-hand side is over the fluxes of all positive ions (the flux of negative ions at discharge wall should satisfy $n_n(R)v_n(R) = 0$ [84]). Finally, the model can be extended to higher pressures ($p > 50$ Torr) by further considering the effects of thermal heating and stepwise ionization, with the consequent decrease in the values of the applied maintenance field.

References

[1] Schottky W 1924 *Phys. Z.* **25** 342
[2] Schottky W 1924 *Phys. Z.* **25** 635
[3] Tonks L and Langmuir I 1929 *Phys. Rev.* **34** 876
[4] Allis W P and Rose D J 1954 *Phys. Rev.* **93** 84
[5] Cobine J D 1958 *Gaseous Conductors* (New York: Dover)
[6] Cohen I M and Kruskal M D 1965 *Phys. Fluids* **8** 920
[7] Self S A and Ewald H N 1966 *Phys. Fluids* **9** 2486
[8] Friedman H W 1967 *Phys. Fluids* **10** 2053
[9] Wilhelm J and Winkler R 1967 *Contrib. Plasma Phys.* **7** 97
[10] Forrest J R and Franklin R N 1968 *J. Phys. D: Appl. Phys.* **1** 1357
[11] Ingold J H 1972 *Phys. Fluids* **15** 75
[12] Tsendin L D 1974 *Sov. Phys.—JETP* **39** 805
[13] Franklin R N 1976 *Plasma Phenomena in Gas Discharges* (Oxford: Clarendon)
[14] Tsendin L D and Golubovskii Yu B 1977 *Sov. Phys. Tech. Phys.* **22** 1066
[15] Ingold J H 1978 *Gaseous Electronics* ed M N Hirsh and H J Oskam (New York: Academic)
[16] Cherrington B E 1979 *IEEE Trans. Electron Devices* **ED-26** 148
[17] Ichikawa Y and Teii S 1980 *J. Phys. D: Appl. Phys.* **13** 2031
[18] Boeuf J P and Marode E 1982 *J. Phys. D: Appl. Phys.* **15** 2169
[19] Dote T and Shimada M 1982 *J. Phys. Soc. Japan* **51** 286
[20] Sommerer T J, Hitchon W N G and Lawler J E 1989 *Phys. Rev.* A **39** 6356
[21] Ingold J H 1989 *Phys. Rev.* A **40** 3855
[22] Raizer Y P 1991 *Gas Discharge Physics* (New York: Springer)
[23] Lister G G 1992 *J. Phys. D: Appl. Phys.* **25** 1649
[24] Hartig M J and Kushner M J 1993 *J. Appl. Phys.* **73** 1080
[25] Kortshagen U 1994 *Phys. Rev.* E **49** 4369
[26] Fiala A, Pitchford L C and Boeuf J P 1994 *Phys. Rev.* E **49** 5607
[27] Parker G J, Hitchon W N G and Lawler J E 1994 *Phys. Rev.* E **50** 3210
[28] Kortshagen U 1995 *Plasma Sources Sci. Technol.* **4** 172
[29] Tsendin L D 1995 *Plasma Sources Sci. Technol.* **4** 200

[30] Busch C and Kortshagen U 1995 *Phys. Rev.* E **51** 280
[31] Bogaerts A, Gijbels R and Goedheer W J 1995 *J. Appl. Phys.* **78** 2233
[32] Uhrlandt D and Winkler R 1996 *J. Phys. D: Appl. Phys.* **29** 115
[33] Uhrlandt D and Winkler R 1996 *Plasma Chem. Plasma Process.* **16** 517
[34] Pfau S, Rohmann J, Uhrlandt D and Winkler R 1996 *Contrib. Plasma Phys.* **36** 449
[35] Kortshagen U, Parker G J and Lawler J E 1996 *Phys. Rev.* E **54** 6746
[36] Behnke J, Golubovskii Yu B, Nisimov S U and Porokhova I A 1996 *Contrib. Plasma Phys.* **36** 75
[37] Behnke J F, Bindemann T, Deutsch H and Becker K 1997 *Contrib. Plasma Phys.* **37** 345
[38] Alves L L, Gousset G and Ferreira C M 1997 *Phys. Rev.* E **55** 890
[39] Ingold J H 1997 *Phys. Rev.* E **56** 5932
[40] Parker G J and Hitchon W N G 1997 *Japan. J. Appl. Phys.* part 1 **36** 4799
[41] Ingold J H 1998 *Electron Kinetics and Applications of Glow Discharges (NATO ASI* vol 369*)* ed U Kortshagen and L D Tsendin (New York: Plenum) p 101
[42] Winkler R and Uhrlandt D 1998 *Electron Kinetics and Applications of Glow Discharges (NATO ASI* vol 369*)* ed U Kortshagen and L D Tsendin (New York: Plenum) p 119
[43] Golubovskii Yu B, Nekuchaev V O and Porokhova I A 1998 *Electron Kinetics and Applications of Glow Discharges (NATO ASI* vol 369*)* ed U Kortshagen and L D Tsendin (New York: Plenum) p 137
[44] Lange H, Leipold F, Otte M, Pfau S and Uhrlandt D 1999 *Plasma Chem. Plasma Process.* **19** 255
[45] Egorov V S, Golubovski Yu B, Kindel E, Mekhov I B and Schimke C 1999 *Phys. Rev.* E **60** 5971
[46] Golubovski Yu B, Porokhova I A, Behnke J and Behnke J F 1999 *J. Phys. D: Appl. Phys.* **32** 456
[47] Lawler J and Kortshagen U 1999 *J. Phys. D: Appl. Phys.* **32** 3188
[48] Richley E A 1999 *Phys. Rev.* E **59** 4533
[49] Uhrlandt D, Schmidt M, Behnke J F and Bindemann T 2000 *J. Phys. D: Appl. Phys.* **33** 2475
[50] Schmidt M, Uhrlandt D and Winkler R 2001 *J. Comput. Phys.* **168** 26
[51] Richley E A 2002 *Phys. Rev.* E **66** 026402
[52] Uhrlandt D and Franke St 2002 *J. Phys. D: Appl. Phys.* **35** 680
[53] Alves L L, Gousset G and Vallée S 2003 *IEEE Trans. Plasma Sci.* **31** 572
[54] Gortchakov S, Lange H and Uhrlandt D 2003 *J. Appl. Phys.* **93** 9508
[55] Golant V E, Zhilinsky A P and Sakharov I E 1980 *Fundamental of Plasma Physics* ed S C Brown (New York: Wiley)
[56] Ferreira C M and Loureiro J 2000 *Plasma Sources Sci. Technol.* **9** 528
[57] Huang K 1963 *Statistical Mechanics* (New York: Wiley)
[58] Balescu R 1975 *Equilibrium and Nonequilibrium Statistical Mechanics* (New York: Wiley)
[59] Chen F F 1984 *Introduction to Plasma Physics and Controlled Fusion* (New York: Plenum)
[60] Goldston R J and Rutherford P H 1995 *Introduction to Plasma Physics* (London: Institute of Physics)
[61] Lieberman M A and Lichtenberg A J 1994 *Principles of Plasma Discharges and Materials Processing* (New York: Wiley)
[62] Allis W P and Brown S C 1952 *Phys. Rev.* **87** 419
[63] Rose D J and Brown S C 1955 *Phys. Rev.* **98** 310
[64] Allis W P 1956 *Handbuck der Physik* vol 21 ed S Flügge (Berlin: Springer) p 383
[65] Muller III C H and Phelps A V 1980 *J. Appl. Phys.* **51** 6141
[66] Ferreira C M and Ricard A 1983 *J. Appl. Phys.* **54** 2261
[67] Valentini H B 1988 *J. Phys. D: Appl. Phys.* **21** 311
[68] Metze A, Ernie D W and Oskam H J 1989 *Phys. Rev.* A **39** 4117
[69] Alves L L, Gousset G and Ferreira C M 1997 *J. Physique IV France* **7-C4** 143
[70] Graves D B and Jensen K F 1986 *IEEE Trans. Plasma Sci.* **PS-14** 78
[71] Boeuf J P 1988 *J. Appl. Phys.* **63** 1342
[72] Meijer P M, Goedheer W J and Passchier J D P 1992 *Phys. Rev.* A **45** 1098
[73] Meyyappan M and Govindan T R 1993 *J. Appl. Phys.* **74** 2250
[74] Nienhuis G J, Goedheer W J, Hamers E A G, van Stark W G J H M and Bezemer J 1997 *J. Appl. Phys.* **82** 2060
[75] Kawamura E and Ingold J H 2001 *J. Phys. D: Appl. Phys.* **34** 3150
[76] Salabas A, Gousset G and Alves L L 2002 *Plasma Sources Sci. Technol.* **11** 448
[77] Alves L L and Ferreira C M 1991 *J. Phys. D: Appl. Phys.* **24** 581
[78] Alves L L, Gousset G and Ferreira C M 1992 *J. Phys. D: Appl. Phys.* **25** 1713
[79] Chanin L M and Biondi M A 1957 *Phys. Rev.* **106** 473
[80] Kaneda T 1979 *J. Phys. D: Appl. Phys.* **12** 61
[81] Sato M 1993 *J. Phys. D: Appl. Phys.* **26** 1687
[82] Bickerton R J and von Engel A 1956 *Proc. Phys. Soc.* B **69** 468
[83] Kimura T, Kano A and Ohe K 1995 *Phys. Plasmas* **2** 4659
[84] Ferreira C M, Gousset G and Touzeau M 1988 *J. Phys. D: Appl. Phys.* **21** 1403

INSTITUTE OF PHYSICS PUBLISHING PLASMA SOURCES SCIENCE AND TECHNOLOGY

Plasma Sources Sci. Technol. **14** (2005) 722–733 doi:10.1088/0963-0252/14/4/011

Solving the Boltzmann equation to obtain electron transport coefficients and rate coefficients for fluid models

G J M Hagelaar and L C Pitchford

Centre de Physique des Plasmas et de leurs Applications de Toulouse,
Université Paul Sabatier, 118 route de Narbonne, 31062 Toulouse Cedex 9, France

Received 13 June 2005
Published 5 October 2005
Online at stacks.iop.org/PSST/14/722

Abstract

Fluid models of gas discharges require the input of transport coefficients and rate coefficients that depend on the electron energy distribution function. Such coefficients are usually calculated from collision cross-section data by solving the electron Boltzmann equation (BE). In this paper we present a new user-friendly BE solver developed especially for this purpose, freely available under the name BOLSIG+, which is more general and easier to use than most other BE solvers available. The solver provides steady-state solutions of the BE for electrons in a uniform electric field, using the classical two-term expansion, and is able to account for different growth models, quasi-stationary and oscillating fields, electron–neutral collisions and electron–electron collisions. We show that for the approximations we use, the BE takes the form of a convection-diffusion continuity-equation with a non-local source term in energy space. To solve this equation we use an exponential scheme commonly used for convection-diffusion problems. The calculated electron transport coefficients and rate coefficients are defined so as to ensure maximum consistency with the fluid equations. We discuss how these coefficients are best used in fluid models and illustrate the influence of some essential parameters and approximations.

1. Introduction

Fluid models of gas discharges describe the transport of electrons, ions and possibly other reactive particle species by the first few moments of the Boltzmann equation (BE): (1) the continuity equation, (2) the momentum equation, usually approximated by the drift-diffusion equation and (3) the energy equation, usually only for electrons. Each of these equations contains transport coefficients or rate coefficients which represent the effect of collisions and which are input data for the fluid model [1–4] (see also references therein).

Transport coefficients and rate coefficients may be rather specific for the discharge conditions. In particular, coefficients concerning electrons depend on the electron energy distribution function (EEDF), which in general is not Maxwellian but varies considerably depending on the conditions. For simple conditions (swarm experiments) and common gases, the electron transport coefficients and rate coefficients have been measured and tabulated as functions of the reduced electric field E/N (ratio of the electric field strength to the gas particle number density) [5].

In general, the EEDF and the electron coefficients for the given discharge conditions can be calculated from the fundamental collision cross-section data by solving the electron BE [6]. A common approach is to solve some approximation of the BE for a series of reduced electric-field values and to put the resulting coefficients in tables versus the reduced field or versus the mean electron energy (disregarding the field values), which are then used in the fluid model to find the transport coefficients and rate coefficients by interpolation. Fluid models without electron energy equation treat the electron coefficients as functions of the local reduced field; models with an electron energy equation treat them as functions of the local mean electron energy.

The BE solvers used to generate the electron-related input data for fluid models are usually based on techniques developed during the 1970s and 1980s, when much work was done on the solution of the BE for the purpose of checking the consistency

between cross-section data and transport coefficients or rate coefficients measured in different experiments [7–16]. These solution techniques originally aimed at simulating specific experiments and calculating the exact physical quantities measured in these experiments with high numerical precision. For fluid discharge modelling, however, one has somewhat different objectives:

(1) the BE solver should work over a large range of discharge conditions (reduced electric field, ionization degree, gas composition, field frequency) rather than simulate a specific experiment;
(2) the calculated transport coefficients and rate coefficients should correspond formally to the same coefficients appearing in the fluid equations (moments of the BE) rather than to quantities measured in experiments; note that the literature gives different definitions of the transport coefficients, some of which are not completely consistent with the fluid equations;
(3) the errors in the calculated transport coefficients and rate coefficients should not limit the accuracy of the fluid model; this is a less strict requirement than the extreme precision (e.g. 0.1% in the drift velocity) needed for the cross-section testing of the 1970s and 1980s;
(4) the BE solver should be fast and reliable without ad hoc calculation parameters to adjust.

There exist several user-friendly BE solvers that are often used and cited by authors in the field of fluid discharge modelling; we mention in particular the commercial ELENDIF [13] and the freeware BOLSIG [17], but there are many others. These solvers however were not designed with the above objectives in mind: they can be applied only for a limited range of discharge conditions, are inconvenient to generate the tables of coefficients or are ill-documented (especially the popular BOLSIG), making it difficult to evaluate the appropriateness of their results for fluid modelling. For years we have felt the need for a new BE solver, able to deal with a larger range of discharge conditions, faster, easier to use and paying more attention to a consistent definition of the calculated coefficients. This is the reason why we have recently developed a new user-friendly BE solver and made it freely available to the discharge modelling community under the name BOLSIG+ [18].

In this paper we document BOLSIG+ in detail. We discuss its physical approximations, numerical techniques, calculated transport coefficients and rate coefficients, and how to use these coefficients in fluid models. In doing so, we provide an extensive discussion on the topic of solving the BE to obtain input data for fluid models. We believe that this is extremely useful: although the techniques used by BOLSIG+ and described in this paper may be well known to BE specialists, developers and users of fluid models are often not aware of them and have little feeling for the precision of the calculated coefficients. The existing literature on BE calculations is so specialized, focusing on specific details, that it is hard to see the consequences for fluid models. This paper looks at the BE from the point of view of a fluid modeller.

2. Boltzmann equation solver

In the following sections we document the physical assumptions and numerical techniques used by our BE solver. We indicate the relation with previous work without trying to be exhaustive; the literature on the electron BE in this context is vast.

The BE for an ensemble of electrons in an ionized gas is

$$\frac{\partial f}{\partial t} + \boldsymbol{v}\cdot\nabla f - \frac{e}{m}\boldsymbol{E}\cdot\nabla_{\boldsymbol{v}} f = C[f], \tag{1}$$

where f is the electron distribution in six-dimensional phase space, $\boldsymbol{v}$ are the velocity coordinates, e is the elementary charge, m is the electron mass, $\boldsymbol{E}$ is the electric field, $\nabla_{\boldsymbol{v}}$ is the velocity-gradient operator and C represents the rate of change in f due to collisions.

To be able to solve the BE, we need to make drastic simplifications. To start with, we limit ourselves to the case where the electric field and the collision probabilities are all spatially uniform, at least on the scale of the collisional mean free path. The electron distribution f is then symmetric in velocity space around the electric field direction. In position space f may vary only along the field direction. Using spherical coordinates in velocity space, we obtain

$$\frac{\partial f}{\partial t} + v\cos\theta\frac{\partial f}{\partial z} - \frac{e}{m}E\left(\cos\theta\frac{\partial f}{\partial v} + \frac{\sin^2\theta}{v}\frac{\partial f}{\partial\cos\theta}\right) = C[f], \tag{2}$$

where v is the magnitude of the velocity, θ is the angle between the velocity and the field direction and z is the position along this direction.

The electron distribution f in equation (2) depends on four coordinates: v, θ, t and z. The next few sections describe how we deal with this. We simplify the θ-dependence by the classical two-term approximation (section 2.1). To simplify the time dependence, we only consider steady-state cases where the electric field and the electron distribution are either stationary or oscillate at high frequency (section 2.3). Additional exponential dependence of f on t or on z is assumed to account for electron production or loss due to ionization and attachment (section 2.2). We then describe the collision term (section 2.4), put all pieces together into one equation for the EEDF (section 2.5), and discuss the numerical techniques we use to solve this equation (section 2.6).

2.1. Two-term approximation

A common approach to solve equation (2) is to expand f in terms of Legendre polynomials of $\cos\theta$ (spherical harmonics expansion) and then construct from equation (2) a set of equations for the expansion coefficients. For high precision results six or more expansion terms are needed [15], but for many cases a two-term approximation already gives useful results. This two-term approximation is often used (e.g. by the BE solvers BOLSIG and ELENDIF) and has been extensively discussed in the literature [19, 20]. Although the approximation is known to fail for high values of E/N when most collisions are inelastic and f becomes strongly anisotropic [21], the errors in the calculated transport coefficients and rate coefficients are acceptable for fluid discharge modelling in the usual range of discharge conditions. Note that when the two-term approximation fails, some other, intrinsic approximations of fluid models also fail.

Using the two-term approximation we expand f as

$$f(v, \cos\theta, z, t) = f_0(v, z, t) + f_1(v, z, t)\cos\theta, \quad (3)$$

where f_0 is the isotropic part of f and f_1 is an anisotropic perturbation. Note that θ is defined with respect to the field direction, so f_1 is negative; this differs from some other texts where θ is defined with respect to the electron drift velocity and f_1 is positive. Also note that f is normalized as

$$\iiint f \,\mathrm{d}^3v = 4\pi \int_0^\infty f_0 v^2 \,\mathrm{d}v = n, \quad (4)$$

where n is the electron number density.

Equations for f_0 and f_1 are found from equation (2) by substituting equation (3), multiplying by the respective Legendre polynomials (1 and $\cos\theta$) and integrating over $\cos\theta$:

$$\frac{\partial f_0}{\partial t} + \frac{\gamma}{3}\varepsilon^{1/2}\frac{\partial f_1}{\partial z} - \frac{\gamma}{3}\varepsilon^{-1/2}\frac{\partial}{\partial \varepsilon}(\varepsilon E f_1) = C_0, \quad (5)$$

$$\frac{\partial f_1}{\partial t} + \gamma\varepsilon^{1/2}\frac{\partial f_0}{\partial z} - E\gamma\varepsilon^{1/2}\frac{\partial f_0}{\partial \varepsilon} = -N\sigma_\mathrm{m}\gamma\varepsilon^{1/2} f_1, \quad (6)$$

where $\gamma = (2e/m)^{1/2}$ is a constant and $\varepsilon = (v/\gamma)^2$ is the electron energy in electronvolts. The right-hand side of equation (5) represents the change in f_0 due to collisions and will be discussed in detail in section 2.4. The right-hand side of equation (6) contains the total momentum-transfer cross-section σ_m consisting of contributions from all possible collision processes k with gas particles:

$$\sigma_\mathrm{m} = \sum_k x_k \sigma_k, \quad (7)$$

where x_k is the mole fraction of the target species of the collision process; realize that the gas can be a mixture of different species, including excited states[1]. For elastic collisions, σ_k is the effective momentum-transfer cross-section, as clearly discussed in [22], accounting for possible anisotropy of the elastic scattering. For inelastic collisions, σ_k is the total cross section, assuming that all momentum is lost in the collision, i.e. that the remaining electron velocity after the collision is scattered isotropically. One needs to be careful about the definition of σ_m: omitting, for example, the contribution from inelastic collisions completely changes the calculation results; some data for σ_m in the literature are unclear on this point.

2.2. Growth of the electron density

We further simplify equations (5) and (6) by making assumptions about the temporal and spatial dependence of f_0 and f_1. In general f cannot be constant in both time and space because some collision processes (ionization, attachment) do not conserve the total number of electrons. Previous work [19, 22–24] proposed a simple technique to approximately describe the effects of net electron production in swarm type experiments. Following this technique, we separate the energy-dependence of f from its dependence on time and space by assuming that

$$f_{0,1}(\varepsilon, z, t) = \frac{1}{2\pi\gamma^3} F_{0,1}(\varepsilon) n(z, t), \quad (8)$$

where the energy distribution $F_{0,1}$ is constant in time and space and normalized by

$$\int_0^\infty \varepsilon^{1/2} F_0 \,\mathrm{d}\varepsilon = 1. \quad (9)$$

The time or space dependence of the electron density n is now related to the net electron production rate. For this, we consider two simple cases corresponding to specific swarm experiments. Most discharges resemble at least one of these cases.

Exponential temporal growth without space dependence. This case corresponds to Pulsed Townsend experiments [11]. The temporal growth rate of the electron number density equals the net production frequency $\bar{\nu}_i$:

$$\frac{1}{n_\mathrm{e}}\frac{\partial n_\mathrm{e}}{\partial t} = \bar{\nu}_i \equiv N\gamma \int_0^\infty \left(\sum_{k=\text{ionization}} x_k\sigma_k - \sum_{k=\text{attachment}} x_k\sigma_k \right) \times \varepsilon F_0 \,\mathrm{d}\varepsilon, \quad (10)$$

where the sum is over the ionization and attachment processes; we remind that x_k is the mole fraction of the target species of collision process k.

Equation (6) becomes

$$F_1 = \frac{E}{N}\frac{1}{\tilde{\sigma}_\mathrm{m}}\frac{\partial F_0}{\partial \varepsilon}, \quad (11)$$

where

$$\tilde{\sigma}_\mathrm{m} = \sigma_\mathrm{m} + \frac{\bar{\nu}_i}{N\gamma\varepsilon^{1/2}}. \quad (12)$$

Substituting this in equation (5), we find

$$-\frac{\gamma}{3}\frac{\partial}{\partial \varepsilon}\left(\left(\frac{E}{N}\right)^2 \frac{\varepsilon}{\tilde{\sigma}_\mathrm{m}}\frac{\partial F_0}{\partial \varepsilon} \right) = \tilde{C}_0 + \tilde{R}, \quad (13)$$

where the collision term

$$\tilde{C}_0 = 2\pi\gamma^3\varepsilon^{1/2}\frac{C_0}{Nn} \quad (14)$$

has been divided by the gas density N and the electron density n with respect to the collision term C_0 in equation (5), which makes it largely independent of these densities[2]. The term

$$\tilde{R} = -\frac{\bar{\nu}_i}{N}\varepsilon^{1/2} F_0 \quad (15)$$

ensures that F_0 remains normalized to unity in the case of net electron production. Previous work [23] interpreted this term as the energy needed to heat the secondary electrons up to the mean electron energy.

[1] The momentum-transfer cross-section σ_m appearing in equation (5) is equivalent to the diffusion cross section discussed in [22]. It can also be identified with the effective momentum-transfer cross-section derived from analysis of swarm experiments, at least at low E/N where ionization can be treated as an excitation process.

[2] Note that $\tilde{C}_0$ and C_0 are physical quantities and not collision operators as used in some other texts.

Exponential spatial growth without time dependence. This case corresponds to Steady State Townsend experiments [11]. While the electrons drift against the electric field their flux and density grow exponentially with a constant spatial growth rate α (Townsend coefficient), which is related to the net electron production by

$$\alpha \equiv -\frac{1}{n}\frac{\partial n}{\partial z} = -\frac{\bar{\nu}_i}{w}, \quad (16)$$

where the mean velocity w is determined by F_1, constant in space and negative.

Using the definition of α, equation (6) becomes

$$F_1 = \frac{1}{\sigma_\mathrm{m}}\left(\frac{E}{N}\frac{\partial F_0}{\partial \varepsilon} + \frac{\alpha}{N}F_0 \right) \quad (17)$$

and equation (5) can again be written in the form

$$-\frac{\gamma}{3}\frac{\partial}{\partial \varepsilon}\left(\left(\frac{E}{N}\right)^2 \frac{\varepsilon}{\tilde{\sigma}_\mathrm{m}}\frac{\partial F_0}{\partial \varepsilon} \right) = \tilde{C}_0 + \tilde{R}, \quad (18)$$

where this time $\tilde{\sigma}_\mathrm{m} = \sigma_\mathrm{m}$ and the growth-renormalization term is

$$\tilde{R} = \frac{\alpha}{N}\frac{\gamma}{3}\left[\frac{\varepsilon}{\sigma_\mathrm{m}}\left(2\frac{E}{N}\frac{\partial F_0}{\partial \varepsilon} + \frac{\alpha}{N}F_0 \right) + \frac{E}{N}F_0\frac{\partial}{\partial \varepsilon}\left(\frac{\varepsilon}{\sigma_\mathrm{m}} \right) \right]. \quad (19)$$

The value of α is found from combining equations (16) and (17):

$$w = \frac{1}{3}\gamma\int_0^\infty F_1 \varepsilon \,\mathrm{d}\varepsilon \equiv -\mu E + \alpha D = -\frac{\bar{\nu}_i}{\alpha}, \quad (20)$$

which yields

$$\alpha = \frac{1}{2D}(\mu E - \sqrt{(\mu E)^2 - 4D\bar{\nu}_i}), \quad (21)$$

where μ and D are written out and identified with the mobility and the diffusion coefficient, respectively, in section 3.1.

2.3. High frequency fields

The quasi-stationary approach of the previous sections assumes that the electric field remains constant on the time scale of the collisions. With some slight modifications, however, the same approach can also be used for high-frequency oscillating fields [19]. Using the complex notation, we express the oscillating electric field as

$$E(t) = E_0 \mathrm{e}^{\mathrm{i}\omega t}. \quad (22)$$

Rather than equation (3), we use the following two-term approximation:

$$f(v, \cos\theta, z, t) = f_0(v, z, t) + f_1(v, z, t)\cos\theta\,\mathrm{e}^{\mathrm{i}\omega t}, \quad (23)$$

where the time-variation of f_0 and f_1 is slow with respect to the oscillation; f_1 may be complex to account for phase shifts with respect to the electric field.

Equation (23) is appropriate if the field frequency is so high that the electron energy lost over one field cycle is small. For elastic collisions this implies that the field frequency should be much greater than the collision frequency times the ratio of the electron mass to the gas particle mass: $\omega/N \gg (2m/M)\sigma_\mathrm{m}\gamma\varepsilon^{1/2}$. A frequency limit related to inelastic collisions is more difficult to estimate. In practice equation (23) is reasonable for field frequencies in the gigahertz range (microwave discharges) and beyond (optical breakdown). For intermediate field frequencies, where the energy transfer per cycle is neither full nor negligible, a more complete solution of the time-dependent BE is necessary [25].

Using equation (23), we proceed exactly as before. Only the temporal growth model makes sense, because the high frequency field does not lead to time-averaged transport, and we find

$$F_1 = \frac{E_0}{N}\frac{\tilde{\sigma}_\mathrm{m} - \mathrm{i}q}{\tilde{\sigma}_\mathrm{m}^2 + q^2}\frac{\partial F_0}{\partial \varepsilon}, \quad (24)$$

where $\tilde{\sigma}_\mathrm{m} = \sigma_\mathrm{m} + \bar{\nu}_i/N\gamma\varepsilon^{1/2}$ and $q = \omega/N\gamma\varepsilon^{1/2}$. Substituting this in the equation for F_0 and averaging the energy absorption over the field cycle, we finally obtain

$$-\frac{\gamma}{3}\frac{\partial}{\partial \varepsilon}\left(\left(\frac{E_0}{N}\right)^2 \frac{\tilde{\sigma}_\mathrm{m}\varepsilon}{2(\tilde{\sigma}_\mathrm{m}^2 + q^2)}\frac{\partial F_0}{\partial \varepsilon} \right) = \tilde{C}_0 + \tilde{R}, \quad (25)$$

where the growth-renormalization term $\tilde{R}$ is given by equation (15).

We remark that in the case of a constant momentum-transfer frequency $\nu = \tilde{\sigma}_\mathrm{m}N\gamma\varepsilon^{1/2}$ (σ_m is inversely proportional to $\varepsilon^{1/2}$), equation (25) can be written exactly as equation (13) for a stationary electric field, where the field E is replaced by an effective field $E_\mathrm{eff} = 2^{-1/2}(1 + \omega^2/\nu^2)^{-1/2}E_0$. This concept of effective field is used by some authors [26] to relate the EEDF and the electron properties in oscillating fields to those in dc fields.

2.4. Collision terms

The right-hand sides of equations (13), (18) and (25) contain the collision term consisting of contributions from all different collision processes k with neutral gas particles and from electron–electron collisions:

$$\tilde{C}_0 = \sum_k \tilde{C}_{0,k} + \tilde{C}_{0,e}. \quad (26)$$

Here we describe these contributions in detail.

Elastic collisions. The effect of elastic collisions can be described by [20]

$$\tilde{C}_{0,k=\text{elastic}} = \gamma x_k \frac{2m}{M_k}\frac{\partial}{\partial \varepsilon}\left[\varepsilon^2\sigma_k\left(F_0 + \frac{k_\mathrm{B}T}{e}\frac{\partial F_0}{\partial \varepsilon} \right) \right], \quad (27)$$

where M_k is the mass of the target particles and T is their temperature. The first term represents the kinetic energy lost to the target particles and the second term is the energy gained from the target particles assuming that these are Maxwellian; this term is important only at very low E/N.

Excitation/de-excitation. Excitation and de-excitation collisions cause a discrete energy loss or gain, continuously removing electrons from the energy distribution and reinserting them somewhere else [19]:

$$\tilde{C}_{0,k=\text{inelastic}} = -\gamma x_k[\varepsilon\sigma_k(\varepsilon)F_0(\varepsilon) - (\varepsilon+u_k)\sigma_k(\varepsilon+u_k)\,F_0(\varepsilon+u_k)], \quad (28)$$

where u_k is the threshold energy of the collision and is negative for de-excitation. The two terms are known, respectively, as the scattering-out and scattering-in terms; the scattering-in term clearly vanishes for $\varepsilon < -u_k$ in the case of de-excitation.

Ionization. The effect of ionization depends on how the remaining energy is shared by the two electrons after ionization. For some gases differential cross sections can be found for the energy sharing, which usually show that the energy is shared less equally as the remaining energy is large [27]. Here we consider only the two limiting cases of equal and zero energy sharing. In the case of equal energy sharing:

$$\tilde{C}_{0,k=\text{ionization}} = -\gamma x_k[\varepsilon\sigma_k(\varepsilon)F_0(\varepsilon) - 2(2\varepsilon+u_k)\sigma_k(2\varepsilon+u_k)F_0(2\varepsilon+u_k)], \quad (29)$$

where the factor 2 in the scattering-in term represents the secondary electrons being inserted at the same energy as the primary electrons. In case the primary electron takes all remaining energy (zero sharing)

$$\tilde{C}_{0,k=\text{ionization}} = -\gamma x_k[\varepsilon\sigma_k(\varepsilon)F_0(\varepsilon) - (\varepsilon+u_k)\sigma_k(\varepsilon+u_k)F_0(\varepsilon+u_k)] + \delta(\varepsilon)\gamma x_k\int_0^\infty u\sigma_k(u)F_0(u)\,\mathrm{d}u, \quad (30)$$

where δ is the Dirac delta-function. The last term denotes the secondary electrons, which are all inserted at zero energy.

Attachment. Attachment simply removes electrons from the energy distribution:

$$\tilde{C}_{0,k=\text{attachment}} = -\gamma x_k\varepsilon\sigma_k(\varepsilon)F_0(\varepsilon). \quad (31)$$

Electron–electron collisions. Previous work [9] gives the following expression for the collision term due to electron–electron collisions, assuming the electron distribution to be isotropic:

$$\tilde{C}_{0,e} = a\frac{n}{N}\left[3\varepsilon^{1/2}F_0^2 + 2\varepsilon^{3/2}\frac{\partial\psi}{\partial\varepsilon}\frac{\partial}{\partial\varepsilon}\left(\varepsilon^{1/2}\frac{\partial F_0}{\partial\varepsilon}\right) + \psi\frac{\partial F_0}{\partial\varepsilon}\right], \quad (32)$$

where

$$\psi = 3A_1 - \frac{A_2}{\varepsilon} + 2\varepsilon^{1/2}A_3, \quad (33)$$

$$A_1 = \int_0^\varepsilon u^{1/2}F_0(u)\,\mathrm{d}u, \quad (34)$$

$$A_2 = \int_0^\varepsilon u^{3/2}F_0(u)\,\mathrm{d}u, \quad (35)$$

$$A_3 = \int_\varepsilon^\infty F_0(u)\,\mathrm{d}u, \quad (36)$$

$$a = \frac{e^2\gamma}{24\pi\varepsilon_0^2}\ln\Lambda, \qquad \Lambda = \frac{12\pi(\varepsilon_0 k_\mathrm{B}T_\mathrm{e})^{3/2}}{e^3 n^{1/2}},$$

$$k_\mathrm{B}T_\mathrm{e} = \frac{2}{3}eA_2(\infty). \quad (37)$$

After some manipulation this becomes:

$$\tilde{C}_{0,e} = a\frac{n}{N}\frac{\partial}{\partial\varepsilon}\left[3A_1F_0 + 2(A_2+\varepsilon^{3/2}A_3)\frac{\partial F_0}{\partial\varepsilon}\right], \quad (38)$$

which expresses the electron–electron collision term as the divergence of the electron flux in energy space. The first term of the flux represents cooling by collisions with colder electrons (A_1 is the fraction of electrons below ε) and the second term is usually heating (diffusion to higher energies). For a Maxwellian distribution function the two terms cancel out, as can be readily seen by substituting $F_0 \propto \exp(-\varepsilon/\tau)$ for arbitrary τ.

2.5. Equation for the EEDF

When combining the previous equations, we find an equation for F_0 that looks like a convection-diffusion continuity-equation in energy space:

$$\frac{\partial}{\partial\varepsilon}\left(\tilde{W}F_0 - \tilde{D}\frac{\partial F_0}{\partial\varepsilon}\right) = \tilde{S}, \quad (39)$$

where

$$\tilde{W} = -\gamma\varepsilon^2\sigma_\varepsilon - 3a\frac{n}{N}A_1, \quad (40)$$

$$\tilde{D} = \frac{\gamma}{3}\left(\frac{E}{N}\right)^2\frac{\varepsilon}{\tilde{\sigma}_\mathrm{m}} + \frac{\gamma k_\mathrm{B}T}{e}\varepsilon^2\sigma_\varepsilon + 2a\frac{n}{N}(A_2+\varepsilon^{3/2}A_3), \quad (41)$$

$$\sigma_\varepsilon = \sum_{k=\text{elastic}}\frac{2m}{M_k}x_k\sigma_k, \quad (42)$$

$$\tilde{S} = \sum_{k=\text{inelastic}}\tilde{C}_{0,k} + G. \quad (43)$$

It is instructive to interpret the left-hand side of equation (39) as the divergence of the electron flux in energy space. This flux then has a convection part with a negative flow velocity $\tilde{W}$, representing cooling by elastic collisions with less energetic particles (neutrals or electrons), and a diffusive part with diffusion coefficient $\tilde{D}$, representing heating by the field and by elastic collisions with more energetic particles. Note that in the case of HF fields the heating term is modified as discussed in section 2.3. Note also that the source term $\tilde{S}$ on the right-hand side of equation (39) has the special property that it is non-local: due to the scattering-in terms it depends on energies elsewhere in energy space. This means that the equation is no ordinary differential equation and solving it requires some special care.

2.6. Numerical solution of the equation

Equation (39) is discretized on a grid in energy space, consisting of a series of subsequent energy intervals, here called grid cells, numbered $i = 1, 2, \ldots$. The subscript i refers to the centre of the grid cell i and the subscript $i+\frac{1}{2}$ to the boundary between the cells i and $i+1$. The energy distribution function F_0 is defined in the cell centres. For each cell i we obtain a linear equation relating the local value $F_{0,i}$ to the values $F_{0,j}$ in the other cells, by integrating the differential equation over the cell:

$$\left[\tilde{W}F_0 - \tilde{D}\frac{\partial F_0}{\partial\varepsilon}\right]_{i+1/2} - \left[\tilde{W}F_0 - \tilde{D}\frac{\partial F_0}{\partial\varepsilon}\right]_{i-1/2} = \int_{\varepsilon_{i-1/2}}^{\varepsilon_{i+1/2}}\tilde{S}\,\mathrm{d}\varepsilon \quad (44)$$

and then discretizing the various terms.

The left-hand side of the equation is discretized by the exponential scheme of Scharfetter and Gummel [28] commonly used for convection-diffusion problems:

$$\left[\tilde{W}F_0 - \tilde{D}\frac{\partial F_0}{\partial\varepsilon}\right]_{i+1/2} = \frac{\tilde{W}_{i+1/2}F_{0,i}}{1-\exp[-z_{i+1/2}]} + \frac{\tilde{W}_{i+1/2}F_{0,i+1}}{1-\exp[z_{i+1/2}]}, \quad (45)$$

where $z_{i+1/2} = \tilde{W}_{i+1/2}(\varepsilon_{i+1}-\varepsilon_i)/\tilde{D}_{i+1/2}$ (Peclet number). This scheme is very accurate when the convection and diffusion terms are about equal, i.e. when inelastic collisions play no important role, and becomes equivalent to a second-order accurate central-difference scheme when the diffusion term is dominant. The electron–electron collision terms in $\tilde{W}$ and $\tilde{D}$ depend on F_0 and require iteration. To speed up convergence these terms are implicitly corrected. In addition, we start the iteration procedure from a Maxwellian distribution function at a temperature deduced from the global energy balance of the electrons.

The inelastic collision terms on the right-hand side are non-local in energy but linear in F_0 and are evaluated fully implicitly, which involves direct inversion of a matrix that is more or less sparse, depending on the different threshold energies of the collisions. We discretize as follows:

$$\int_{\varepsilon_{i-1/2}}^{\varepsilon_{i+1/2}}\tilde{S}\,\mathrm{d}\varepsilon \equiv -P_iF_{0,i} + \sum_j Q_{i,j}F_{0,j}, \quad (46)$$

where the two terms represent scattering-out and scattering-in:

$$P_i = \sum_{\text{inelastic}}\gamma x_k\int_{\varepsilon_{i-1/2}}^{\varepsilon_{i+1/2}}\varepsilon\sigma_k\exp[(\varepsilon_i-\varepsilon)g_i]\,\mathrm{d}\varepsilon, \quad (47)$$

$$Q_{i,j} = \sum_{\text{inelastic}}\gamma x_k\int_{\varepsilon_1}^{\varepsilon_2}\varepsilon\sigma_k\exp[(\varepsilon_j-\varepsilon)g_j]\,\mathrm{d}\varepsilon, \quad (48)$$

where the interval $[\varepsilon_1, \varepsilon_2]$ is the overlap of cell j, and cell i shifted by the threshold energy u_k:

$$\varepsilon_1 = \min(\max(\varepsilon_{i-1/2}+u_k, \varepsilon_{j-1/2}), \varepsilon_{j+1/2}), \quad (49)$$

$$\varepsilon_2 = \min(\max(\varepsilon_{i+1/2}+u_k, \varepsilon_{j-1/2}), \varepsilon_{j+1/2}). \quad (50)$$

The exponential factors in the P- and Q-integrals assume the distribution F_0 to be piecewise exponential, with a (local) logarithmic slope estimated as

$$g_i = \frac{1}{\varepsilon_{i+1}-\varepsilon_{i-1}}\ln\left(\frac{F_{0,i+1}}{F_{0,i-1}}\right). \quad (51)$$

This technique requires iteration but converges extremely rapidly. The P- and Q-integrals are calculated exactly, assuming the cross sections to be linear in between the points specified by the user in a table of cross section versus energy.

For simplicity we have not written out the effects of ionization or attachment in the above equations. In the case of ionization the scattering-in term accounts for the secondary electrons, as discussed before, and in the case of attachment there is no scattering-in. In either case an additional growth-renormalization term is included accounting for temporal or spatial growth, as discussed before. The growth-renormalization term is non-linear in F_0 and also requires iteration. To ensure convergence, however, this term must be linearized and partly evaluated implicitly. We use different ways of linearizing this term depending on the growth type (temporal growth or spatial growth) and on the sign of the net electron production (production or loss). We impose that the term integrated over all energies equals exactly the net production.

We impose the boundary condition that there is no flux in energy space at zero energy. In addition we impose the normalization condition.

3. Coefficients for fluid equations

Although more flexible than BOLSIG and most other solvers, our BE solver only describes the simplest discharge conditions: uniform electric field, uniform or exponentially growing electron density, etc. We now want to use the results from the BE solver to obtain transport coefficients and rate coefficient for fluid models which describe much more general conditions: arbitrarily varying electric fields, electron densities, etc. This implies a generalization of the coefficients as a function of E/N or mean electron energy, which is difficult to justify and should be seen as just an assumption made out of technical necessity. However, if we are careful about the definition of the coefficients, we can ensure that whenever the fluid model is used for the simple conditions assumed by the BE solver, it yields exactly the same mean velocity and mean energy as the solver. We thus obtain maximum consistency between the fluid model and the BE.

In order to find out how best to calculate the transport coefficients and rate coefficients from the energy distribution function F_0, we need to make the link between the two-term formulation of the BE equation, represented by equations (5) and (6), and the fluid equations. In the next few sections we discuss this for common fluid equations and their coefficients.

3.1. Electron transport

The continuity equation for electrons can be obtained from equation (5) by multiplying by $\varepsilon^{1/2}$ and integrating over all energies:

$$\frac{\partial n}{\partial t} + \frac{\partial\Gamma}{\partial z} = S, \quad (52)$$

where S is the net electron source term and the electron flux is

$$\Gamma = nw = n\frac{\gamma}{3}\int_0^\infty\varepsilon F_1\,\mathrm{d}\varepsilon. \quad (53)$$

Combining this with equation (6), we find the well-known drift-diffusion equation

$$\Gamma = -\mu En - \frac{\partial(Dn)}{\partial z}, \quad (54)$$

where the mobility and diffusion coefficient are given by

$$\mu N = -\frac{\gamma}{3}\int_0^\infty\frac{\varepsilon}{\tilde{\sigma}_\mathrm{m}}\frac{\partial F_0}{\partial\varepsilon}\mathrm{d}\varepsilon, \quad (55)$$

$$DN = \frac{\gamma}{3}\int_0^\infty\frac{\varepsilon}{\tilde{\sigma}_\mathrm{m}}F_0\,\mathrm{d}\varepsilon. \quad (56)$$

The effective momentum-transfer cross-section $\tilde{\sigma}_\mathrm{m}$ in these equations includes the effect of possible temporal growth as

given by equation (12). Although the normalized energy distribution F_0 is assumed to be independent of space when solving the BE, the above fluid equations and coefficient definitions are also valid in case the energy distribution is space dependent. The diffusion coefficient in equation (54) then clearly appears inside the divergence and can generally not be put in front of it, as is done in Fick's law.

3.2. Energy transport

Similar to the derivation of the continuity equation in the previous section, the energy equation is obtained from equation (5) by multiplying by $\varepsilon^{3/2}$ and integrating:

$$\frac{\partial n_\varepsilon}{\partial t} + \frac{\partial \Gamma_\varepsilon}{\partial z} + E\Gamma = S_\varepsilon, \tag{57}$$

where the energy density and the energy flux are given by

$$n_\varepsilon = n\int_0^\infty \varepsilon^{3/2} F_0 \,\mathrm{d}\varepsilon \equiv n\bar{\varepsilon}, \tag{58}$$

$$\Gamma_\varepsilon = n\frac{\gamma}{3}\int_0^\infty \varepsilon^2 F_1 \,\mathrm{d}\varepsilon, \tag{59}$$

where $\bar{\varepsilon}$ is the mean electron energy in electronvolts. The last term on the left-hand side of equation (57) represents heating by the electric field; the term S_ε on the right-hand side is the total energy transfer (usually loss) due to collisions. Using equation (6), we can write the energy flux as well in a drift-diffusion form:

$$\Gamma_\varepsilon = -\mu_\varepsilon E n_\varepsilon - \frac{\partial(D_\varepsilon n_\varepsilon)}{\partial z}, \tag{60}$$

where the energy mobility and the energy diffusion coefficient are defined by

$$\mu_\varepsilon N = -\frac{\gamma}{3\bar{\varepsilon}}\int_0^\infty \frac{\varepsilon^2}{\tilde{\sigma}_\mathrm{m}}\frac{\partial F_0}{\partial \varepsilon}\,\mathrm{d}\varepsilon, \tag{61}$$

$$D_\varepsilon N = \frac{\gamma}{3\bar{\varepsilon}}\int_0^\infty \frac{\varepsilon^2}{\tilde{\sigma}_\mathrm{m}} F_0 \,\mathrm{d}\varepsilon. \tag{62}$$

The above formulation of the energy equation is somewhat unusual but we recommend it because of its consistency with the two-term BE. The formulation is basically equivalent to that of Allis [29]; our energy mobility and diffusion coefficient are straightforwardly related to Allis' thermoelectricity β and heat diffusion G as $\mu_\varepsilon = \beta/\bar{\varepsilon}$ and $D_\varepsilon = G/\bar{\varepsilon}$; some other authors using this approach are Ingold [30] and Alves *et al* [31].

Other formulations of the energy equation found in the literature [32] show a separation of the electron energy flux into a convective part proportional to the electron flux and a thermal conduction part proportional to the gradient of the mean electron energy; this however involves additional assumptions and may lead to ambiguity in the definition of the energy transport coefficients (e.g. the thermal conductivity appearing in such energy equations); some further discussion on this issue is given in section 4.5.

Note also that the above formulation of the energy equation is technically convenient because it has exactly the same form as the particle continuity equation and can be solved for n_ε by the same numerical routine. The mean energy is subsequently obtained by dividing, $\bar{\varepsilon} = n_\varepsilon/n$. A semi-implicit technique to avoid numerical instabilities due to the possible energy-dependence of the source term S_ε has previously been developed [33] and proved to work very well.

3.3. Source terms

Various coefficients can be defined for the purpose of calculating the reaction rates appearing in the source terms of fluid equations. Most straightforward is to define rate coefficients (in units of volume per time) as

$$k_k = \gamma\int_0^\infty \varepsilon\sigma_k F_0 \,\mathrm{d}\varepsilon, \tag{63}$$

from which the reaction rate for the collision processes k is obtained by multiplication by the density of the electrons and the target species:

$$R_k = k_k x_k N n. \tag{64}$$

In an alternative approach one can define Townsend coefficients α_k (in units of inverse length) such that

$$R_k = \alpha_k x_k |\Gamma|. \tag{65}$$

For the cases of temporal and spatial growth discussed in section 2.2, these Townsend coefficients are then given by

$$\frac{\alpha_k}{N} = \frac{k_k \alpha}{\bar{\nu}_i} \tag{66}$$

and

$$\frac{\alpha_k}{N} = \frac{k_k}{\mu E}. \tag{67}$$

Using Townsend coefficients, the reaction rates are calculated from the electron flux rather than from the electron density. Clearly this makes no difference for the cases of pure spatial or temporal growth, but in general equations (66) and (67) yield different results. It is recommended to use rate coefficients in situations where the electrons diffuse against the electric force (plasma bulk) and Townsend coefficients in situations where the flux is field driven. The use of Townsend coefficients is especially recommended for modelling the cathode region in dc discharges, where the poor physical reality of the drift-diffusion equation leads to large errors in the electron density but hardly affects the electron flux; models without energy equation may not even have a solution when rate coefficients are used in the cathode fall.

3.4. High frequency momentum equation

Some models of HF discharges use an electron momentum equation of the form

$$\frac{\partial w}{\partial t} + \bar{\nu}_\mathrm{eff} w = -\phi\frac{e}{m}E, \tag{68}$$

where w is the electron drift velocity and $\bar{\nu}_\mathrm{eff}$ is an effective collision frequency. The factor ϕ is usually omitted, but we show here that this factor is needed to be consistent with the BE. According to the two-term approach of section 2.3, and using the complex notation, the electron drift velocity in HF fields is equal to

$$w = \gamma \mathrm{e}^{\mathrm{i}\omega t}\int_0^\infty \varepsilon F_1 \,\mathrm{d}\varepsilon = -\frac{\gamma E}{3N}\int_0^\infty \varepsilon\frac{\tilde{\sigma}_\mathrm{m} - \mathrm{i}q}{\tilde{\sigma}_\mathrm{m}^2 + q^2}\frac{\partial F_0}{\partial \varepsilon}\mathrm{d}\varepsilon$$
$$\equiv -(\mu_r + \mathrm{i}\mu_i)E, \tag{69}$$

which defines a complex electron mobility $\mu = \mu_r + \mathrm{i}\mu_i$. Substituting this in the momentum equation, we find that the coefficients must be calculated as

$$\bar{\nu}_\mathrm{eff} = -\frac{\mu_r}{\mu_i}\omega, \tag{70}$$

$$\phi = -\frac{\mu_r^2 + \mu_i^2}{\mu_i}\frac{m_\mathrm{e}\omega}{e}. \tag{71}$$

The factor ϕ equals unity for a constant momentum-transfer frequency (σ_m inversely proportional to $\varepsilon^{1/2}$) but may be quite different from unity in case the momentum-transfer frequency depends on energy. This has been pointed out previously [34] but is frequently overlooked.

We remark that, strictly speaking, the momentum equation (68) is not very useful to describe the electron motion in a pure harmonic HF field, since the electron drift velocity w can be obtained directly from the complex mobility by equation (69). However, the momentum equation is useful to describe more general cases where the electric field is not purely harmonic, but resembles a harmonic oscillation at a certain frequency.

4. Examples of results

We have extensively tested our BE solver for the gases argon and nitrogen. These are model gases used in many BE calculations described in the literature; we use the cross sections recommended by Phelps [35]. As default options for our calculations we consider the assumptions done by BOLSIG and most other BE solvers available: exponential temporal growth, quasi-stationary electric field, only collisions with ground state gas particles. For these assumptions our calculation results are identical to those obtained with BOLSIG. We consider that this exact agreement obtained using two very different solution techniques validates each. The typical calculation time for one EEDF is on the order of a few tens of milliseconds on a standard 2 GHz PC.

Calculation results for the default options are so well known from previous work that there is no use showing them again in this paper. Instead, we show results for options different from default, not included in BOLSIG and most other solvers. The next few sections illustrate the influence of the growth model (section 4.1), electron–electron collisions (section 4.2), electron collisions with excited neutrals (section 4.3), high frequency field oscillations (section 4.4), and some commonly used assumptions concerning the transport coefficients (section 4.5). Similar results have been presented previously and are known to BE specialists, but often overlooked by developers and users of fluid models. Our aim here is to provide a feeling of how and when the new options of our BE solver should be used and how they might affect the fluid model coefficients. We do not intend to be exhaustive; the presented results are just illustrative examples and more systematic investigation is saved for future work.

4.1. Influence of growth model

When solving the BE one needs to make assumptions on what happens if collision processes (ionization, attachment) do not conserve the total number of electrons. In section 2.2 we discussed two model cases included in our BE solver, where the net production (loss) of electrons leads to exponential temporal growth (decay) and exponential spatial growth (decay) of the electron density. Clearly these are only ideal cases that do not always exactly fit real discharges. Some discharges, such as a fully developed dc glow discharge between parallel plates, closely resemble the case of exponential spatial growth. Other discharge situations, such as the ignition of a dielectric barrier discharge, have features of both spatial and temporal growth. Yet other discharge situations cannot be described by either of the exponential growth models; in a dc positive column, for example, net production is balanced by transverse diffusion loss. There is no growth model that works for all discharges, but we estimate that for many cases the exponential spatial growth model is probably the most realistic. Note however that BOLSIG and most other solvers assume exponential temporal growth.

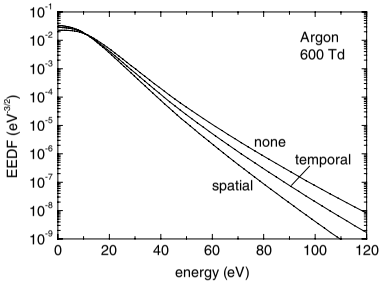

Figure 1. EEDF for 600 Td in argon calculated using the exponential temporal growth model, exponential spatial growth model, and neglecting growth (treating ionization as excitation).

In general the growth effects reduce the mean electron energy (for a given E/N) but have only a minor influence on the shape of the EEDF (for a given mean energy). This is illustrated for argon by figure 1, which compares the EEDFs for the different exponential growth models with the EEDF when growth is neglected, i.e. when ionization is treated as an excitation process and no secondary electrons are inserted. Note that the difference between the two exponential growth models is on the same order as the difference between the temporal growth model and no growth model at all. Figure 2 then shows the influence of the growth effects on the ionization rate coefficient in argon. Although the differences between the curves for the different growth models in figure 2 seem relatively small, our experience is that they can have serious consequences for the fluid simulation results. More systematic investigation on this point is definitely needed but beyond the scope of this paper.

4.2. Influence of electron–electron collisions

Electron–electron collisions cause the EEDF to tend towards a Maxwellian distribution function. The influence of these collisions depends essentially on the ionization degree n/N and is known to become significant for $n/N > 10^{-6}$ in some gases. Note from equation (32) that there is also a

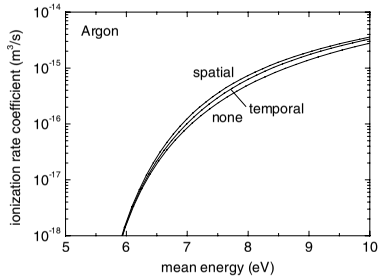

Figure 2. Ionization rate coefficient in argon for different exponential growth models.

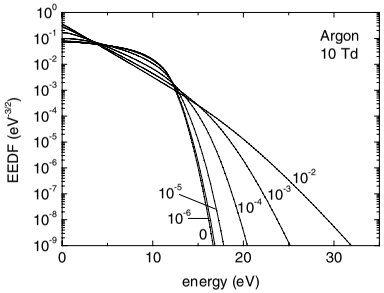

Figure 3. EEDF for 10 Td in argon, taking into account electron–electron collisions, for different ionization degrees.

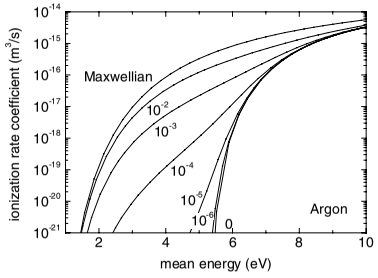

Figure 4. Ionization rate coefficient in argon, taking into account electron-electron collisions, for different ionization degrees and for a Maxwellian EEDF.

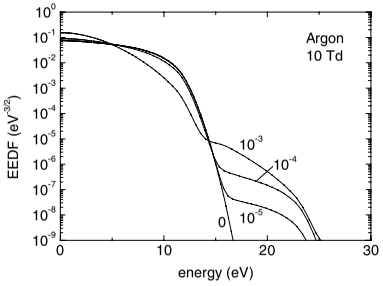

Figure 5. EEDF for 10 Td in argon, taking into account collisions with excited neutrals, for different excitation degrees.

weak dependence on the plasma density which appears in the Coulomb logarithm accounting for the screening of the Coulomb potential by space charge effects. Figure 3 shows the EEDF in argon for different ionization degrees, a plasma density of 10^{18} m^{-3} and a weak reduced electric field of 10 Td. For increasing ionization degree the EEDF resembles more and more a Maxwellian distribution function, i.e. a straight line in the logarithmic plot of figure 3.

These effects are usually neglected in fluid models, but is this justified? The most important consequence of electron–electron collisions for fluid models is that they increase the rate coefficients of inelastic collisions (ionization, excitation) by repopulating the tail of the EEDF. This is illustrated by figure 4 which shows the ionization rate coefficient of ground state argon for different ionization degrees. The inelastic rate coefficients may be strongly increased for ionization degrees of 10^{-5} and higher, but only at low mean electron energy, because the cross-section for electron–electron collisions drops off rapidly with increasing electron energy.

The eventual consequences of this for fluid simulations clearly depend on the discharge conditions. Many discharges have such low ionization degree or such high mean electron energy that it is perfectly justified to neglect the influence of electron–electron collisions. Some discharges, however, operate at precisely those conditions where electron–electron collisions are important; microwave discharges, for example, can have a high ionization degree beyond 10^{-5} and a low electron mean energy of only a few electronvolts. These conditions occur typically in discharges sustained by stepwise ionization and where the EEDF is also influenced by electron collisions with excited neutrals; see section 4.3.

We remark that it may be technically cumbersome to account for the influence of electron–electron collisions in a fluid model: due to these collisions the rate coefficients are functions not only of E/N or the mean energy, but also of the ionization degree n/N; this implies using two-dimensional interpolation tables.

4.3. *Influence of collisions with excited neutrals*

Collisions with excited neutrals may be super-elastic and accelerate electrons immediately into the tail of the EEDF. The influence of this on the EEDF is shown by figure 5 for argon for different excitation degrees (fractional densities of excited neutrals). The results in this figure have been obtained by regrouping all excited argon states in one compound state, for which we estimated an overall super-elastic cross-section by detailed balancing, taking into account only transitions to the ground state.

As with electron–electron collisions, the most important consequence for fluid simulations is an increase of the rate

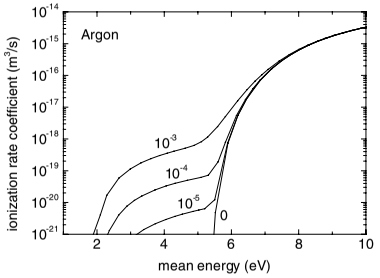

Figure 6. Ionization rate coefficient in argon, taking into account collisions with excited neutrals, for different excitation degrees.

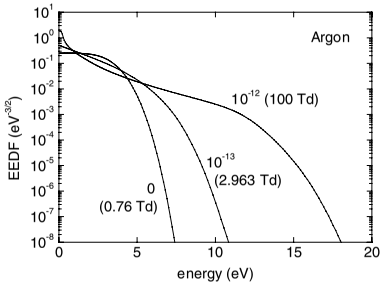

Figure 7. EEDF in argon for oscillating electric fields with different amplitudes and different reduced frequencies ω/N (in units of m^3 s^{-1}), each having the same mean electron energy of 2.150 eV.

coefficients of inelastic collisions at low mean electron energy. Figure 6 shows the ionization rate coefficient of ground state argon. See further our discussion on electron–electron collisions.

4.4. *Influence of high-frequency oscillations*

In HF oscillating fields with a frequency comparable with or greater than the collision frequency, the electron heating is less efficient than in dc fields. As a result, a stronger reduced field is required to achieve the same mean electron energy. In addition the shape of the EEDF may be different (for the same mean energy), because the electron heating depends differently on collisional momentum transfer: in dc fields collisions impede the heating whereas in HF fields they enhance it; compare the electron heating terms in equations (13) and (25). In gases where the momentum-transfer frequency depends strongly on the electron energy, this leads to large differences in the shape of EEDF. This is illustrated by figure 7, which shows the EEDF in argon for the same mean energy and for different reduced field-frequencies ω/N.

Rate coefficients for fluid models of HF discharges (e.g. microwave discharges) need to account for the field-oscillation effects on the shape of the EEDF. Figure 8 shows the ionization rate coefficient of ground state argon as a function of the mean energy for different reduced frequencies. The effects are important mainly at lower mean electron energy (where more electrons see the Ramsauer minimum in the elastic collision cross section) which is exactly where most HF discharges operate. The influence of the oscillations is much less important in gases with a more constant collision frequency, as is illustrated in figure 8 for the case of nitrogen.

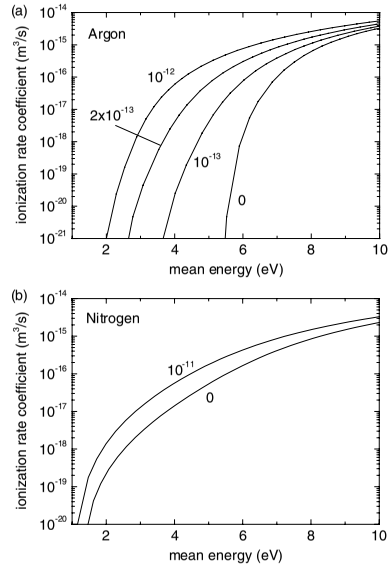

Figure 8. Ionization coefficient in (*a*) argon and (*b*) nitrogen for oscillating electric fields with different reduced frequencies ω/N (in units of m^3 s^{-1}).

When implementing the high-frequency rate coefficients in a fluid model a technical complication can arise when the gas is heated by the discharge such that ω/N is not constant; two-dimensional interpolation tables may then be necessary. We also remark that for some gases and some values of ω/N the mean energy may not be a monotonic function of E/N: there may exist two different EEDFs with the same mean energy, so that it becomes impossible to define rate coefficients or transport coefficients as unique functions of the mean energy. We found this behaviour for argon for a wide range of ω/N (10^{-13}–10^{-11} m^3 s^{-1}) and low mean energies (around 2 eV), but not for nitrogen.

4.5. *Accuracy of some common approximations*

Fluid models often use approximations concerning the transport coefficients, such as the Einstein relation between the diffusion coefficient and the mobility. In this section we check some of these approximations against the results of our BE solver in order to get an idea of their accuracy.

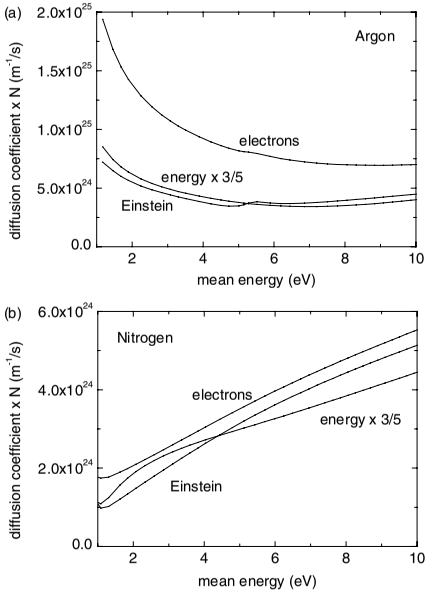

Figure 9. Diffusion coefficients in (*a*) argon and (*b*) nitrogen for electrons and electron energy, calculated precisely and calculated from the Einstein relation.

The commonly used Einstein relation is [36]:

$$D = \tfrac{2}{3}\mu\bar{\varepsilon}, \tag{72}$$

which is exact for a Maxwellian EEDF or a constant momentum-transfer frequency (σ_m inversely proportional to $\varepsilon^{1/2}$) but more or less approximate for real discharge situations. To illustrate the possible errors of the Einstein relation, figure 9 shows the diffusion coefficient in argon and in nitrogen calculated exactly from equation (62) and calculated from the Einstein relation. For argon the Einstein relation is off by a factor 2 due to the strong energy-dependence of the momentum-transfer frequency; for nitrogen the errors are much smaller.

One must realize, however, that the results of our BE solver are approximations as well. For instance, more detailed analysis [37] shows different diffusion coefficients for transport along and perpendicular to the electric field direction, whereas this distinction vanishes with our BE solver based on the two-term expansion. Realize also that for many discharge conditions the drift-diffusion equation itself gives a rather bad description of reality, without this having too serious consequences for the discharge simulation as a whole [38]. In the cathode region of dc discharges the drift-diffusion equation is known to lead to large errors in the electron density without seriously affecting the rest of the discharge; also see our also remarks in section 3.3.

Further common approximations concern the electron energy transport. Many fluid models in the literature use an electron energy equation where (once written as equation (60)) the energy transport coefficients are given by

$$\mu_\varepsilon = \tfrac{5}{3}\mu \qquad \text{and} \qquad D_\varepsilon = \tfrac{5}{3}D. \tag{73}$$

These approximations can be derived by assuming a Maxwellian EEDF, a constant momentum-transfer frequency and constant kinetic pressure [36]. The approximations allow the separation of the energy flux into a part proportional to the electron flux and a part proportional to the gradient of the mean energy, as in classical fluid mechanics:

$$\Gamma_\varepsilon = \tfrac{5}{3}\Gamma\bar{\varepsilon} - \tfrac{5}{3}nD\nabla\bar{\varepsilon}, \tag{74}$$

where the factor in front of the energy gradient is the electron thermal conductivity.

Some authors [29–31] however avoid the approximations given by equation (73) and calculate the energy transport coefficients more precisely as discussed in section 3.2. To illustrate the difference between the approximations and the more precise expressions given by equations (61) and (62), figure 9 also shows the energy diffusion coefficient D_ε calculated from equation (62) and multiplied by 3/5, which (according to equation (73)) is to be compared with the electron diffusion coefficient D. Once again the difference is about a factor 2 for argon and much smaller for nitrogen. For the energy mobility μ_ε the difference is usually much smaller than for D_ε. To our knowledge the consequences of equation (73) for fluid simulations have never been investigated systematically, but one can imagine that for some gases they are quite significant.

5. Conclusions

We have developed a new user-friendly BE solver to calculate the electron transport coefficients and rate coefficients that are input data for fluid models. Our BE solver is called the BOLSIG+ and is available as a freeware [18]. The solver provides steady-state solutions of the BE for electrons in a uniform electric field, using the classical two-term expansion, and is able to account for different growth models, quasi-stationary and oscillating fields, electron–neutral collisions and electron–electron collisions. We show that for the approximations we use, the BE takes the form of a convection-diffusion continuity-equation with a non-local source term. To solve this equation we use an exponential scheme commonly used for convection-diffusion problems. The calculation time for one EEDF is on the order of tens of milliseconds on a standard 2 GHz PC. The calculated electron coefficients are defined so as to ensure maximum consistency with the fluid equations. Special care must be taken of the transport coefficients for electron energy, for which we recommend the formulation proposed previously by Allis [29].

We have illustrated the influence of several non-standard options included in our BE solver, frequently overlooked by users and developers of fluid models. The results from our BE solver show that growth effects significantly reduce the mean electron energy and the ionization rate coefficient; there are also significant differences between the exponential models for temporal and spatial growth. Electron–electron collisions may strongly increase the rate coefficients of

inelastic collisions (excitation, ionization) for low electron mean energies ($\ll$ threshold energy) and ionization degrees of 10^{-5} and higher; these conditions are present in some common gas discharges. A similar increase in the inelastic rate coefficients can be due to super-elastic collisions with excited neutrals for excitation degrees of 10^{-5} and higher. In HF oscillating fields the shape of the EEDF can be strongly modified by oscillation effects, causing large differences in the electron coefficients as a function of mean electron energy with respect to dc fields, especially for gases where the momentum-transfer frequency depends strongly on energy. For such gases also the Einstein relation can be wrong by as much as a factor 2, and special care must be taken about the definition of energy transport coefficients. All results presented here are just illustrative examples; more systematic investigation is necessary to obtain a complete picture of when and how best to use the different options of our BE solver.

References

[1] Ingold J H 1989 *Phys. Rev.* A **40** 3855–63
[2] Graves D B and Jensen K F 1986 *IEEE Trans. Plasma Sci.* **PS-14** 78
[3] Boeuf J-P 1987 *Phys. Rev.* A **36** 2782
[4] Salabas A, Gousset G and Alves L L 2002 *Plasma Sources Sci. Technol.* **11** 448
[5] Dutton J 1975 *J. Phys. Chem. Ref. Data* **4** 577
[6] Frost L S and Phelps A V 1962 *Phys. Rev.* **127** 1621
[7] Wilhelm R and Winkler R 1969 *Ann. Phys.* **23** 28
[8] Winkler R *et al* 1984 *Beitr. Plasmaphys.* **24** 657–74
[9] Rockwood S D 1973 *Phys. Rev.* A **40** 399
[10] Luft P E 1975 *JILA Information Center Report* No. 14 University of Colorado, Boulder
[11] Tagashira H, Sakai Y and Sakamoto S 1977 *J. Phys. D: Appl. Phys.* **10** 1051–63
[12] Morgan W L 1979 *JILA Information Center Report* No. 19 University of Colorado, Boulder
[13] Morgan W L and Penetrante B M 1990 *Comput. Phys. Commun.* **58** 127–52
[14] Lin S L, Robson R E and Mason E A 1979 *J. Chem. Phys.* **71** 3483–98
[15] Pitchford L C, ONeil S V and Rumble J J R 1981 *Phys. Rev.* A **23** 294
[16] Segur P *et al* 1983 *J. Comput. Phys.* **50** 116
[17] BOLSIG 1997 CPAT: http://www.cpat.ups-tlse.fr/operations/operation_03/POSTERS/BOLSIG/index.html
[18] BOLSIG+ 2005 CPAT: http://www.codiciel.fr/plateforme/plasma/bolsig/bolsig.php
[19] Holstein T 1946 *Phys. Rev.* **70** 367
[20] Allis W P 1956 *Handbuch der Physik* ed S Flugge (Berlin: Springer) p 383
[21] Allis W P 1982 *Phys. Rev.* A **26** 1704–12
[22] Phelps A V and Pitchford L C 1985 *Phys. Rev.* A **31** 2932–49
[23] Thomas W R L 1969 *J. Phys. B: At. Mol. Opt. Phys.* **2** 551
[24] Brunet H and Vincent P 1979 *J. Appl. Phys.* **50** 4700
[25] Wilhelm J and Winkler R 1979 *J. Phys.* **40** C7-251
[26] McDonald A D 1953 *Microwave Breakdown in Gases* (London: Oxford University Press)
[27] Opal C B, Peterson W K and Beaty E C 1971 *J. Chem. Phys.* **55** 4100
[28] Scharfetter D L and Gummel H K 1969 *IEEE Trans. Electron. Devices* **16** 64
[29] Allis W P 1967 *Electrons, Ions, and Waves* (Cambridge: MIT Press)
[30] Ingold J H 1997 *Phys. Rev.* E **56** 5932–44
[31] Alves L L, Gousset G and Ferreira C M 1997 *Phys. Rev.* E **55** 890–906
[32] Boeuf J P and Pitchford L C 1995 *Phys. Rev.* E **51** 1376–90
[33] Hagelaar G J M and Kroesen G M W 2000 *J. Comput. Phys.* **159** 1–12
[34] Whitmer R F and Herrmann G F 1966 *Phys. Fluids* **9** 768–73
[35] Phelps A V ftp://jila.colorado.edu/collision_data/.
[36] Bittencourt J A 1986 *Fundamentals of Plasma Physics* (Oxford: Pergamon)
[37] Parker J H and Lowke J J 1969 *Phys. Rev.* **181** 290–301
[38] Hagelaar G J M and Kroesen G M W 2000 *Plasma Sources Sci. Technol.* **9** 605–14

Low Temperature Plasma Physics: Basics and Applications

October 4 – 9, 2014

Electron Kinetics in Atomic and Molecular Plasmas

L.L. Alves
llalves@tecnico.ulisboa.pt

Instituto de Plasmas e Fusão Nuclear

Instituto Superior Técnico, Lisbon, Portugal

Outline

- The particle distribution function
- The Boltzmann equation (kinetic equation for low temperature plasmas)
- The Boltzmann equation for electrons (the small anisotropy approximation)
- Solving the electron Boltzmann equation (difficulties and simplifications)
- The homogeneous electron Boltzmann equation
- Results for argon (atomic gas) - variation with E/N, ω/N and n_e/N
- Results for nitrogen (molecular gas) - influence of the VDF

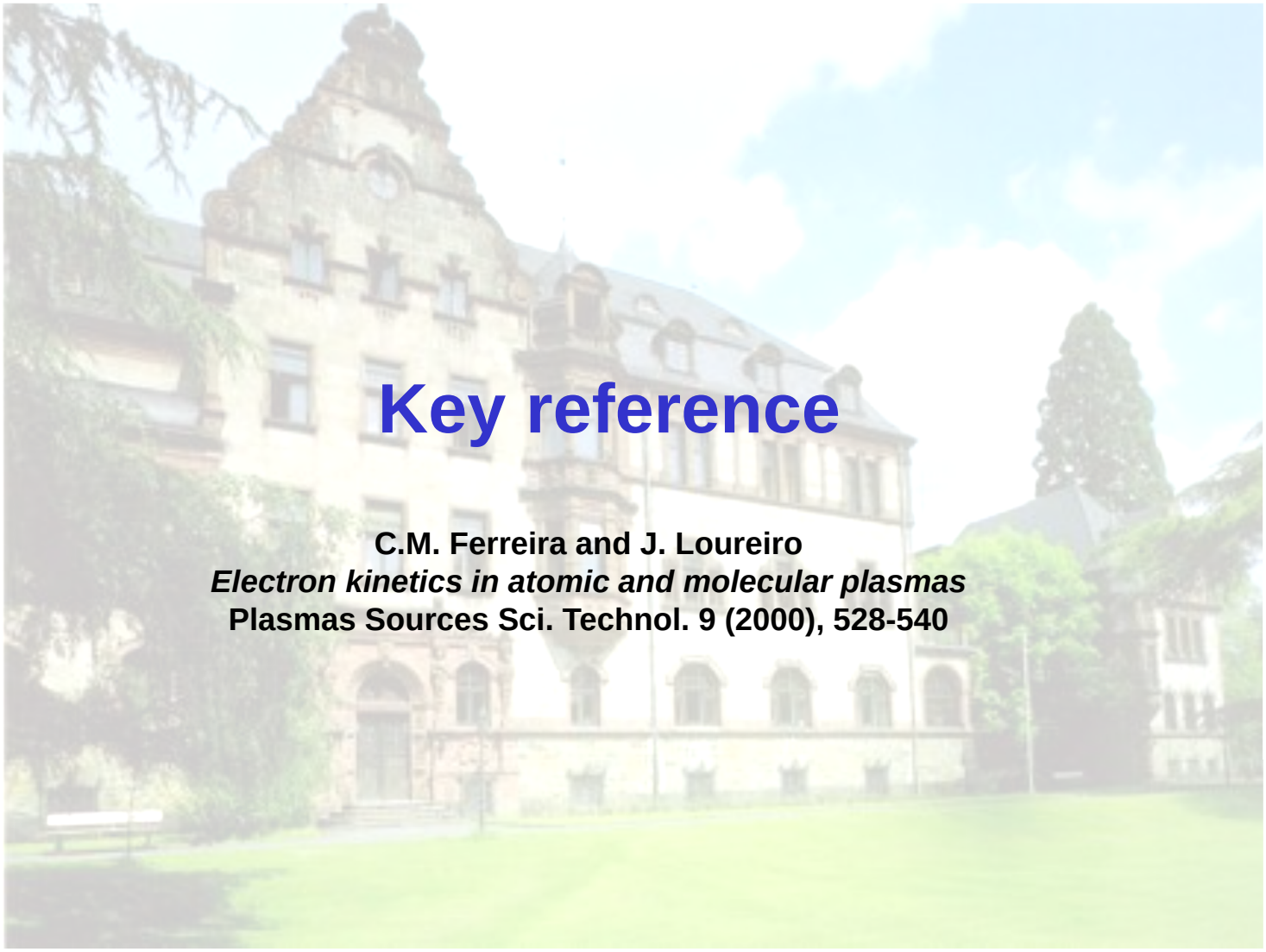

Key reference

C.M. Ferreira and J. Loureiro
Electron kinetics in atomic and molecular plasmas
Plasmas Sources Sci. Technol. 9 (2000), 528-540

Electron kinetics in atomic and molecular plasmas

The particle distribution function

To study the kinetic behavior of particles in a discharge plasma ...

- description in configuration space

  $\vec{r}\,(x, y, z)$

- description in velocity space (in energy space)

  $\vec{v}\,(v_x, v_y, v_z)$

- description in time

  t

Definition of the **PARTICLE DISTRIBUTION FUNCTION**

$$F(\vec{r}, \vec{v}, t)$$

Electron kinetics in atomic and molecular plasmas

The particle distribution function

The **particle distribution function** $F(\mathbf{r}, \mathbf{v}, t)$ represents the number of particles per unit volume of phase space ($\mathbf{r}$, $\mathbf{v}$), at time t.

The number of particles per unit volume of configuration space, at position $\mathbf{r}$ and time t, with velocity components between v_x and $v_x + dv_x$, v_y and $v_y + dv_y$, and v_z and $v_z + dv_z$ is

$$F(x, y, z, v_x, v_y, v_z, t)dv_x dv_y dv_z$$

- Normalization to the density of particles

$$n(\vec{r}, t) = \int_{-\infty}^{\infty} dv_x \int_{-\infty}^{\infty} dv_y \int_{-\infty}^{\infty} dv_z F(\vec{r}, \vec{v}, t) = \int_{-\infty}^{\infty} F(\vec{r}, \vec{v}, t)\, d^3v = \int_{-\infty}^{\infty} F(\vec{r}, \vec{v}, t)\, d\vec{v}$$

- Normalization as a probability

$$F(\vec{r}, \vec{v}, t) = n(\vec{r}, t)\, f(\vec{r}, \vec{v}, t) \qquad \int_{-\infty}^{\infty} f(\vec{r}, \vec{v}, t)\, d\vec{v} = 1$$

Electron kinetics in atomic and molecular plasmas

The particle distribution function

The main problem in kinetic theory …

$$f(\vec{r}, \vec{v}, t) = ?$$

- Thermodynamic equilibrium

$$f(\vec{r}, \vec{v}, t) = f_M(v) = (m/2\pi k_B T)^{3/2}\, exp[-(v_x^2 + v_y^2 + v_z^2)/v_{\rm th}^2]$$

Maxwellian isotropic distribution function

$v_{\rm th} \equiv (2k_B T/m)^{1/2}$ (thermal velocity)

- Non-equilibrium situations

$f(\vec{r}, \vec{v}, t)$ calculated from the solution to a kinetic equation

Electron kinetics in atomic and molecular plasmas

The Boltzmann equation (kinetic equation for low temperature plasmas)

$$\frac{\partial F}{\partial t} + \vec{v}\cdot\vec{\nabla}F + \frac{\vec{X}}{m}\cdot\frac{\partial F}{\partial \vec{v}} = \left(\frac{\partial F}{\partial t}\right)_c$$

Rate of change of *F*

- in time
- in configuration space
- in velocity space
- due to collisions
- Force acting on particles

➢ Gradient in configuration space

$$\vec{\nabla} \equiv \frac{\partial}{\partial x}\vec{e_x} + \frac{\partial}{\partial y}\vec{e_y} + \frac{\partial}{\partial z}\vec{e_z}$$

➢ Gradient in velocity space

$$\frac{\partial}{\partial \vec{v}} \equiv \frac{\partial}{\partial v_x}\vec{e_{v_x}} + \frac{\partial}{\partial v_y}\vec{e_{v_y}} + \frac{\partial}{\partial v_z}\vec{e_{v_z}}$$

Electron kinetics in atomic and molecular plasmas

The Boltzmann equation

$$\frac{\partial F}{\partial t} + \vec{v}\cdot\vec{\nabla}F + \frac{\vec{X}}{m}\cdot\frac{\partial F}{\partial \vec{v}} = \left(\frac{\partial F}{\partial t}\right)_c$$

The convective derivative of *F* (in phase space) ...

$$\frac{dF}{dt}(x,y,z,v_x,v_y,v_z,t) = \frac{\partial F}{\partial t} + \underbrace{\frac{\partial F}{\partial x}\frac{\partial x}{\partial t} + \frac{\partial F}{\partial y}\frac{\partial y}{\partial t} + \frac{\partial F}{\partial z}\frac{\partial z}{\partial t}}_{\vec{v}\cdot\vec{\nabla}F} + \underbrace{\frac{\partial F}{\partial v_x}\frac{\partial v_x}{\partial t} + \frac{\partial F}{\partial v_y}\frac{\partial v_y}{\partial t} + \frac{\partial F}{\partial v_z}\frac{\partial v_z}{\partial t}}_{\frac{d\vec{v}}{dt}\cdot\frac{\partial F}{\partial \vec{v}} = \frac{\vec{X}}{m}\cdot\frac{\partial F}{\partial \vec{v}}}$$

Electron kinetics in atomic and molecular plasmas

The Boltzmann equation

- In the absence of collisions

$$\frac{dF}{dt} = 0$$ The density of particles in phase space is constant in time

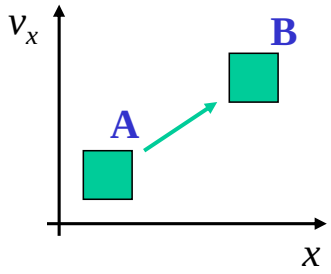

- In the presence of collisions

$$\frac{dF}{dt} = \left(\frac{\partial F}{\partial t}\right)_c$$ (scattering; production of new particles)

Electron kinetics in atomic and molecular plasmas

The Boltzmann equation for electrons

Working conditions ...

- The total electric field acting on electrons has the form

$$\vec{E} = \vec{E}_s(\vec{r}) + \vec{E}_p \exp(j\omega t)$$

dc space-charge field hf field at frequency ω

- No external magnetic field
- The electron distribution function F is expanded

  in spherical harmonics in velocity space

  in Fourier series in time

$$F = \sum_l \sum_p F_p^l P_l(\cos\theta) \exp(jp\omega t)$$

Electron kinetics in atomic and molecular plasmas

The Boltzmann equation for electrons

The small anisotropy approximation ...

- the electron mean free path is much smaller than any relevant dimension of the container, $\lambda_e \ll L$
- the energy gained from the electric field per collision by a representative electron is much smaller than the thermal energy of the electrons
- the oscillation amplitude of the electron motion under the action of the hf field is small as compared to L
- the characteristic frequency for the electron energy relaxation by collisions is much smaller than the oscillation frequency of the hf field, $\tau_e^{-1} \ll \omega$

$$F(\vec{r},v) \simeq F_0^0(\vec{r},v) + (\vec{v}/v)\cdot\left[\vec{F}_0^1(\vec{r},v) + \vec{F}_1^1(\vec{r},v)\exp(j\omega t)\right]$$

Isotropic component (energy relaxation)

Anisotropic components (transport)

Electron kinetics in atomic and molecular plasmas

The Boltzmann equation for electrons

The two-term expansion ...

- The isotropic equation

$$\frac{v}{3}\vec{\nabla}\cdot\vec{F}_0^1 - \frac{1}{v^2}\frac{\partial}{\partial v}\left\{\left(\frac{ev^2}{6m}\right)\left[Re\left(\vec{E}_p\cdot\vec{F}_1^1\right) + 2\vec{E}_s\cdot\vec{F}_0^1\right] + \frac{m}{M}\nu_c v^3 F_0^0\right\} = (q-\nu_x-\nu_i)F_0^0$$

elastic collision operator

inelastic collision operator

- The anisotropic equations

$$\nu_c\vec{F}_0^1 = -v\vec{\nabla}F_0^0 + \frac{e}{m}\vec{E}_s\frac{\partial F_0^0}{\partial v} \quad > 0$$

$$(\nu_c + j\omega)\vec{F}_1^1 = \frac{e\vec{E}_p}{m}\frac{\partial F_0^0}{\partial v} \quad < 0$$

Electron kinetics in atomic and molecular plasmas

The Boltzmann equation for electrons

The inelastic collision operator ...

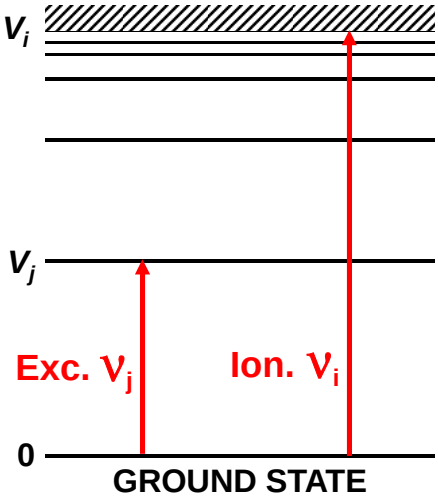

$$qF_0^0 - (\nu_x + \nu_i) F_0^0$$

Entrance Exit

$$\nu_x = \sum_j \nu_j$$

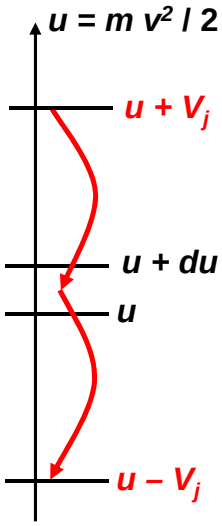

$$\int qF_0^0 d^3v = n\left(\langle\nu_x\rangle + 2\langle\nu_i\rangle\right)$$

Electron kinetics in atomic and molecular plasmas

Solving the electron Boltzmann equation

Difficulties ...

- Crossed space and velocity terms involving $\boldsymbol{E}_s(r)$ $\Rightarrow$ $F_0^0(\vec{r},v) \neq n(\vec{r}) f_0(v)$
- Self-consistent calculation of $\boldsymbol{E}_s(r)$ involves coupling to ion kinetics

$$\frac{v}{3}\vec{\nabla}\cdot\vec{F}_0^1 - \frac{1}{v^2}\frac{\partial}{\partial v}\left\{\left(\frac{ev^2}{6m}\right)\left[Re\left(\vec{E}_p\cdot\vec{F}_1^1\right) + 2\vec{E}_s\cdot\vec{F}_0^1\right] + \frac{m}{M}\nu_c v^3 F_0^0\right\} = (q - \nu_x - \nu_i) F_0^0$$

$$\nu_c\vec{F}_0^1 = -v\vec{\nabla}F_0^0 + \frac{e}{m}\vec{E}_s\frac{\partial F_0^0}{\partial v}$$

$$(\nu_c + j\omega)\vec{F}_1^1 = \frac{e\vec{E}_p}{m}\frac{\partial F_0^0}{\partial v}$$

Electron kinetics in atomic and molecular plasmas

Solving the electron Boltzmann equation

Space-charge separation ...

$$\cancel{\frac{v}{3}\vec{\nabla}\cdot\vec{F}_0^1} - \frac{1}{v^2}\frac{\partial}{\partial v}\left\{\left(\frac{ev^2}{6m}\right)\left[Re\left(\vec{E}_p\cdot\vec{F}_1^1\right)+\cancel{2\vec{E}_s\cdot\vec{F}_0^1}\right]+\frac{m}{M}\nu_c v^3 F_0^0\right\}$$

$$= \left(q-\nu_x-\nu_i\right)F_0^0$$

$$\cancel{\nu_c\vec{F}_0^1 = -v\vec{\nabla}F_0^0 + \frac{e}{m}\vec{E}_s\frac{\partial F_0^0}{\partial v}}$$

$$(\nu_c + j\omega)\vec{F}_1^1 = \frac{e\vec{E}_p}{m}\frac{\partial F_0^0}{\partial v}$$

OK at high pressures

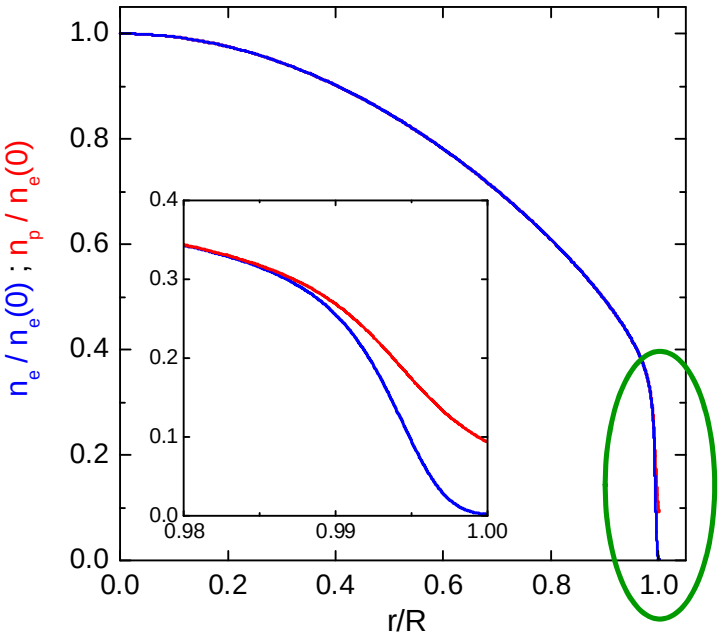

Electron kinetics in atomic and molecular plasmas

Solving the electron Boltzmann equation

$$-\frac{1}{v^2}\frac{\partial}{\partial v}\left\{\left(\frac{ev^2}{6m}\right)Re\left(\vec{E}_p\cdot\vec{F}_1^1\right)+\frac{m}{M}\nu_c v^3 F_0^0\right\} = \left(q-\nu_x-\nu_i\right)F_0^0$$

$$(\nu_c + j\omega)\vec{F}_1^1 = \frac{e\vec{E}_p}{m}\frac{\partial F_0^0}{\partial v}$$

$$\int qF_0^0 d^3v = n\left(\langle\nu_x\rangle + \langle\nu_i\rangle\right)$$

Ionization is treated like an ordinary excitation mechanism

Electron kinetics in atomic and molecular plasmas

The homogeneous electron Boltzmann equation

$$\frac{dG(u)}{du} = [q(u) - \nu_x(u) - \nu_i(u)]\, f(u)\sqrt{u}$$

$$G(u) = G_E(u) + G_c(u)$$ The total upflux in energy space

$$G_E(u) = -\frac{2}{3}u^{3/2}\nu_c(u)u_c(u)\frac{df(u)}{du}$$ The applied field energy gain

$$G_c(u) = -\frac{2}{3}u^{3/2}\nu_c(u)\frac{3m}{M}f(u)$$ The elastic collision energy losses

- The electron energy distribution function

$$f(u)\sqrt{u}du = \frac{F_0^0(\vec{r},v)4\pi v^2 dv}{n(\vec{r})} \Longrightarrow \int_0^\infty f(u)\sqrt{u}du = 1$$

- The time-average energy gained from the hf field per collision

$$u_c(u) = \frac{(eE_p)^2}{2m\left(\nu_c^2 + \omega^2\right)}$$

Electron kinetics in atomic and molecular plasmas

The homogeneous electron Boltzmann equation

$$\frac{dG(u)}{du} = [q(u) - \nu_x(u) - \nu_i(u)]\, f(u)\sqrt{u}$$ **The collision operator…**

$$= \sum_{i,j}\left[(u+V_{ij})^{1/2} f(u+V_{ij})\nu_{ij}(u+V_{ij}) - u^{1/2} f(u)\nu_{ij}(u)\right]$$

$$\sum_{j,i}\left[(u-V_{ij})^{1/2} f(u-V_{ij})\nu_{ji}(u-V_{ij}) - u^{1/2} f(u)\nu_{ji}(u)\right]$$

ENTRANCE

EXIT

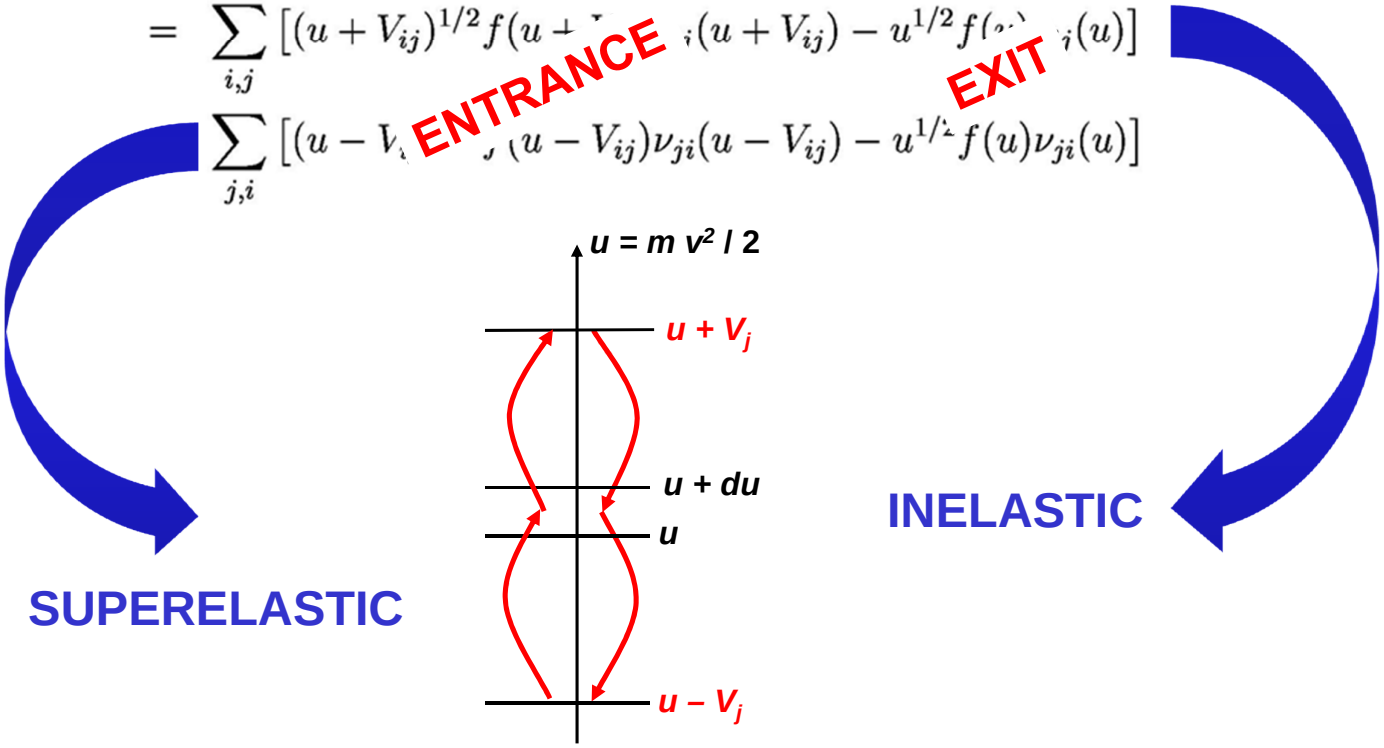

Electron kinetics in atomic and molecular plasmas

The homogeneous electron Boltzmann equation

$$\frac{dG(u)}{du} = [q(u) - \nu_x(u) - \nu_i(u)]\, f(u)\sqrt{u}$$

- Boundary conditions

$$G(u=0) = G(u=\infty) = 0$$

- Solution for no inelastic collisions

$$\frac{dG}{du} = 0 \;\Rightarrow\; G = -\frac{2}{3}u^{3/2}\nu_c\left[\frac{(eE_p)^2}{2m\,(\nu_c^2+\omega^2)}\frac{df}{du} + \frac{3m}{M}f\right] = 0$$

$$\Rightarrow\; f(u) = A\exp\left[-\int_0^u \frac{3m}{M}\frac{du}{u_c(u)}\right]$$

Druyvestein's electron distribution function

Electron kinetics in atomic and molecular plasmas

Input data

Collision frequencies …

$$\frac{d}{du}\left[-\frac{2}{3}u^{3/2}\nu_c\left(u_c\frac{df}{du} + \frac{3m}{M}f\right)\right] = q - \nu_x - \nu_i\; f\sqrt{u}$$

$$\nu_c = N\sigma_c\left(2eu/m\right)^{1/2} \qquad q,\nu = N_i\sigma_{ij}\left(2eu/m\right)^{1/2}$$

$N_{i=0} = N$ ⇒ **Gas density**

$N_{i\neq 0}$ ⇒ **Collisional-radiative model**

Electron kinetics in atomic and molecular plasmas

Input data

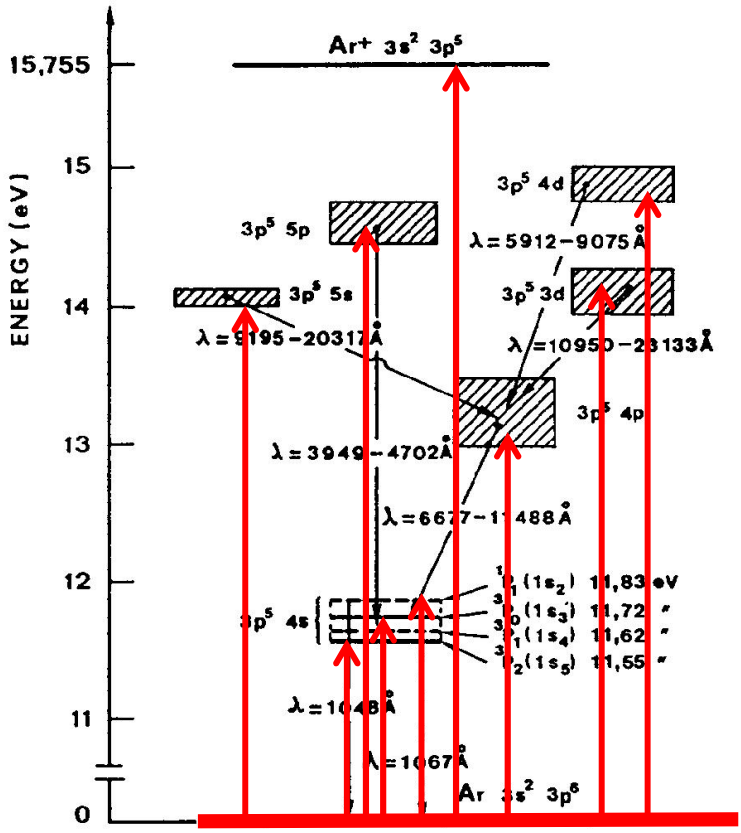

Inelastic collisions
from ground-state

Electron kinetics in atomic and molecular plasmas

Input data

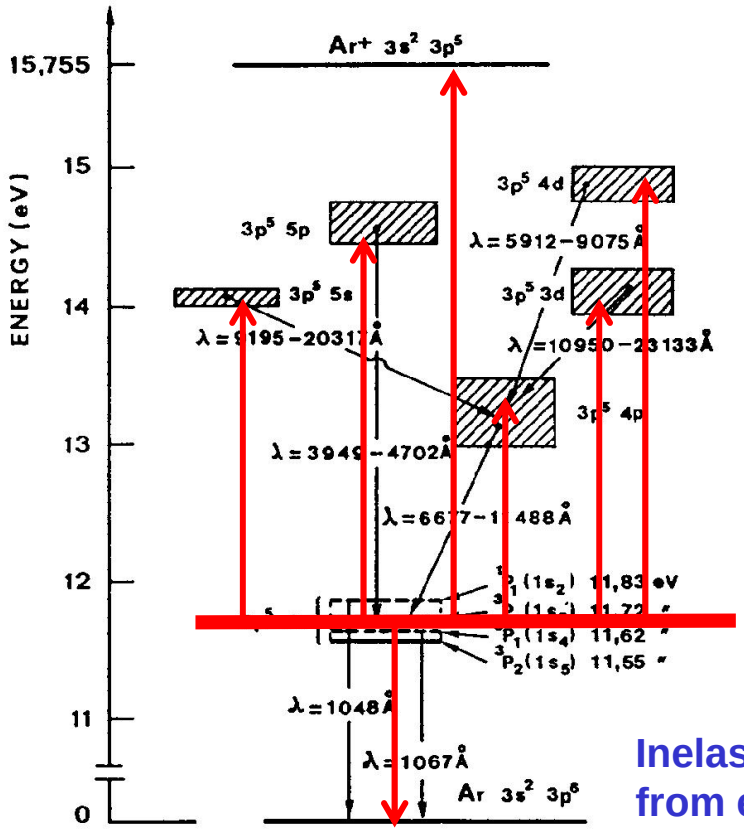

Inelastic + superelastic collisions
from excited states

Electron kinetics in atomic and molecular plasmas

Input data

Cross sections…

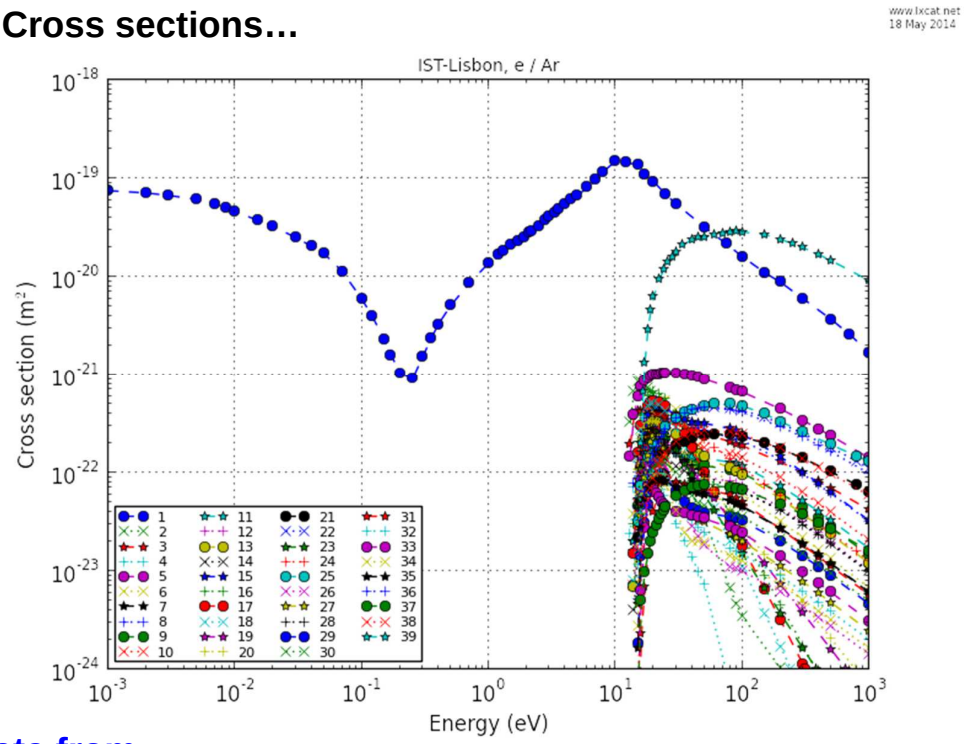

Data from…

- Bibliography
- Databases (e.g. LXCat: www.lxcat.net)

Electron kinetics in atomic and molecular plasmas

Input data

Independent reduced parameters …

$$\frac{d}{du}\left[-\frac{2}{3}u^{3/2}\nu_c\left(u_c\frac{df}{du}+\frac{3m}{M}f\right)\right]=\left(q-\nu_x-\nu_i\right)f\sqrt{u}$$

$$u_c=\frac{\left(eE_p\right)^2}{2m\left(\nu_c^2+\omega^2\right)}=\frac{e^2}{2m}\frac{\left(E_p/N\right)^2}{\left(\nu_c/N\right)^2+\left(\omega/N\right)^2}$$

Independent parameters

$$\frac{E_p}{N},\frac{\omega}{N}$$

Electron kinetics in atomic and molecular plasmas

Results for argon (atomic gas)

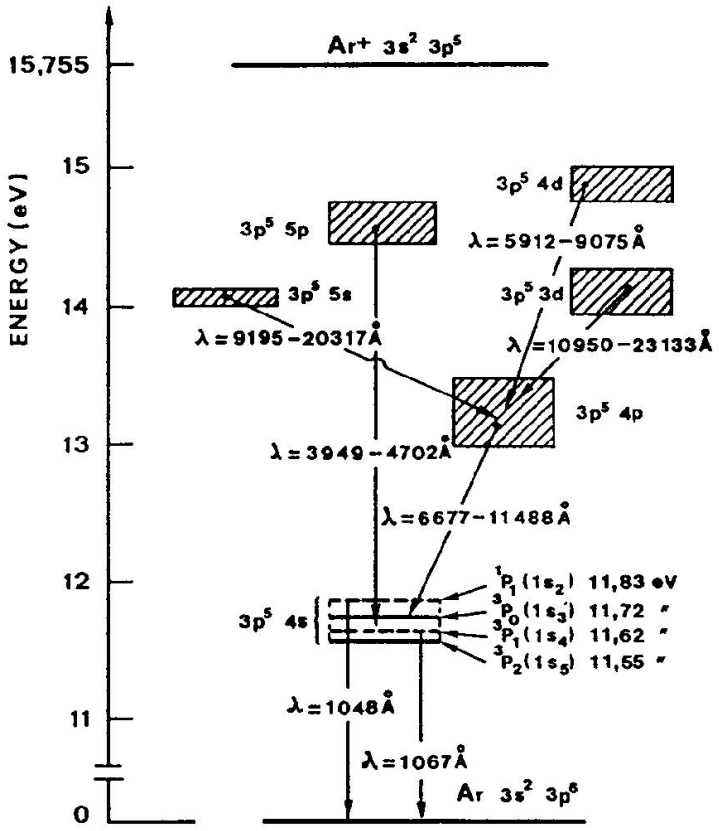

Electron kinetics in …

Results for argon (atomic gas)

Variation with *E/N* …

$10^{-18} < E/N < 10^{-15}$ (V cm^2)

$\omega = 0$

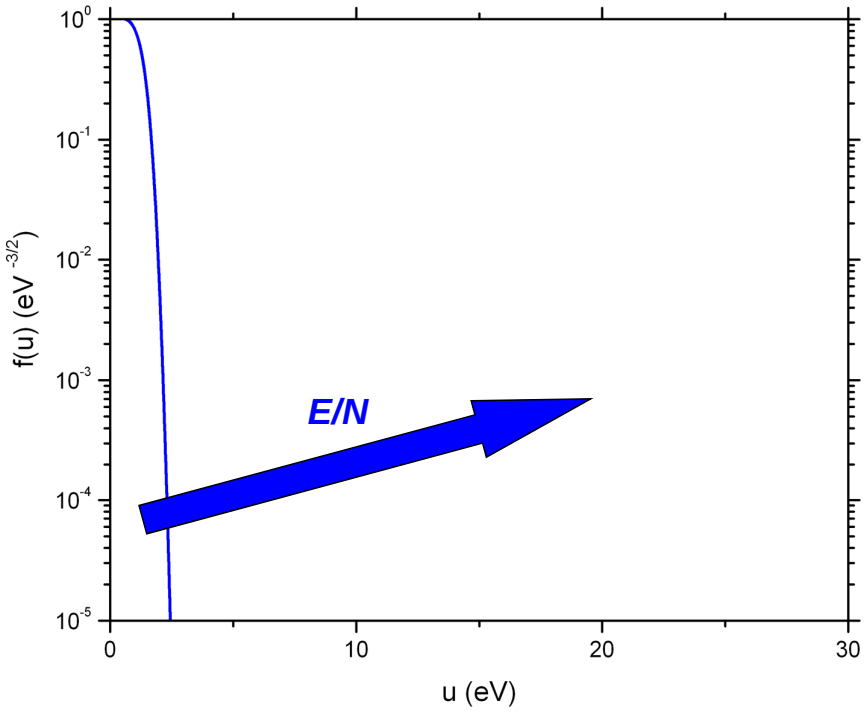

Electron kinetics in atomic and molecular plasmas

Results for argon (atomic gas)

Variation with ω/N ...

Average power transferred from the hf field to electrons of energy u

$$u_c(u)\nu_c(u) = \frac{(eE_p)^2}{2m}\frac{\nu_c(u)}{\nu_c^2(u)+\omega^2}$$

- dc case ($\omega = 0$)

$$u_c(u)\nu_c(u) = \frac{(eE_p)^2}{2m}\frac{1}{\nu_c(u)}$$

No collisions ⇒ increased heating

- hf case ($\omega >> \nu_c$)

$$u_c(u)\nu_c(u) \simeq \frac{(eE_p)^2}{2m}\frac{\nu_c(u)}{\omega^2}$$

No collisions ⇒ no heating

Electron kinetics in …

Results for argon (atomic gas)

$$u_c(u)\nu_c(u) \simeq \frac{(eE_p)^2}{2m}\frac{\nu_c(u)}{\omega^2}$$

Variation with ω/N ...

$10^{-7} < \omega/N < 10^{-5}$ ($cm^3\ s^{-1}$)
$E/N = 10^{-16}$ V cm^2

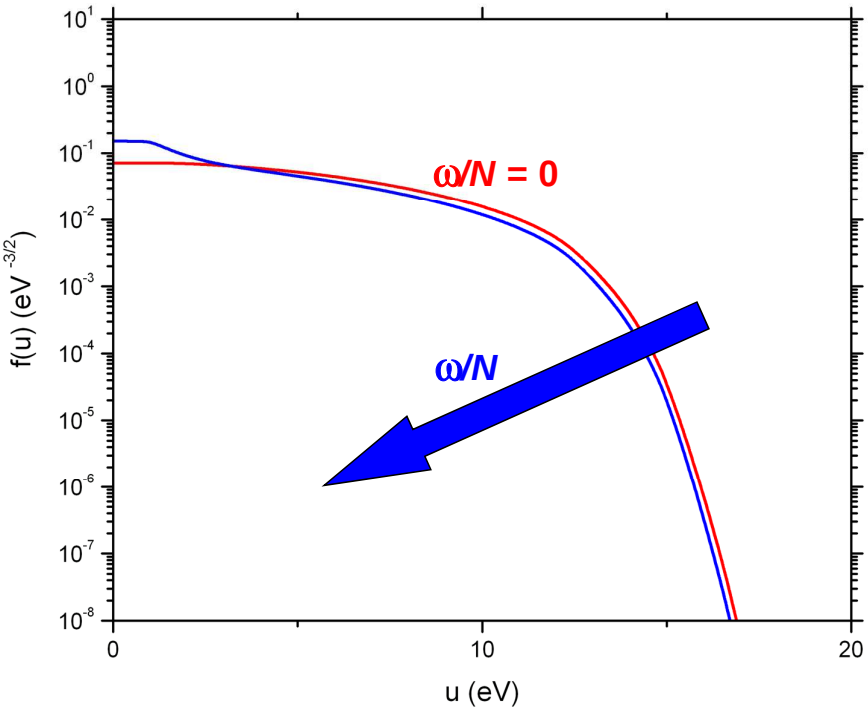

Electron kinetics in atomic and molecular plasmas

Results for argon (atomic gas)

Variation with ω/N ...

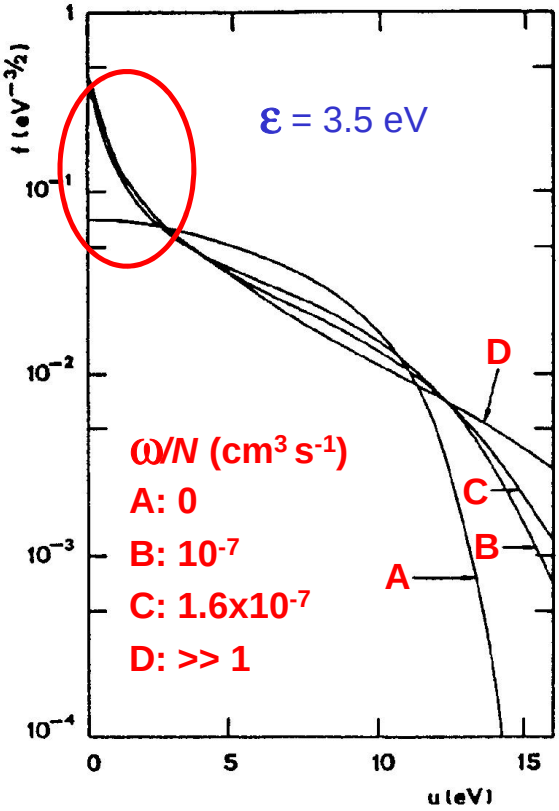

Influence of ν_c/N ...

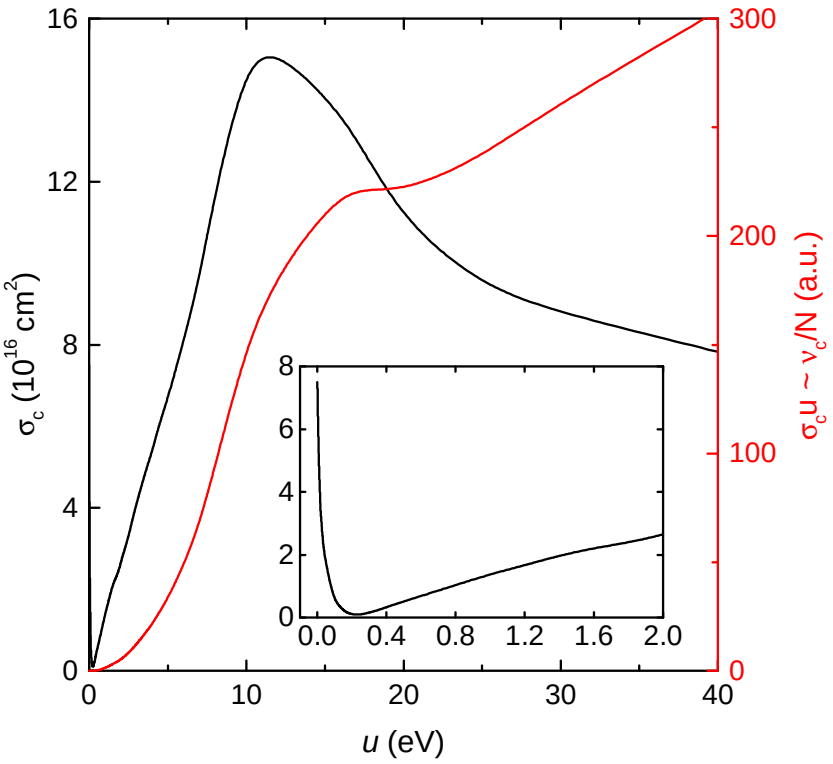

Electron kinetics in atomic and molecular plasmas

Results for argon (atomic gas)

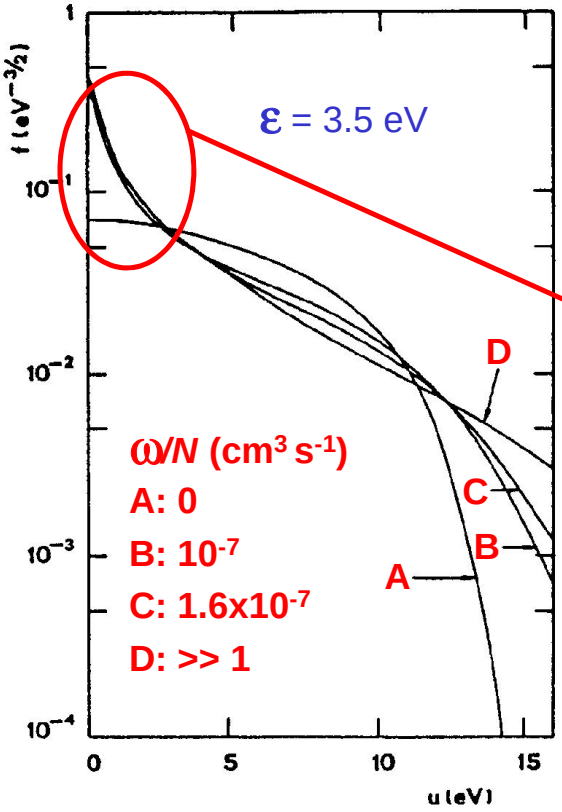

Non-physical solution

Electron kinetics in atomic and molecular plasmas

Results for argon (atomic gas)

Influence of electron-electron collisions ...

$$\frac{dG(u)}{du} = [q(u) - \nu_x(u) - \nu_i(u)]\, f(u)\sqrt{u}$$

$$G(u) = G_E(u) + G_c(u) + G_{ee}(u)$$

$$G_{ee}(u) = -2\nu_{ee}(u)u^{3/2}\left[I(u)f(u) + J(u)\frac{df(u)}{du}\right]$$

$$I(u) = \int_0^u f(u')\sqrt{u'}du'$$

$$J(u) = \frac{2}{3}\left(\int_0^u f(u')u'^{3/2}du' + u^{3/2}\int_u^\infty f(u')du'\right)$$

$$\nu_{ee}(u) = 4\pi\left(\frac{e^2}{4\pi\varepsilon_0 m}\right)^2 \frac{\ln\Lambda_c}{v^3} n_e$$

$$\Lambda_c = 12\pi n_e \lambda_D^3$$

Independent parameters

$$\frac{E_p}{N}, \frac{\omega}{N}, \frac{n_e}{N}$$

Electron kinetics in …

Results for argon (atomic gas)

Variation with n_e/N ...

A:

ω/N = 0

E/N = 3x10^{-16} V cm^2

B:

ω/N = 2x10^{-6} cm^3 s^{-1}

E/N = 3x10^{-15} V cm^2

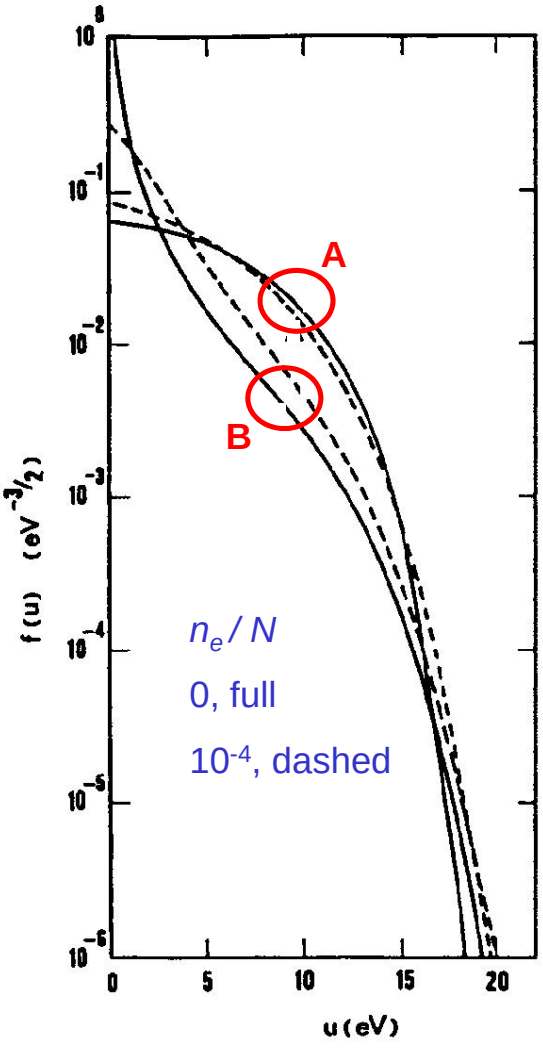

Electron kinetics in atomic and molecular plasmas

Results for nitrogen (molecular gas)

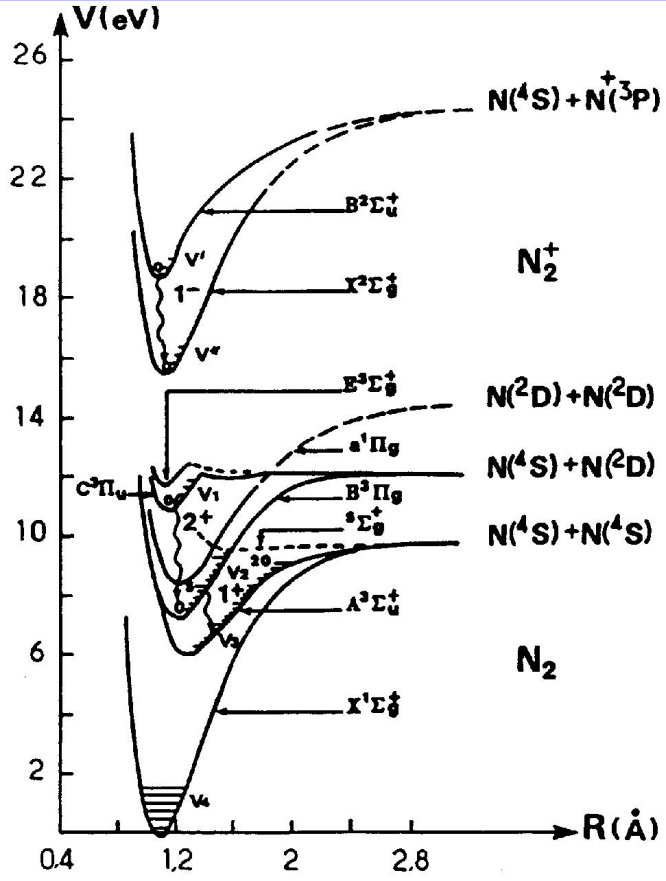

Electron kinetics in atomic and molecular plasmas

Results for nitrogen (molecular gas)

Modifications to the homogeneous electron Boltzmann equation ...

$$\frac{d}{du}\left[-\frac{2}{3}u^{3/2}\nu_c\left(u_c\frac{df}{du}+\frac{3m}{M}f\right)+6B_0u^{1/2}\nu_0 f\right]$$

$$=\sum_{i,j}\left[(u+V_{ij})^{1/2}f(u+V_{ij})\nu_{ij}(u+V_{ij})-u^{1/2}f(u)\nu_{ij}(u)\right]$$

$$+\sum_{j,i}\left[(u-V_{ij})^{1/2}f(u-V_{ij})\nu_{ji}(u-V_{ij})-u^{1/2}f(u)\nu_{ji}(u)\right]$$

$$\nu_{ij}=N_i\sigma_{ij}(2eu/m)^{1/2}$$

→ Populations of vibrational excited levels

Electron kinetics in atomic and molecular plasmas

Results for nitrogen (molecular gas)

Rate balance equations for the vibrational levels ...

$$n_e \sum_{w=0,w\neq v}^{45} N_w C_{w,v} - n_e N_v \sum_{w=0,w\neq v}^{45} C_{v,w}$$
$$+ \quad N_{v-1} NP_{v-1,v} + N_{v+1} NP_{v+1,v} - N_v (P_{v,v-1} + P_{v,v+1})$$
$$+ \quad N_{v-1} \sum_{w=0}^{44} N_{w+1} Q_{v-1,v}^{w+1,w} + N_{v+1} \sum_{w=0}^{45} N_w Q_{v+1,v}^{w,w+1}$$
$$- \quad N_v \left(\sum_{w=0}^{44} N_{w+1} Q_{v,v+1}^{w+1,w} + \sum_{w=0}^{45} N_w Q_{v,v-1}^{w,w+1} \right) + R(v) = 0$$

- electron-vibration

$$\mathrm{e} + \mathrm{N}_2(v) \underset{C_{v,w}}{\overset{C_{w,v}}{\rightleftharpoons}} \mathrm{e} + \mathrm{N}_2(w)$$

Electron kinetics in atomic and molecular plasmas

Results for nitrogen (molecular gas)

Rate balance equations for the vibrational levels ...

$$n_e \sum_{w=0,w\neq v}^{45} N_w C_{w,v} - n_e N_v \sum_{w=0,w\neq v}^{45} C_{v,w}$$
$$+ \quad N_{v-1} NP_{v-1,v} + N_{v+1} NP_{v+1,v} - N_v (P_{v,v-1} + P_{v,v+1})$$
$$+ \quad N_{v-1} \sum_{w=0}^{44} N_{w+1} Q_{v-1,v}^{w+1,w} + N_{v+1} \sum_{w=0}^{45} N_w Q_{v+1,v}^{w,w+1}$$
$$- \quad N_v \left(\sum_{w=0}^{44} N_{w+1} Q_{v,v+1}^{w+1,w} + \sum_{w=0}^{45} N_w Q_{v,v-1}^{w,w+1} \right) + R(v) = 0$$

- vibration-translation

$$\begin{cases} \mathrm{N}_2 + \mathrm{N}_2(v) \underset{P_{v,v-1}}{\overset{P_{v-1,v}}{\rightleftharpoons}} \mathrm{N}_2 + \mathrm{N}_2(v-1) \\ \mathrm{N}_2 + \mathrm{N}_2(v+1) \underset{P_{v+1,v}}{\overset{P_{v,v+1}}{\rightleftharpoons}} \mathrm{N}_2 + \mathrm{N}_2(v) \end{cases}$$

Electron kinetics in atomic and molecular plasmas

Results for nitrogen (molecular gas)

Rate balance equations for the vibrational levels ...

$$n_e \sum_{w=0,w\neq v}^{45} N_w C_{w,v} - n_e N_v \sum_{w=0,w\neq v}^{45} C_{v,w}$$
$$+ \quad N_{v-1} N P_{v-1,v} + N_{v+1} N P_{v+1,v} - N_v (P_{v,v-1} + P_{v,v+1})$$
$$+ \quad N_{v-1} \sum_{w=0}^{44} N_{w+1} Q_{v-1,v}^{w+1,w} + N_{v+1} \sum_{w=0}^{45} N_w Q_{v+1,v}^{w,w+1}$$
$$- \quad N_v \left(\sum_{w=0}^{44} N_{w+1} Q_{v,v+1}^{w+1,w} + \sum_{w=0}^{45} N_w Q_{v,v-1}^{w,w+1} \right) + R(v) = 0$$

Atom kinetics

- vibration-vibration

$$\begin{cases} \mathrm{N}_2(v) + \mathrm{N}_2(w) \underset{Q_{v,v-1}^{w,w+1}}{\overset{Q_{v-1,v}^{w+1,w}}{\rightleftharpoons}} \mathrm{N}_2(v-1) + \mathrm{N}_2(w+1) \\ \mathrm{N}_2(v+1) + \mathrm{N}_2(w) \underset{Q_{v+1,v}^{w,w+1}}{\overset{Q_{v,v+1}^{w+1,w}}{\rightleftharpoons}} \mathrm{N}_2(v) + \mathrm{N}_2(w+1) \end{cases}$$

Electron kinetics in atomic and molecular plasmas

Results for nitrogen (molecular gas)

$$n_e \sum_{w=0,w\neq v}^{45} N_w C_{w,v} - n_e N_v \sum_{w=0,w\neq v}^{45} C_{v,w}$$
$$+ \quad N_{v-1} N P_{v-1,v} + N_{v+1} N P_{v+1,v} - N_v (P_{v,v-1} + P_{v,v+1})$$
$$+ \quad N_{v-1} \sum_{w=0}^{44} N_{w+1} Q_{v-1,v}^{w+1,w} + N_{v+1} \sum_{w=0}^{45} N_w Q_{v+1,v}^{w,w+1}$$
$$- \quad N_v \left(\sum_{w=0}^{44} N_{w+1} Q_{v,v+1}^{w+1,w} + \sum_{w=0}^{45} N_w Q_{v,v-1}^{w,w+1} \right) + R(v) = 0$$

Independent parameters ...

$$\frac{E_p}{N}, \frac{\omega}{N}, \frac{n_e}{N} \rightarrow T_v$$

Vibrational temperature

Electron kinetics in atomic and molecular plasmas

Results for nitrogen (molecular gas)

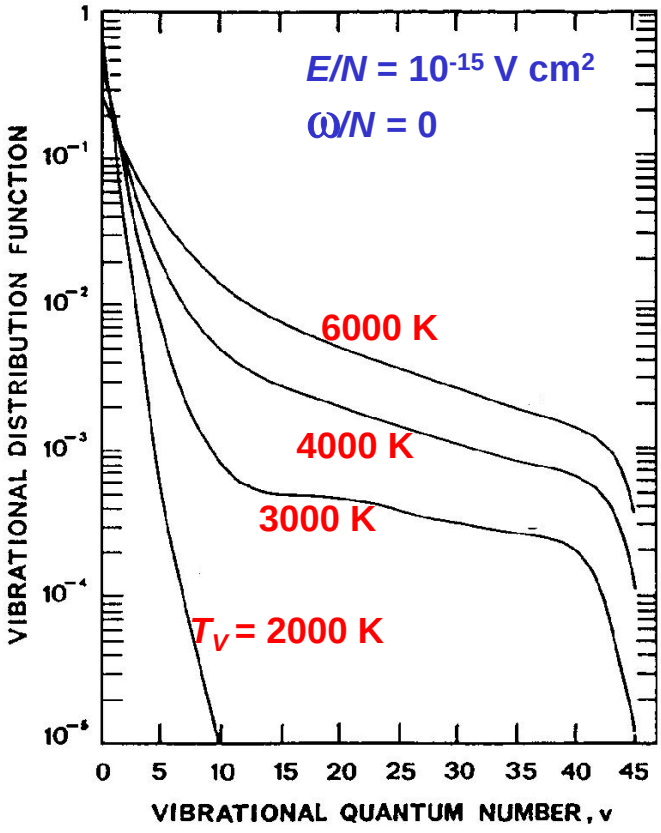

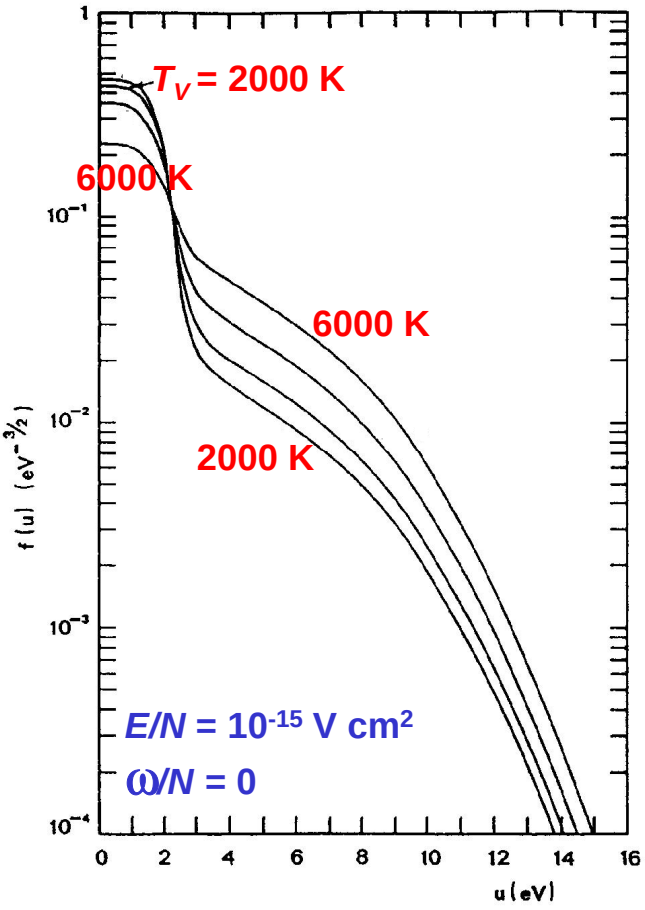

Low Temperature Plasma Physics: Basics and Applications

October 4 – 9, 2014

Fluid Modelling of dc Discharge Plasmas

L.L. Alves
llalves@tecnico.ulisboa.pt

Instituto de Plasmas e Fusão Nuclear

Instituto Superior Técnico, Lisbon, Portugal

Outline

- Introduction
- Moments of the electron Boltzmann equation (dc case)
- The positive column of a dc discharge plasma
- Fluid model of a dc positive column (equations, boundary conditions, eigenvalues)
- Classical ambipolar solution - high pressure limit
  (Bessel solution and Schottky condition)
- Application to a discharge in helium

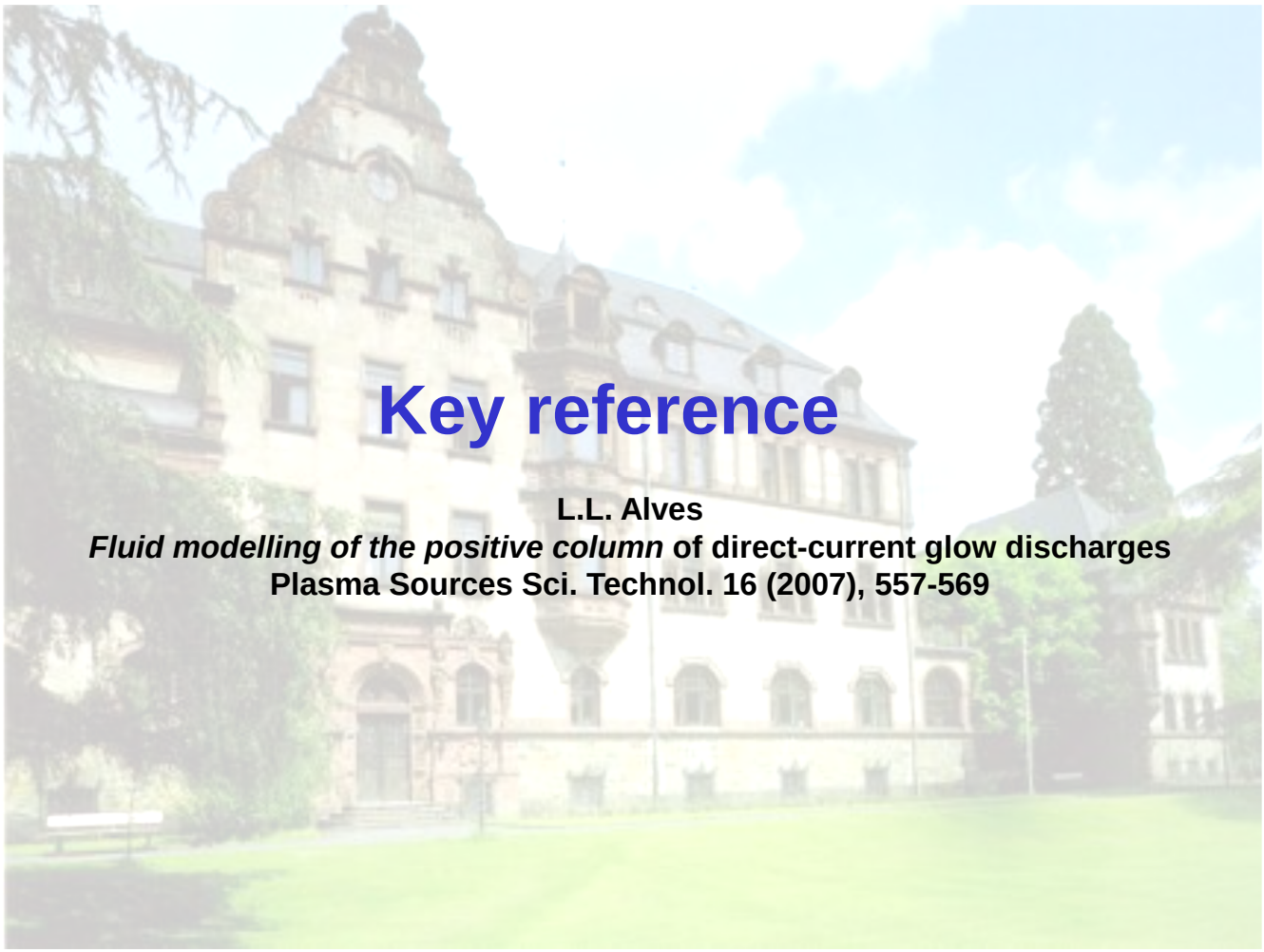

Key reference

L.L. Alves
***Fluid modelling of the positive column* of direct-current glow discharges**
Plasma Sources Sci. Technol. 16 (2007), 557-569

Fluid modelling of dc discharge plasmas

Introduction

FLUID MODELLING OF DC DISCHARGE PLASMAS

Hidrodynamic (fluid) transport equations
for electrons and ions

FLUID MODELLING OF DC DISCHARGE PLASMAS

Direct-current discharge (ω=0)

Fluid modelling of dc discharge plasmas
Introduction

FLUID MODELLING OF DC DISCHARGE PLASMAS

Details on plasma excitation
Definition of boundaries

Fluid modelling of dc discharge plasmas

Moments of the electron Boltzmann equation (dc case)

$$\frac{v}{3}\vec{\nabla}\cdot\vec{F}_0^1 - \frac{1}{v^2}\frac{\partial}{\partial v}\left\{\left(\frac{ev^2}{6m}\right)\left[Re\left(\vec{E}_p\cdot\vec{F}_1^1\right)+2\vec{E}_s\cdot\vec{F}_0^1\right]+\frac{m}{M}\nu_c v^3 F_0^0\right\}$$

$$= (q-\nu_x-\nu_i)\,F_0^0$$

$$\nu_c\vec{F}_0^1 = -v\vec{\nabla}F_0^0 + \frac{e}{m}\vec{E}_s\frac{\partial F_0^0}{\partial v}$$

$$(\nu_c+j\omega)\vec{F}_1^1 = \frac{e\vec{E}_p}{m}\frac{\partial F_0^0}{\partial v}$$

Fluid modelling of dc discharge plasmas

Moments of the electron Boltzmann equation (dc case)

$$\frac{v}{3}\vec{\nabla}\cdot\vec{F}_0^1 - \frac{1}{v^2}\frac{\partial}{\partial v}\left\{\frac{ev^2}{3m}\vec{E}\cdot\vec{F}_0^1+\frac{m}{M}\nu_c v^3 F_0^0\right\} = (q-\nu_x-\nu_i)\,F_0^0$$

$$\nu_c\vec{F}_0^1 = -v\vec{\nabla}F_0^0 + \frac{e}{m}\vec{E}\frac{\partial F_0^0}{\partial v}$$

$\int_0^\infty \cdots 4\pi v^2 dv$ Particle balance equation

$\int_0^\infty \frac{mv^2}{2e}\times\cdots 4\pi v^2 dv$ Energy balance equation

$\int_0^\infty v\times\cdots 4\pi v^2 dv$ Particle flux equation

$\int_0^\infty \frac{mv^2}{2e}v\times\cdots 4\pi v^2 dv$ Energy flux equation

Fluid modelling of dc discharge plasmas

Moments of the electron Boltzmann equation (dc case)

$$\vec{\nabla}\cdot\int_0^\infty \vec{F}_0^1\frac{v}{3}4\pi v^2 dv - \int_0^\infty \frac{1}{v^2}\frac{\partial}{\partial v}\left\{\frac{ev^2}{3m}\vec{E}\cdot\vec{F}_0^1 + \frac{m}{M}\nu_c v^3 F_0^0\right\}4\pi v^2 dv$$

$$= \int_0^\infty (q-\nu_x-\nu_i)\,F_0^0 4\pi v^2 dv$$

The electron particle balance equation (continuity equation)

$$\vec{\nabla}\cdot\vec{\Gamma} - 0 = n_e\langle\nu_i\rangle$$

Fluid modelling of dc discharge plasmas

Moments of the electron Boltzmann equation (dc case)

$$\int_0^\infty \frac{v}{3}\vec{F}_0^1\,4\pi v^2 dv = -\vec{\nabla}\left[\int_0^\infty \frac{v^2}{3\nu_c}F_0^0\,4\pi v^2 dv\right] - \left[\int_0^\infty -\frac{ev}{3m\nu_c}\frac{\partial F_0^0}{\partial v}\,4\pi v^2 dv\right]\vec{E}$$

The electron flux equation

$$\vec{\Gamma} = -\vec{\nabla}\left(D_e n_e\right) - n_e\mu_e\,\vec{E}$$

Drift-diffusion approximation

The electron transport coefficients

$$D_e n_e = \int_0^\infty \frac{v^2}{3\nu_c}F_0^0\,4\pi v^2 dv$$

Electron free diffusion coefficient

$$\mu_e n_e = -\int_0^\infty \frac{ev}{3m\nu_c}\frac{\partial F_0^0}{\partial v}\,4\pi v^2 dv$$

Electron mobility

Fluid modelling of dc discharge plasmas

Moments of the electron Boltzmann equation (dc case)

$$-\vec{\nabla}\cdot\int_0^\infty \frac{mv^2}{2e}\vec{F}_0^1\frac{v}{3}4\pi v^2dv+\int_0^\infty \frac{mv^2}{2e}\frac{1}{v^2}\frac{\partial}{\partial v}\left[\frac{ev^2}{3m}\vec{E}\cdot\vec{F}_0^1\right]4\pi v^2dv$$

$$=-\int_0^\infty \frac{mv^2}{2e}\frac{1}{v^2}\frac{\partial}{\partial v}\left[\frac{m}{M}\nu_c v^3F_0^0\right]4\pi v^2dv$$

$$-\int_0^\infty \frac{mv^2}{2e}(q-\nu_x-\nu_i)F_0^0\,4\pi v^2dv$$

The electron energy balance equation

$$-\vec{\nabla}\cdot\vec{\Gamma}_\varepsilon-\vec{\Gamma}\cdot\vec{E}=\frac{2m}{M}\left\langle\frac{mv^2}{2e}\nu_c\right\rangle+\sum_j V_j\langle\nu_j\rangle+V_i\langle\nu_i\rangle\equiv\theta_{\text{coll}}$$

Fluid modelling of dc discharge plasmas

Moments of the electron Boltzmann equation (dc case)

$$\int_0^\infty \frac{v}{3}\frac{mv^2}{2e}\vec{F}_0^1\,4\pi v^2dv=-\vec{\nabla}\left[\int_0^\infty \frac{v^2}{3\nu_c}\frac{mv^2}{2e}F_0^0\,4\pi v^2dv\right]-\left[\int_0^\infty -\frac{ev}{3m\nu_c}\frac{mv^2}{2e}\frac{\partial F_0^0}{\partial v}4\pi v^2dv\right]\vec{E}$$

The electron energy flux equation

$$\vec{\Gamma}_\varepsilon=-\vec{\nabla}\left(D_\varepsilon n_e\varepsilon\right)-n_e\varepsilon\mu_\varepsilon\vec{E}$$

Drift-diffusion approximation

The electron energy transport coefficients

$$\varepsilon n_e=\int_0^\infty \frac{mv^2}{2e}F_0^0\,4\pi v^2dv$$ Electron mean energy (density)

$$D_\varepsilon=\frac{\int_0^\infty \frac{mv^2}{2e}\frac{v^2}{3\nu_c}F_0^0\,4\pi v^2dv}{\int_0^\infty \frac{mv^2}{2e}F_0^0\,4\pi v^2dv}$$ Diffusion coefficient for elec. energy transport

$$\mu_\varepsilon=-\frac{\int_0^\infty \frac{mv^2}{2e}\frac{ev}{3m\nu_c}\frac{\partial F_0^0}{\partial v}4\pi v^2dv}{\int_0^\infty \frac{mv^2}{2e}F_0^0\,4\pi v^2dv}$$ Mobility for elec. energy transport

Fluid modelling of dc discharge plasmas

Electron parameters

$$\frac{v}{3}\vec{\nabla}\cdot\vec{F}_0^1 - \frac{1}{v^2}\frac{\partial}{\partial v}\left\{\frac{ev^2}{3m}\vec{E}\cdot\vec{F}_0^1 + \frac{m}{M}\nu_c v^3 F_0^0\right\} = (q-\nu_x-\nu_i)\,F_0^0$$

$$\nu_c\vec{F}_0^1 = -v\vec{\nabla}F_0^0 + \frac{e}{m}\vec{E}\frac{\partial F_0^0}{\partial v} \qquad \Rightarrow F_0^0, \vec{F}_0^1\left(E/N, \omega/N = 0\right)$$

All macroscopic quantities obtained by integration over the eedf are **exclusive functions of the independent reduced parameters**

$$\frac{E}{N}, \frac{\omega}{N}(\text{non-dc case}), \frac{n_e}{N}(\text{e}-\text{e included})$$

Fluid modelling of dc discharge plasmas

Electron parameters (example): reduced free diffusion coefficient

$$D_e N = \int_0^\infty \frac{Nv^2}{3\nu_c}\frac{F_0^0}{n_e}4\pi v^2 dv = \frac{2e}{3m}\int_0^\infty \frac{u^{3/2}}{\left(\nu_c/N\right)} f\, du = \text{function}\left(E/N\right)$$

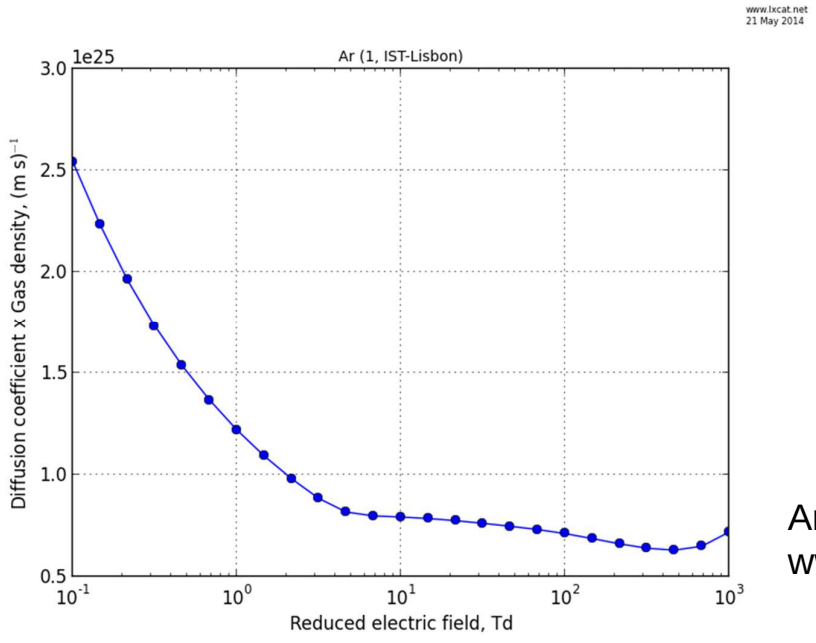

1 Td ≡ 10^{-17} V cm^2

Ar @ IST-LISBON
www.lxcat.net

Fluid modelling of dc discharge plasmas

The positive column of a dc discharge plasma

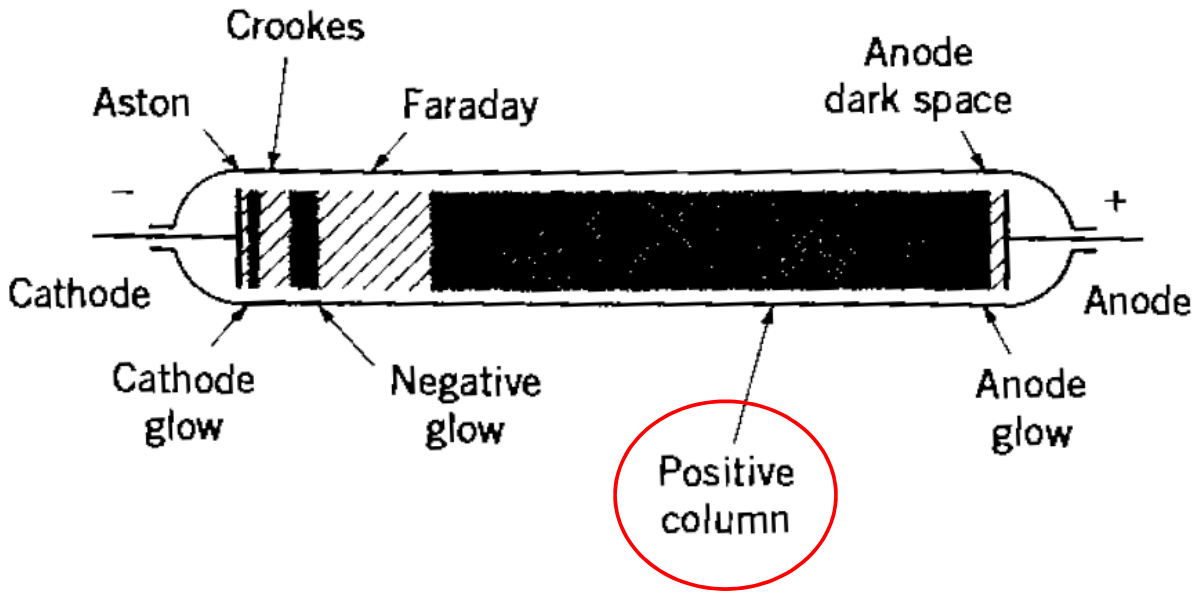

Fluid modelling of dc discharge plasmas

The positive column of a dc discharge plasma

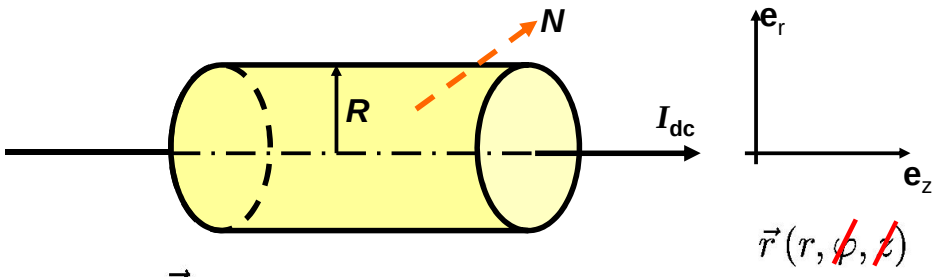

$$\vec{E} = E_r(r)\,\vec{e}_r + E_z\,\vec{e}_z$$

Radial dc space-charge field — Axial external field

- Reduced independent variables used in fluid description

$$x \equiv \frac{r}{R},\ \frac{E_z}{N},\ NR,\ n_e \rightarrow I_{\mathrm{dc}}$$

Fluid modelling of dc discharge plasmas

Fluid model of a dc positive column

Electron transport equations (4x 1st order PDE's)

$$\frac{1}{x}\frac{d}{dx}(x\Gamma) = NR\,\frac{\langle\nu_i\rangle}{N}\,n_e$$

$$\Gamma = -\frac{1}{NR}\frac{d}{dx}\left[(D_e N)\;n_e\right] - (\mu_e N)\frac{E_r}{N}\,n_e$$

$$(\mu_e N)\left(\frac{E_z}{N}\right)^2 n_e - \frac{1}{NR}\frac{1}{x}\frac{d}{dx}(x\Gamma_\varepsilon) = \Gamma\frac{E_r}{N} + \frac{\theta_{\text{coll}}}{N}$$

$$\Gamma_\varepsilon = -\frac{1}{NR}\frac{d}{dx}\left[(D_\varepsilon N)\;\varepsilon\,n_e\right] - (\mu_\varepsilon N)\frac{E_r}{N}\,\varepsilon\,n_e$$

- Solution: radial profiles of

$$n_e,\;\Gamma,\;\varepsilon,\;\Gamma_\varepsilon$$

Fluid modelling of dc discharge plasmas

Fluid model of a dc positive column

Poisson's equation (1st order PDE)

$$\frac{1}{x}\frac{d}{dx}\left(x\frac{E_r}{N}\right) = \frac{eR^2}{\varepsilon_o NR}\,(n_i - n_e)$$

- Solution: radial profile of

$$\frac{E_r}{N}$$

Fluid modelling of dc discharge plasmas

Fluid model of a dc positive column

Ion transport equations (2x 1st order PDE's)

(moments of the ion Boltzmann equation)

$$\frac{1}{x}\frac{d}{dx}\left(x n_p v_p\right) = NR\,\frac{\langle \nu_i \rangle}{N}\,n_e$$

$$\left[n_p + \frac{\langle \nu_i \rangle / N}{\nu_p / N}\,n_e\right] v_p + \frac{1}{NR}\frac{n_p v_p}{\nu_p / N}\frac{dv_p}{dx} - (\mu_p N)\;n_p\left[\frac{E_r}{N} - \frac{k_B T_p}{e}\frac{1}{NR}\frac{1}{n_p}\frac{dn_p}{dx}\right] = 0$$

- Solution: radial profiles of

$$n_p,\;\; v_p$$

Fluid modelling of dc discharge plasmas

Fluid model of a dc positive column

Spatial dependence for the electron transport parameters

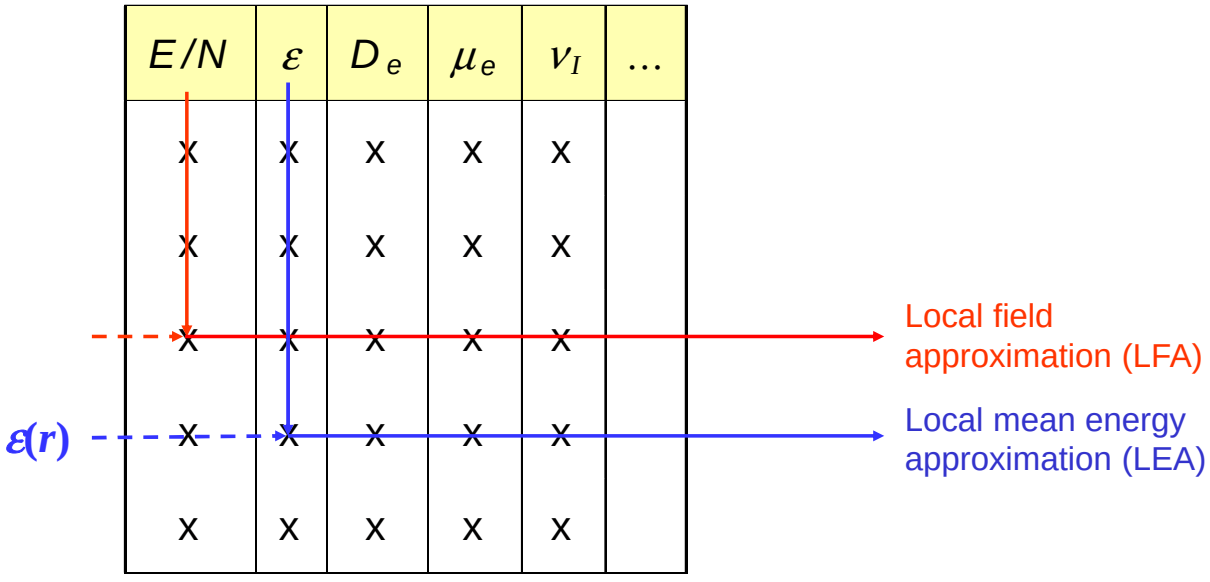

Table constructed by solving the homogeneous electron Boltzmann equation

Fluid modelling of dc discharge plasmas

Fluid model of a dc positive column

Boundary conditions

➢ Axi-symmetry conditions

$$\left.\frac{dn_e}{dx}\right|_{x=0} = 0$$

$$\left.\frac{dn_p}{dx}\right|_{x=0} = 0 \rightarrow n_p(0) = \cdots$$

$$\left.\frac{d\varepsilon}{dx}\right|_{x=0} = 0$$

$$\frac{E_r}{N}(0) = 0$$

➢ Wall flux conditions

$$\Gamma(R) = \frac{1}{2} n_e(R)\langle v\rangle(R)$$

$$\Gamma_\varepsilon(R) = \frac{1}{2} n_e(R)\langle uv\rangle(R)$$

➢ Current conservation

$$\Gamma(R) = n_p(R)v_p(R) \implies \Gamma(r) = n_p(r)v_p(r)$$

➢ Axis electron density

$$n_{e0} \longrightarrow I_{\rm dc}$$

$\Rightarrow$ **8 boundary conditions**

Fluid modelling of dc discharge plasmas

The wall boundary condition

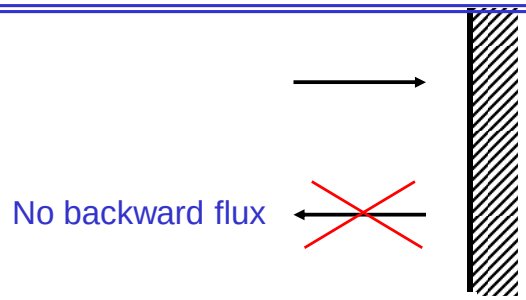

$$\int_0^\infty v^2 dv \int_\pi^{\pi/2} \sin\theta d\theta \int_0^{2\pi} d\varphi \; F(R,\vec{v})\, v_r = 0$$

$$\int_0^\infty v^2 dv \int_\pi^{\pi/2} \sin\theta d\theta \; 2\pi \; \left[F_0^0(R,v) + F_0^1(R,v)\cos\theta\right] v\cos\theta = 0$$

$$\int_0^\infty v F_0^0(R,v)\; 4\pi v^2 dv \int_\pi^{\pi/2} \sin\theta\cos\theta d\theta - \int_0^\infty \frac{v}{3} F_0^1(R,v)\; 4\pi v^2 dv \int_\pi^{\pi/2} (-3)\sin\theta\cos^2\theta d\theta = 0$$

$$\Gamma(R) = \frac{1}{2} n_e(R)\langle v\rangle(R)$$

Fluid modelling of dc discharge plasmas

Fluid model of a dc positive column

Eigenvalue calculation

- Discharge parameters

$$\frac{E_z}{N},\ NR,\ I_{\rm dc}$$

- Discharge current

$$I_{\rm dc} = e\,n_{e0}\int_0^R \mu_e(r)\,E_z\,\frac{n_e(r)}{n_{e0}}\,2\pi r\,dr \;=\; \cdots$$

- Eigenvalue calculation

$$NR,\ I_{\rm dc} \;\Longrightarrow\; \frac{E_z}{N}$$

Fluid modelling of dc discharge plasmas

Classical ambipolar solution - high pressure limit

$$\Gamma \;=\; n_p v_p \qquad \text{Flux conservation}$$
$$n_e \;\simeq\; n_p \equiv n \qquad \text{Quasi-neutrality}$$

$$\begin{cases} \Gamma \simeq -\dfrac{D_e N}{NR}\dfrac{dn}{dx} - (\mu_e N)\dfrac{E_r}{N}\,n \\ \left[n + \dfrac{\langle \nu_i\rangle/N}{\nu_p/N}\,n\right] v_p + \dfrac{1}{NR}\dfrac{n v_p}{\nu_p/N}\dfrac{dv_p}{dx} - (\mu_p N)\,n\left[\dfrac{E_r}{N} - \dfrac{k_B T_p}{e}\dfrac{1}{NR}\dfrac{1}{n}\dfrac{dn}{dx}\right] = 0 \end{cases}$$

$$\Longrightarrow \begin{cases} \Gamma \;\simeq\; -\dfrac{D_A N}{NR}\dfrac{dn}{dx} \\ \dfrac{E_r}{N} \;\simeq\; -u_k\dfrac{1}{n}\dfrac{dn}{dx} \end{cases}$$

- Ambipolar diffusion coefficient

$$D_A N \;=\; -u_k\,(\mu_p N)$$

$$u_k \;=\; \frac{D_e N}{\mu_e N}$$

- Characteristic energy

Fluid modelling of dc discharge plasmas

Classical ambipolar solution - high pressure limit

$$\begin{cases} \dfrac{1}{x}\dfrac{d}{dx}(x\Gamma) = NR\dfrac{\langle\nu_i\rangle}{N}n \\ \Gamma \simeq -\dfrac{D_A N}{NR}\dfrac{dn}{dx} \end{cases} \Rightarrow \frac{1}{x}\frac{d}{dx}\left(x\frac{dn}{dx}\right) = -\frac{n}{(\Lambda_{\text{eff}}/R)^2}$$

- Effective diffusion length

$$\left(\frac{\Lambda_{\text{eff}}}{R}\right)^2 = \frac{D_A N}{(NR)^2\langle\nu_i\rangle/N}$$

SCHOTTKY CONDITION

- Bessel solution

$$n(r) = n_0 J_0\left(r/\Lambda_{\text{eff}}\right)$$

Fluid modelling of dc discharge plasmas

Classical ambipolar solution - high pressure limit

Eigenvalue calculation

- Boundary condition: zero density at wall

$$n(R) = 0 \;\Rightarrow\; J_0\left(R/\Lambda_{\text{eff}}\right) = 0 \;\Rightarrow\; \frac{\Lambda_{\text{eff}}}{R} \simeq 0.42$$

- Electron gain/loss balance

$$\frac{\langle\nu_i\rangle}{N} = \frac{D_A N}{(NR)^2\left(\Lambda_{\text{eff}}/R\right)^2}$$

$$\frac{E_z}{N}$$

EIGENVALUE

Fluid modelling of dc discharge plasmas

Application to a discharge in helium

Working conditions

- Pressure 0.1 - 10 Torr
- Discharge currents 50, 150, 200 mA
- Gas temperature 500 K
- Radius 1 cm

Zero density at wall (typical ambipolar boundary condition) $\Rightarrow \Lambda_{eff\ (amb)} = 0.42$

Schottky condition (for model results at high pressures) $\Rightarrow \Lambda_{eff} = 0.37$

Fluid modelling of dc discharge plasmas

Application to a discharge in helium

Charged particle radial profiles

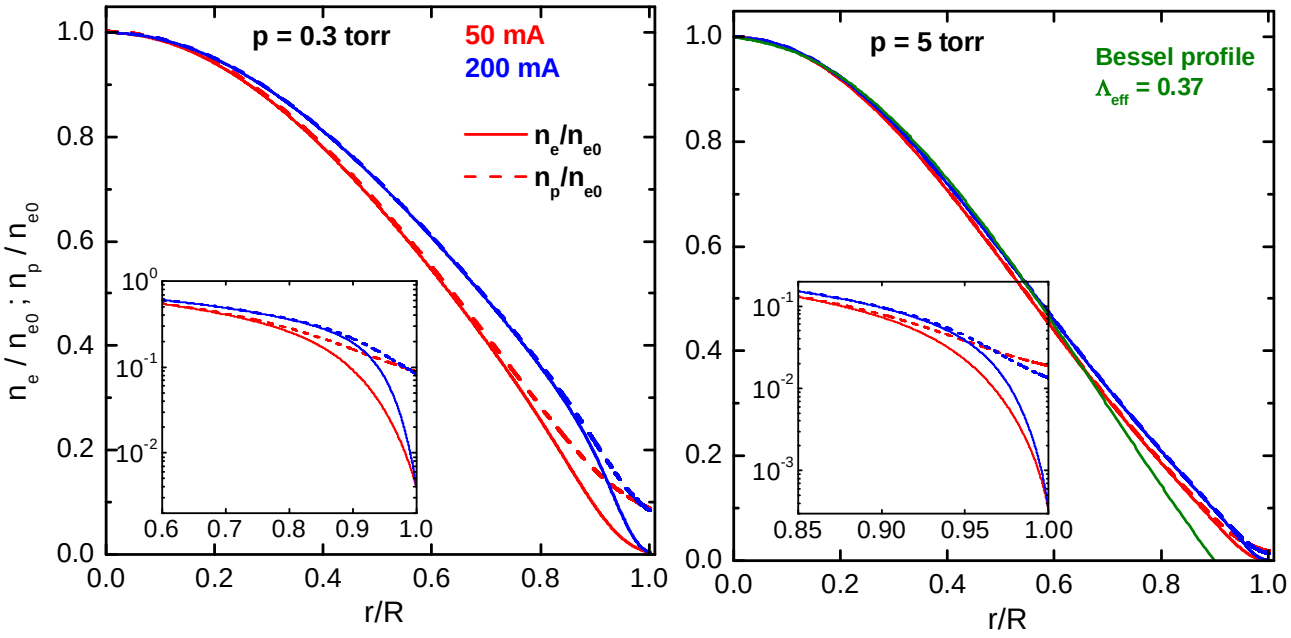

Fluid modelling of dc discharge plasmas

Application to a discharge in helium

Space-charge field radial profile

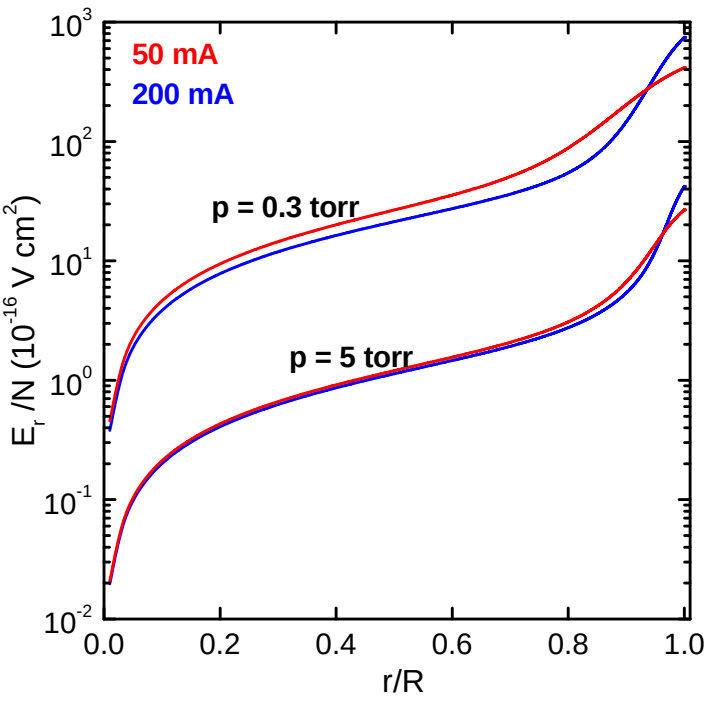

→ ~ 100's V cm^{-1}

Fluid modelling of dc discharge plasmas

Application to a discharge in helium

Space-charge potential radial profile

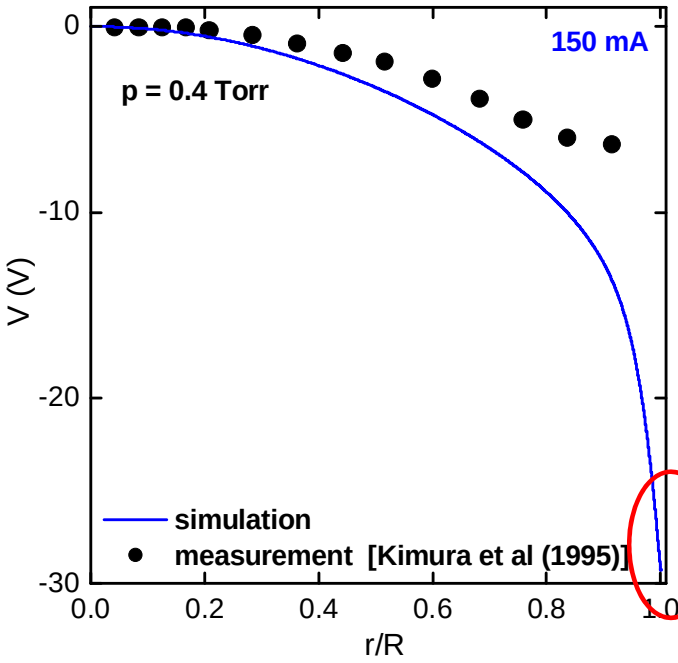

Wall potential

Fluid modelling of dc discharge plasmas

Application to a discharge in helium

Plasma wall potential vs. NR

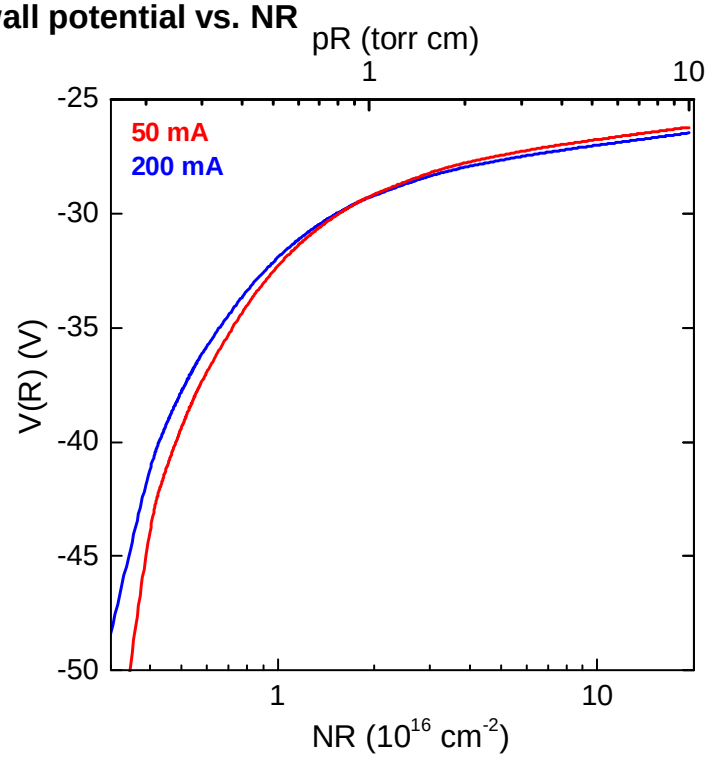

Fluid modelling of dc discharge plasmas

Application to a discharge in helium

Electron mean energy radial profile

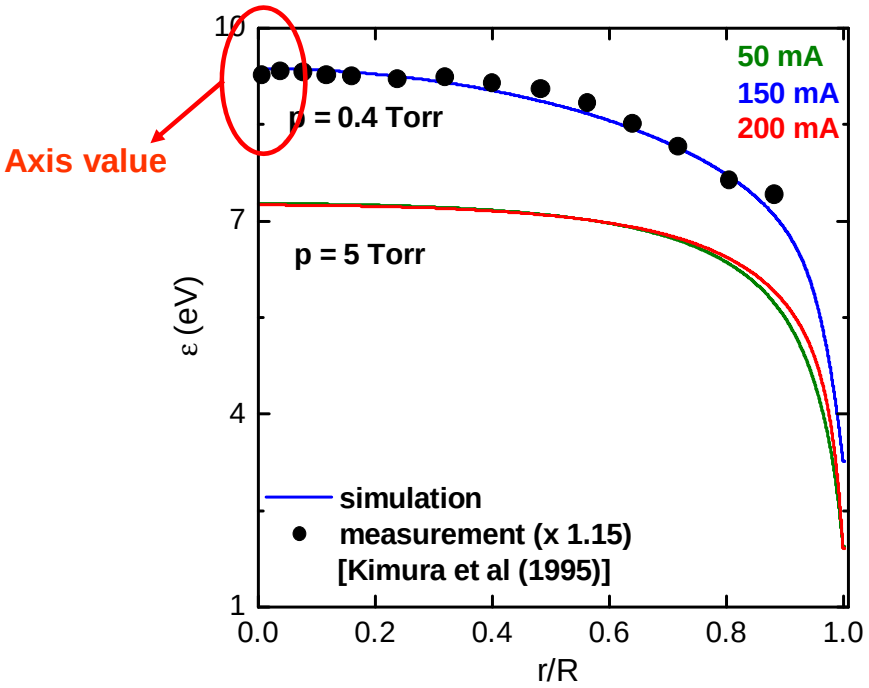

Fluid modelling of dc discharge plasmas

Application to a discharge in helium

Electron mean energy at discharge axis vs. NR

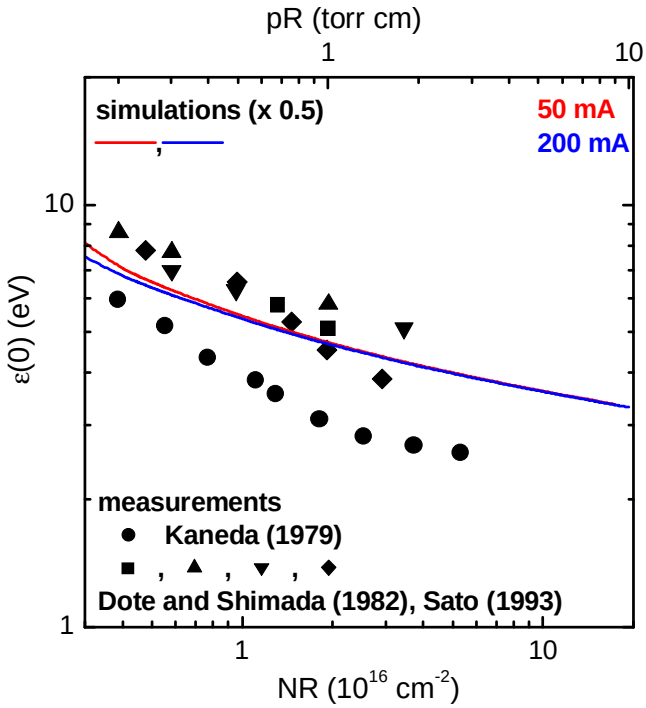

Fluid modelling of dc discharge plasmas

Application to a discharge in helium

Power transfer radial profile

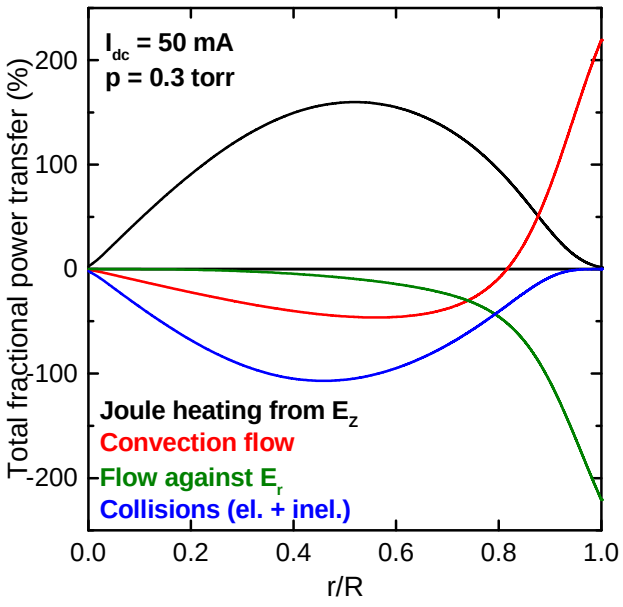

Percentages are calculated relative to the total (radially integrated across the discharge) power gained from the field

$$-\Gamma_z E_z = \nabla_r \Gamma_\varepsilon + \Gamma E_r + \theta_{\text{coll}}$$

Fluid modelling of dc discharge plasmas

Application to a discharge in helium

Power transfer radial profile

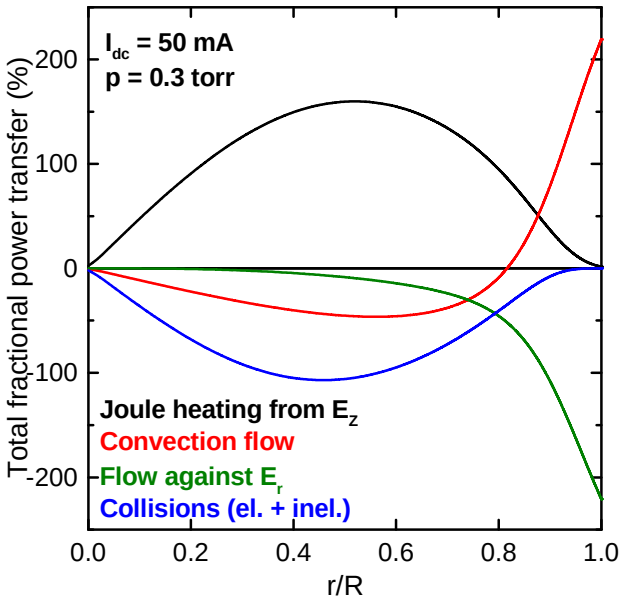

Percentages are calculated relative to the total (radially integrated across the discharge) power gained from the field

$$-\Gamma_z E_z = \nabla_r \Gamma_\varepsilon + \Gamma E_r + \theta_{\text{coll}}$$

Fluid modelling of dc discharge plasmas

Application to a discharge in helium

Power transfer radial profile

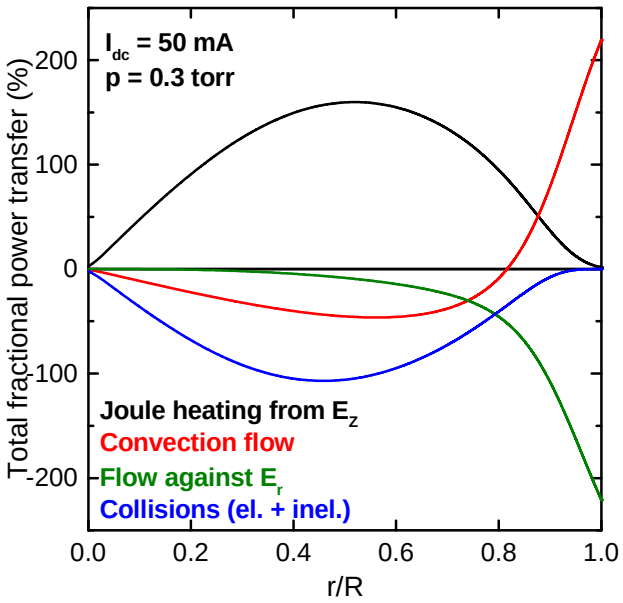

Percentages are calculated relative to the total (radially integrated across the discharge) power gained from the field

$$-\Gamma_z E_z = \nabla_r \Gamma_\varepsilon + \Gamma E_r + \theta_{\text{coll}}$$

Fluid modelling of dc discharge plasmas

Application to a discharge in helium

Power transfer radial profile

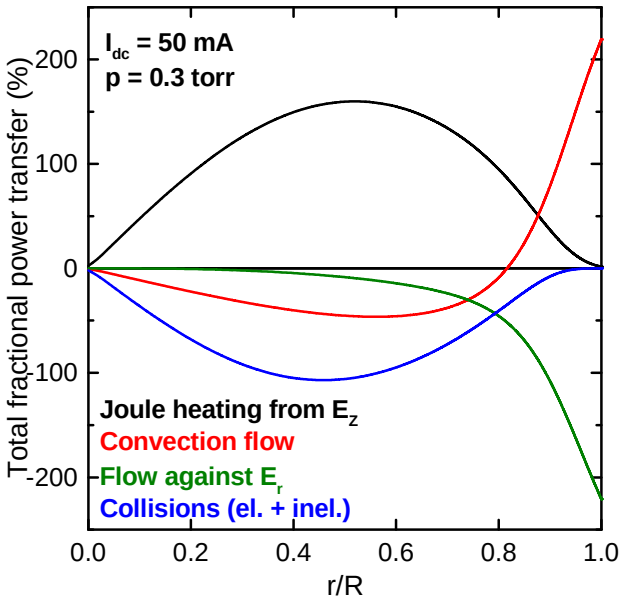

Percentages are calculated relative to the total (radially integrated across the discharge) power gained from the field

$$-\Gamma_z E_z = \nabla_r \Gamma_\varepsilon + \Gamma E_r + \theta_{\text{coll}}$$

Fluid modelling of dc discharge plasmas

Application to a discharge in helium

Power transfer radial profile

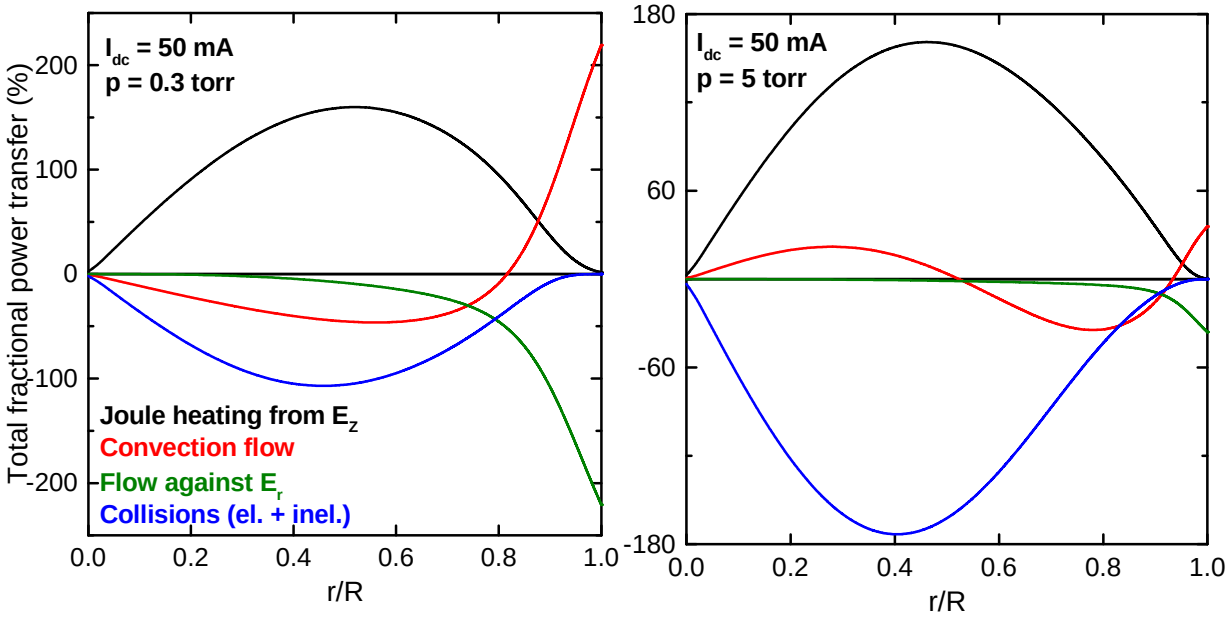

Percentages are calculated relative to the total (radially integrated across the discharge) power gained from the field

Final remarks

Modelling – looks complicated

$$\frac{v}{3}\vec{\nabla}\cdot\vec{F}_0^1 \;-\; \frac{1}{v^2}\frac{\partial}{\partial v}\left\{\left(\frac{ev^2}{6m}\right)\left[Re\left(\vec{E}_p\cdot\vec{F}_1^1\right)+2\vec{E}_s\cdot\vec{F}_0^1\right]+\frac{m}{M}\nu_c v^3 F_0^0\right\}$$

$$= \;(q-\nu_x-\nu_i)\,F_0^0$$

$$\nu_c\vec{F}_0^1 = -v\vec{\nabla}F_0^0+\frac{e}{m}\vec{E}_s\frac{\partial F_0^0}{\partial v}$$

$$(\nu_c+j\omega)\vec{F}_1^1 = \frac{e\vec{E}_p}{m}\frac{\partial F_0^0}{\partial v}$$

$$\frac{1}{x}\frac{d}{dx}\left(xn_pv_p\right) = NR\,\frac{\langle\nu_i\rangle}{N}\,n_e$$

$$\left[n_p+\frac{\langle\nu_i\rangle/N}{\nu_p/N}\,n_e\right]v_p+\frac{1}{NR}\frac{n_pv_p}{\nu_p/N}\frac{dv_p}{dx}-(\mu_pN)\;n_p\left[\frac{E_r}{N}-\frac{k_BT_p}{e}\frac{1}{NR}\frac{1}{n_p}\frac{dn_p}{dx}\right]=0$$

$$\frac{1}{x}\frac{d}{dx}\left(x\Gamma\right) = NR\,\frac{\langle\nu_i\rangle}{N}\,n_e$$

$$\Gamma = -\frac{1}{NR}\frac{d}{dx}\left[(D_eN)\;n_e\right]-(\mu_eN)\,\frac{E_r}{N}\,n_e$$

$$(\mu_eN)\left(\frac{E_z}{N}\right)^2 n_e-\frac{1}{NR}\frac{1}{x}\frac{d}{dx}\left(x\Gamma_\varepsilon\right) = \Gamma\,\frac{E_r}{N}+\frac{\theta_{\text{coll}}}{N}$$

$$\Gamma_\varepsilon = -\frac{1}{NR}\frac{d}{dx}\left[(D_\varepsilon N)\;\varepsilon\,n_e\right]-(\mu_\varepsilon N)\,\frac{E_r}{N}\,\varepsilon\,n_e$$

Final remarks

Modelling – practical results: discharge characteristic (in helium)